

INSTITUTO POTOSINO DE INVESTIGACIÓN  
CIENTÍFICA Y TECNOLÓGICA  
DEPARTAMENTO DE MATERIALES AVANZADOS

**“MICRO-SCALE SYSTEMS  
AND CELLULAR AUTOMATA:  
Spatio-Temporal Dynamics”**

Tesis que presenta

**M.C. Jaime Enrique Pérez Terrazas**

Para obtener el grado de Doctor en Ciencias Aplicadas  
en la especialidad de Nanociencias y Nanotecnología

*Director de Tesis:*

Dr. Haret Codratian Rosu

SAN LUIS POTOSÍ, S. L. P., MÉXICO

NOVIEMBRE DEL 2009

INSTITUTE FOR SCIENTIFIC AND TECHNOLOGICAL  
RESEARCH OF SAN LUIS POTOSÍ  
ADVANCED MATERIALS DEPARTMENT

**“MICRO-SCALE SYSTEMS  
AND CELLULAR AUTOMATA:  
Spatio-Temporal Dynamics”**

by

**M.Sc. Jaime Enrique Pérez Terrazas**

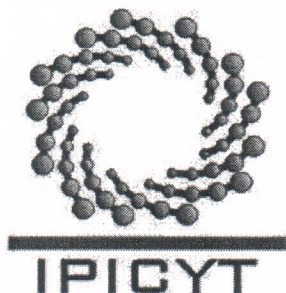
Thesis submitted to the Advanced Materials Department of  
the Institute for Scientific and Technological Research of San  
Luis Potosí, in partial fulfillment of the requirements for the  
degree of PhD in Applied Sciences

*Thesis Advisor:*

Ph.D. Haret Codratian Rosu

NOVEMBER, 2009

SAN LUIS POTOSÍ, S. L. P., MÉXICO



# Instituto Potosino de Investigación Científica y Tecnológica, A.C.

## Acta de Examen de Grado

El Secretario Académico del Instituto Potosino de Investigación Científica y Tecnológica, A.C., certifica que en el Acta 029 del Libro Primero de Actas de Exámenes de Grado del Programa de Doctorado en Ciencias Aplicadas en la opción de Nanociencias y Nanotecnología está asentado lo siguiente:

En la ciudad de San Luis Potosí a los 20 días del mes de noviembre del año 2009, se reunió a las 16:00 horas en las instalaciones del Instituto Potosino de Investigación Científica y Tecnológica, A.C., el Jurado integrado por:

<b>Dr. José Salomé Murguía Ibarra</b>	<b>Presidente</b>	<b>UASLP</b>
<b>Dr. Román López Sandoval</b>	<b>Secretario</b>	<b>IPICYT</b>
<b>Dr. Florentino López Urías</b>	<b>Sinodal</b>	<b>IPICYT</b>
<b>Dr. Haret-Codratian Rosu Barbus</b>	<b>Sinodal</b>	<b>IPICYT</b>
<b>Dr. José Luis Rodríguez López</b>	<b>Sinodal</b>	<b>IPICYT</b>

a fin de efectuar el examen, que para obtener el Grado de:

**DOCTOR EN CIENCIAS APLICADAS  
EN LA OPCIÓN DE NANOCIENCIAS Y NANOTECNOLOGÍA**

sustento el C.

**Jaime Enrique Pérez Terrazas**

sobre la Tesis intitulada:

*Micro-scale Systems and Cellular Automata: Spatio-temporal Dynamics*

que se desarrolló bajo la dirección de

**Dr. Haret-Codratian Rosu Barbus**

El Jurado, después de deliberar, determinó

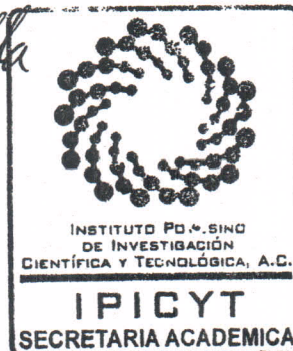
**APROBARLO**

Dandose por terminado el acto a las 18:10 horas, procediendo a la firma del Acta los integrantes del Jurado. Dando fe el Secretario Académico del Instituto.

A petición del interesado y para los fines que al mismo convengan, se extiende el presente documento en la ciudad de San Luis Potosí, S.L.P., México, a los 20 días del mes de noviembre de 2009.

*Manuel Bonilla*  
**Dr. Marcial Bonilla Marín**  
Secretario Académico

*Ivonne Lizette Cuevas Vélez*  
**Mtra. Ivonne Lizette Cuevas Vélez**  
Jefa del Departamento de Asuntos Escolares



# Abstract

This work contains the results from the simulations performed according to two computational models. The first one refers to a chemical system within a Continuously Stirred Tank Reactor (CSTR), while the second deals with a physico-chemical system of self-assembling pieces under different conditions. In addition, two mathematical analyses are also included. One is for waves along microtubules at the brain scale and the other is a wavelet processing of data from time series of Elementary Cellular Automata (ECA). The results of this thesis are mainly based on cellular automata as a tool for modeling and producing complex spatio-temporal dynamics.

me the confidence and self-esteem that have always maintained my hopes in a high level education even in hard times.

*To my parents;  
to my wife, Dulce;  
and to my son, Arturo Rafael.*

# Summary

In this work, the results from the simulations according to two computational models are presented. The first one refers to a chemical system within a continuously stirred tank reactor (CSTR) while the second deals with a physical system of self-assembling pieces under different conditions. In addition, two mathematical analyses are presented, for waves along microtubules at the brain scale, and a wavelet processing of data from time series of elementary cellular automata (ECA). The results of the work are mainly based on cellular automata as a tool for modeling and producing complex spatio-temporal dynamics.

A cellular automata approach for the CSTR with a cooling jacket is presented in Chapter 3. It could reproduce the CSTR dynamical behavior calculated by ODE's with a good approximation and in an easy way. The presented stochastic model allows us to study what could be the behavior of the variables of the tank when the reaction probability depends on the local temperature. It also gives us an approach to study systems of reduced content, such as micro and nanoreactors or reactor and jacket geometries different from the common ones.

In Chapter 4, the mathematical technique of factorization of differential operators is applied to two different problems. After a brief overview on microtubules, previous results are reviewed related to the supersymmetry of the Montroll kinks moving onto the microtubule walls as well as mentioning the sine-Gordon model for the microtubule nonlinear excitations. Next, new analytic formulas are presented for a class of one-parameter solutions of a sort of diffusion equation of Bessel type that is obtained by supersymmetry from the homogeneous form of a simple damped

---

wave equations derived from previous work in the literature of the corticothalamic system. A possible interpretation of the diffusion equation in the brain context is presented.

In Chapter 5, the discussion is focused on a model for the aggregation of pieces (or molecules), dynamically interacting according to LGCA methods. In addition to traditional models, we considered that particles are not just point-like, but they have a cross shape. This implies the consideration of rotations and orientation of pieces and gives us the possibility of considering a huge spectra of different pieces by defining different kinds of extremes and interactions between them. It is shown that selection of pieces and densities have a major effect on the morphology of the aggregates at different scales. In addition, three appropriate measures for characterizing the aggregates are proposed. The results suggest that it is possible to create experimental aggregated structures at the micro- and nano-scales with partial control on their local and global structural properties. This would allow to produce small structures with enhanced properties for physical or chemical absorption, or special microlocal surface properties.

Chapter 6 focuses on the analysis of the time series of the so-called row sum (or total activity) ECA signals, i.e., the sum of ones in sequences of rows, employing Daubechies (Db) wavelets. An algorithmic implementation that embeds the discrete wavelet transform in the Multifractal Detrended Fluctuation (MF-DFA) technique is proposed. With it, we get similar results to the other methods but computationally faster because we employ a lesser number of windows. Our results represent a confirmation of the fact that ECA patterns (rules 90, 105 and 150) of different magnitudes follow different scaling laws, *i.e.*, the ECA have intrinsic multifractality that does not depend on the set of initial data that we used.

# Abbreviations in this work

<i>CA</i>	Cellular Automata
<i>CSTR</i>	Continuously Stirred Tank Reactor
<i>ECA</i>	Elementary Cellular Automata
<i>FHP model</i>	Frisch, Hasslacher and Pomeau model
<i>FWT</i>	Fast Wavelet Transform
<i>HPP model</i>	Hardy, Pomeau and de Pazzis model
<i>LGCA</i>	Lattice Gas Cellular Automata
<i>MF-DFA</i>	Multifractal Detrended Fluctuation Analysis
<i>MRA</i>	Multi-Resolution Analysis
<i>MT</i>	Microtubule
<i>ODE</i>	Ordinary Differential Equation
<i>QCA</i>	Quantum Cellular Automata
<i>WMF-DFA</i>	Wavelet Multifractal Detrended Fluctuation Analysis

# Acknowledgments

This thesis document presents the results of the multi-disciplinary activity in which I was involved during the last four years. The touched issues are as diverse as chemical reactors, reaction-diffusion equations, cytoskeletal structures, self-assembly, fractal and multifractal properties, wavelet approaches and cellular automata, as well as others that did not make all the way in order to be part of a full project presented here: quantum dots, neuronal memory processes, quantification of information, consciousness, simulated annealing and others. Working on a project with such diversity of issues has been a really tough journey for which, I realized now at the end that I was barely prepared. So, I want to acknowledge the friendship and collaboration given to me along this journey, but also, and mainly, I feel myself grateful to those actions, people and support that kept me working on, and surpassing those moments when my “academic faith” was declining.

I thank to all people that has been part of the Advanced Materials Department these years. All of them, in their specific role, have provided me with smiles, friendship, support and excellent companionship. Specially to Ph.D. Aldo Romero and Ph.D. Mauricio Terrones for all their work and guidance towards achieving my first publication, to Gaby for all her help making arrangements for my academic trips abroad, to Ph.D. José Luis Rodríguez for his natural way of friendship with students and constant book supply, and to my office partners Pili, Jorge, Pedro and Jessica (unofficial office partner) for their magnificent friendship, valuable technical advice and the sharing of joy, worries, ideas, pizzas, books, news, hobbies and time spent together.

Of course, Ph.D. Haret Codratian Rosu, my advisor, deserves a special place. He was the leading force that promoted colaborations and kept them working in a proper way. He has been always willing and collaborative to resolve any request about books, support for academic events and any other necessities of the work. However, what I want to recognize over all things is that he is always there for his students. Almost any hour of the day, any day of the whole week he is willing to give help and guidance to students in order to achieve the completion of a proper work. I thank him all his colaboration and constant support to achieve my academic goals as well as his large patience for the completion of the present work.

I thank also to Ph.D. José Salomé Murguía, Ph.D. Vrani Ibarra and Ph.D. Octavio Cornejo by giving me their best advices on their own specialities in order to make a successfull colaboration leading to new scientific work. Especially to José Salomé Murguía, whose colaboration lasted a longer time being plenty of friendly and fruitful talks and worthy advices.

I want to express my admiration to Ph.D. Ignacio Barradas, Ph.D. Harry Swinney, and Ph.D. Joel Urias. Although they have not been directly involved on this work, they are, for me, the mixed models of what I want to become some day as a scientist, as a teacher and as an advisor.

I am grateful to my family that has been always the strongest pillar of my achievements. I thank to my father and my mother for their love, support and constant confidence in me. To my brother, Efrén, by walking with me on the scientific road and by his advices. To my brother, Javier, for letting me know about different views of science. To my son, Arturo Rafael, and my wife, Dulce, for waiting for me living with them in Saltillo and sharing with me their beautiful smiles and happiness, toghether with their lovely support and patience.

Finally, I dedicate this work to my mother, not only this written document but the whole “Ph.D. achievement”. All her love given to me in my childhood built in

# Contents

<b>1</b>	<b>Introduction</b>	<b>1</b>
1.1	Brief history . . . . .	1
1.2	Motivation . . . . .	7
1.2.1	Molecular systems . . . . .	7
1.2.2	Reaction and diffusion in Micro-Scale Systems . . . . .	9
1.3	Aims of the work . . . . .	12
<b>2</b>	<b>Cellular automata modeling</b>	<b>16</b>
2.1	Definitions and considerations . . . . .	16
2.1.1	Cellular automata . . . . .	16
2.1.2	Neighborhood and boundary conditions . . . . .	18
2.1.3	The rule: options for cellular automata modeling . . . . .	20
2.2	A simple model: Directed percolation . . . . .	21
2.3	Lattice gas CA Models . . . . .	24
2.3.1	The HPP rule . . . . .	24
2.3.2	The FHP model . . . . .	25
2.4	Why CA and LGCA Simulations? . . . . .	28
2.4.1	Modeling Nature . . . . .	28
2.4.2	Cellular automata as a modeling tool . . . . .	30
<b>3</b>	<b>Continuous Stirred Tank Reactor CA model</b>	<b>34</b>
3.1	Models in Chemistry . . . . .	34
3.2	The CA model for CSTR . . . . .	36
3.2.1	Introduction . . . . .	37

3.2.2	The ODE-based model of jacketed CSTR . . . . .	39
3.2.3	Stochastic CA model for Jacketed CSTR . . . . .	40
3.2.4	Simulations . . . . .	43
3.2.5	Concluding Remarks . . . . .	46
<b>4</b>	<b>A Biological System</b>	<b>52</b>
4.1	Supersymmetric methods in the traveling variable: inside neurons and at the brain scale . . . . .	52
4.1.1	Microtubule structure and dynamics, brief overview . . . . .	53
4.1.2	Nonlinear biological excitations . . . . .	55
4.1.3	Supersymmetric MT Kinks . . . . .	57
4.1.4	The sine-Gordon MT solitons . . . . .	61
4.1.5	More on the hydrolysis and solitary waves in MTs . . . . .	63
4.2	Quantum information in the MT walls . . . . .	64
4.2.1	Supersymmetry at the Brain Scale . . . . .	65
<b>5</b>	<b>A CA model for Self-Assembling</b>	<b>72</b>
5.1	Self-assembly: an overview . . . . .	72
5.1.1	What is self-assembly? . . . . .	72
5.1.2	Self-assembly research revisited . . . . .	75
5.2	Description of the proposed LGCA model . . . . .	79
5.3	Self-assembly model in action . . . . .	81
5.3.1	Tests . . . . .	81
5.3.2	Density effects . . . . .	83
5.3.3	Systems with pieces with induced defects . . . . .	89
5.4	Conclusions and perspectives . . . . .	99
<b>6</b>	<b>Wavelet Analysis of Elementary Cellular Automata Signals</b>	<b>105</b>
6.1	Overview . . . . .	105
6.1.1	Elementary Cellular Automata . . . . .	105
6.1.2	Wavelet Method . . . . .	107

---

6.2	Multifractal properties of elementary cellular automata in a discrete wavelet approach of MF-DFA . . . . .	110
6.2.1	Introduction . . . . .	110
6.2.2	DFA with wavelets . . . . .	112
6.2.3	Application to one-dimensional CAs . . . . .	114
6.2.4	Conclusions . . . . .	115
<b>7</b>	<b>Concluding remarks and future work</b>	<b>122</b>
7.1	Contributions . . . . .	122
7.2	Future research . . . . .	126
<b>A</b>	<b>Cellular Automata Model for Reaction-Diffusion Systems</b>	<b>128</b>
<b>B</b>	<b>Multi-Resolution Analysis</b>	<b>132</b>

# List of Tables

3.1	Parameters of the model . . . . .	41
6.1	Hurst exponent for three ECAs under different initial conditions, MF-DFA method . . . . .	116
6.2	Hurst exponent for three ECAs under different initial conditions, WMF-DFA method . . . . .	117

# List of Figures

1.1	Game of Life: Glider . . . . .	3
1.2	Wolfram's rule 90: Sierpinski triangle . . . . .	4
1.3	Quantum dots cellular automata . . . . .	6
2.1	Cellular automata grids and cell's states. . . . .	17
2.2	Cellular automata rule application. . . . .	18
2.3	Von Neumann and Moore neighborhoods . . . . .	19
2.4	Directed percolation problem . . . . .	22
2.5	Parameter space of directed percolation . . . . .	23
2.6	HPP Model. . . . .	25
2.7	Collision in the HPP Model. . . . .	26
2.8	Types of collisions in the FHP model. . . . .	27
3.1	Schematic representation of the jacketed CSTR. . . . .	40
3.2	Comparison between the curves from the differential equations and the curves obtained from simulations with the CA approach. . . . .	44
3.3	Comparison between the tank temperature evolution curves for a ki- netic constant based on average temperature and for kinetics constant calculated on the base of the local temperature. . . . .	45
3.4	Behaviors that could be found in systems with small number of elements	47
3.5	Different concentration behaviors of chemical A for systems of the same size. . . . .	48
4.1	Microtubule structure and assembly . . . . .	54
4.2	Microtubule behavior . . . . .	55

---

4.3	Stochastic CA Model of Microtubule Assembly/Disassembly . . . . .	56
4.4	Single electron within the traveling double-well potential $u(\xi)$ as a qubit. . . . .	58
5.1	Self-assembly: biological examples . . . . .	73
5.2	Ordered structure made up by complementary components. . . . .	74
5.3	Crystalline aggregates made by self-assembly. . . . .	75
5.4	General molecular method for designing and producing self-assembling pieces. . . . .	76
5.5	Structures assembled with DNA strands . . . . .	77
5.6	Formation of virus capsides in a molecular dynamics model . . . . .	78
5.7	Comparison between a multiagent model for self-assembly and Monte Carlo method . . . . .	78
5.8	Pieces assembled in a ordered structure, square lattice . . . . .	80
5.9	Evolution of an aggregate: test try . . . . .	82
5.10	Conversion speed for three different systems . . . . .	83
5.11	Cluster formed at an initial density of 0.2 pieces per node. . . . .	85
5.12	Conversion speed for five different densities . . . . .	86
5.13	Relation between perimeter and area for five different densities. . . . .	87
5.14	Time evolution of the measure $F$ for different initial densities. . . . .	89
5.15	Cluster formed by pieces without defects. . . . .	91
5.16	Cluster formed by normal pieces and M1 mutant pieces. . . . .	91
5.17	Cluster formed by normal pieces and M2L mutant pieces. . . . .	92
5.18	Cluster formed by normal pieces and M2I mutant pieces. . . . .	93
5.19	Cluster formed by normal pieces and M3 mutant pieces. . . . .	93
5.20	Cluster formed by normal pieces and M4 mutant pieces. . . . .	94
5.21	Conversion speed for systems with mutant pieces . . . . .	95
5.22	Perimeter vs area evolution for systems with mutant pieces . . . . .	97
5.23	The non sticky perimeter vs total perimeter for systems with mutant pieces . . . . .	98
5.24	Time evolution of the measure $F$ for systems with mutant pieces . . . . .	99
5.25	Formation of covalently connected networks . . . . .	101

---

6.1	ECA number 90 evolution . . . . .	106
6.2	Four Wavelets . . . . .	109
6.3	Properties of the rule 90 time series . . . . .	115
6.4	Properties of the rule 150 time series . . . . .	116
6.5	Properties of the rule 105 time series . . . . .	117
6.6	Log-log plot of the fluctuation function $F_2$ versus scale for: (a) rule 90, (b) rule 150, and (c) rule 105. . . . .	118
A.1	Summary of moving average cellular automaton. . . . .	129
B.1	The structure of a three-level FWT. . . . .	135

# Chapter 1

## Introduction

### 1.1 Brief history

The elaboration of the cellular automata method is due to John von Neumann, who at the end of the 1940s was involved in the design of the first digital computers. Von Neumann wanted to know how to imitate the power of human brain for solving very complex problems. Even more, he wished to find how to reproduce the organic properties of self-control and self-repair. Those thoughts led him to the also very complicated problem of designing a self-replicating machine, capable of building itself out of some available material in its environment. He found a theoretical procedure to solve this problem: a cellular automaton.

Following the suggestions of S. Ulam, Neumann developed a model using a discrete two-dimensional universe made up of cells, each one being in a defined internal state. Neumann suggested a system evolution performed in discrete time steps, where the cells only know a simple recipe, the same for all of them, to compute their new internal state. Such recipe, or rule, is defined as a function of the states of the neighbor cells and is applied synchronously on all cells. These fully discrete dynamical systems are now referred as cellular automata.

Neumann succeeded in designing a structure of cells, with given initial states and a defined rule, able to generate new identical structures. They contained in

themselves the information and the algorithm that gave them the capacity of self-reproduction. This artificial life model was based on a two-dimensional square lattice, a set of 29 possible states, a rule applied to each cell that is function of the four closest neighbors and the cell itself, and, finally, an initial structure of several thousand elementary cells. A new tool was born, although Neumann's replicator needed to wait further development of computers in order to be simulated.

Cellular automata was almost forgotten until 1970, when M. Gardner presented the Conway's "Game of Life" [1]. This was intended to simulate an ecological model, by means of a two-dimensional square lattice as space and two possible states: alive or dead. The rule is defined as follows (see figure 1.1):

- a dead cell surrounded by exactly three living cells comes back to life,
- a living cell surrounded by less than two living neighbors dies of isolation,
- a living cell surrounded by more than three neighbors dies of overcrowding,
- in any other case the cell does not change

Here, the surrounding cells correspond to the neighborhood composed of the four nearest cells (north, south, east and west) plus the four second nearest neighbors, along the diagonals. This simple model is capable of unexpected rich and complex behavior. Complex structures can emerge from the initial system state, and some of them evolve in a way that produce the sensation of seeing interacting living things, colliding, evolving, traveling through the grid. Such richness of behavior brought the concept of cellular automata to the attention of a wide audience.

In the 1980's Stephen Wolfram performed detailed studies on one-dimensional cellular automata [3]. He was interested in cellular automata not only as a modeling tool but also as systems that deserve being studied. He showed that cellular automata can exhibit many of the behaviors found in continuous systems, such as complexity, but in simpler framework and without truncation errors, due to their discrete nature. Wolfram numbered the rules for one-dimensional cellular automata

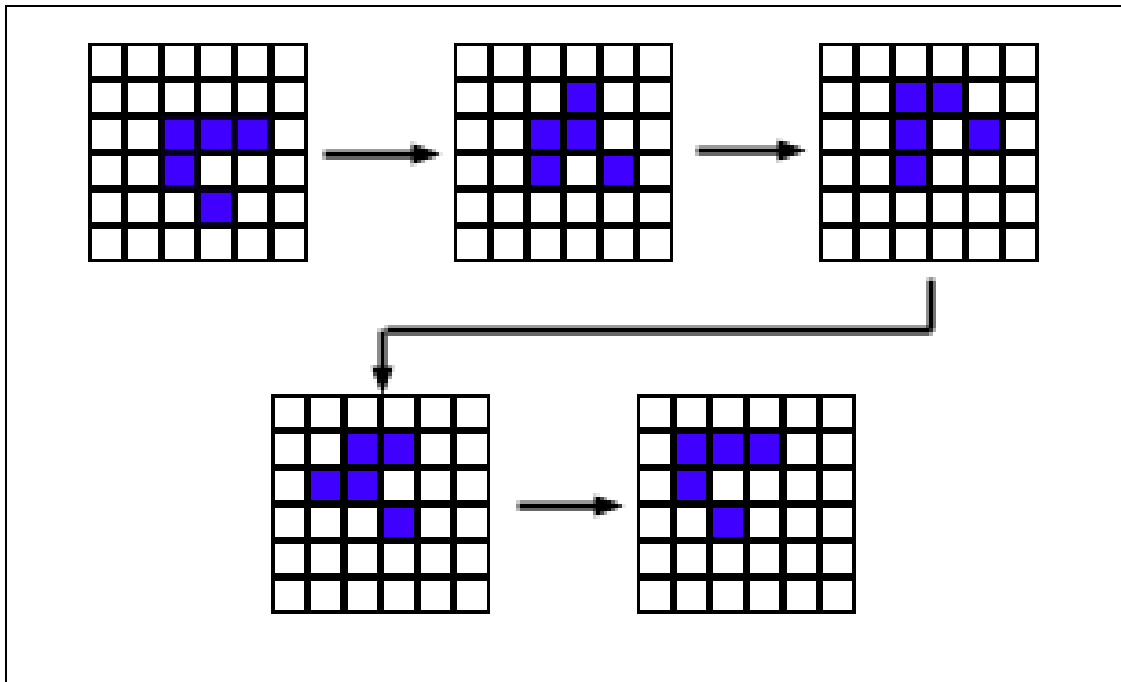


Figure 1.1: Glider, self-sustainable structure in the Game of Life. Black cells represent alive cells, white cells represent dead cells. Figure from [2]

with two states and rules defined as function of the two nearest neighbors and the evolving cell itself. He found complex behaviors in the evolution of some of those 256 rules and proved that they are important objects to consider for statistical mechanics studies. In figure 1.2 it is shown a fractal structure that is obtained from the evolution of Wolfram's rule 90. Nowadays, Wolfram's rules, as well as other cellular automata schemes, are still the topic of much active research. Some issues related with cellular automata and typically studied using them are: chaos synchronization [4], as an alternative to differential equations in modeling physics [5], as models of complexity [3], damage spreading [7], self-organization [8], etc.

Von Neumann's automaton, Conway's Game of Life and Wolfram's 110 rule have the special property of being universal computers. This means that they can perform any possible algorithmic procedure if proper initial conditions and data coding are set. This motivated Toffoli and Margolus to build the first general purpose cellular automata machines (called CAM-6) in the 1980's. The distributed nature of such computers gave them the capability of a supercomputer of that time.

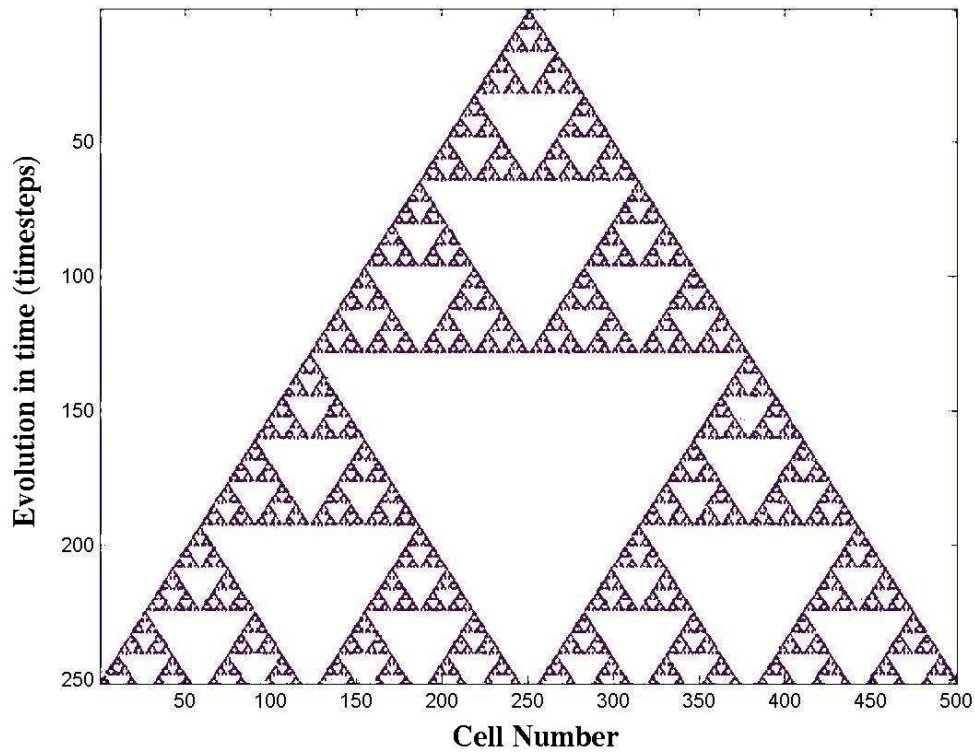


Figure 1.2: Sierpinski triangle made by Wolfram's rule 90

In the 1970 Hardy, Pomeau and de Pazzis developed the HPP lattice gas model [4]. However, in the 1980's it was recognized that this model was in fact a cellular automata, being termed Lattice Gas Automata (LGA). The main idea was to represent particles in a gas, colliding and moving in a squared lattice, in such a way that momentum and particle number were conserved. Therewith, fundamental statistical properties can be calculated from the model. Since then, cellular automata rules have been viewed as an alternative form of microscopic reality which bears the expected macroscopic behavior. In 1986, U. Frisch, B. Hasslacher and Y. Pomeau developed a similar model, now called FHP, but in an hexagonal grid [16]. Due to the improve of the symmetry, this model reproduce, in some appropriate limits, the behavior prescribed by the Navier-Stokes equation of hydrodynamics. More about these models will be discussed in the following chapters.

In 2002, Wolfram published his famous book "A New Kind of Science" [2]. In this book, he claims that complex behavior could come from computation in a sys-

tem that is following simple rules. The main issues discussed are computability and complexity in nature. However, the principal tools and system paradigm used in the book are cellular automata. He gives an impressive number of examples of cellular automata simulations that resembles the behavior of several physical and biological systems. He even discusses about the possibility that the physical world could be a very large cellular automaton. Although many of the ideas presented are controversial [12], this book is still considered the most important exposition of cellular automata systems to the scientific community.

When looking for technical applications, one of the most interesting applications of cellular automata is their use in quantum computation. Here are implemented quantum-dot cellular automata, that conform a transistorless computational paradigm. In denser and denser arrangements with smaller devices, quantum-dot could allow to built devices able to take advantage of quantum phenomena, instead of reducing performance as would happen with transistor systems. Using a cellular automata paradigm addresses also the interconnection problem due to the fact that it is local and dependent of the state of neighbors.

The quantum-dot cellular automata was proposed by Lent and coworkers [13]. Each cell is made of by four quantum-dots in a square, and the state is given by the position of two extra electrons. Because of coulombic repulsion they are in opposite sides in diagonal direction, giving two possible states (see figure 1.3). The spatial arrangement and the coulombic repulsion allow the creation of logic gates AND, OR and NOT, making general purpose computing possible. Until now, only small arrangements have been made experimentally, using aluminum islands and aluminum-oxide tunnel junctions, fabricated on an oxidized silicon wafer [14]. There is also theoretical work on quantum computation with quantum cellular automata. Several schemes have been proposed in order to obtain universal computability, reliable implementation at room temperature as well as local and unitary evolution (see, for instance, [15]).

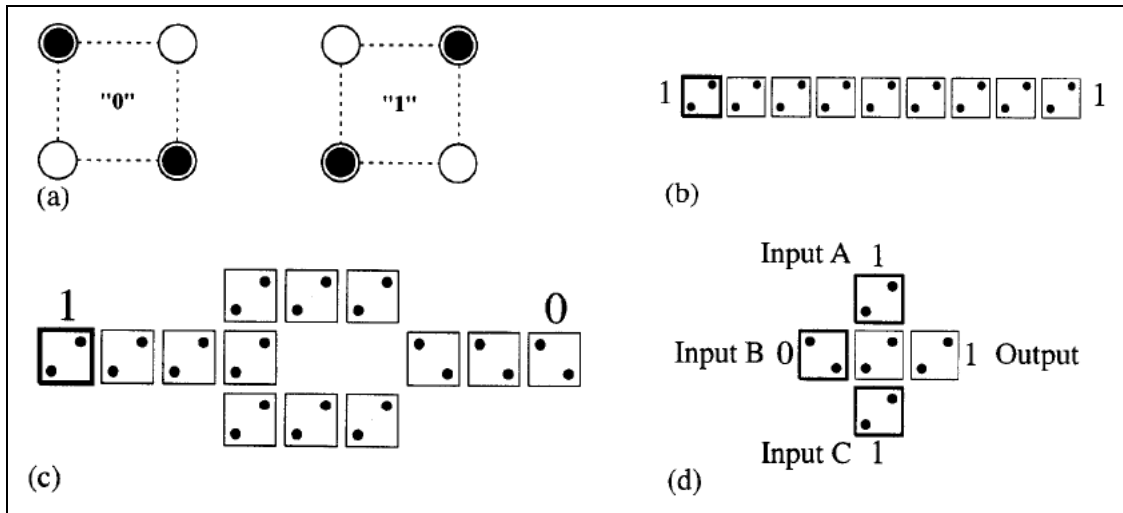


Figure 1.3: (a) QCA cells showing the two possible polarizations. (b) QCA line. (c) Inverter. (d) Majority gate. Figure from [14]

Nowadays, the efficiency of cellular automata as a modeling tool is manifest. They have been used for the study and simulation of a broad range of physical, biological, chemical, and sociological phenomena. Some examples are: excitable media [17,38], evolutionary game theory [18], self-replicating structures [19], migration of glioma cells [20], stock market dynamics [21], dynamics of HIV infection [22], formation of patterns in chemical systems [3], recrystallization [24], ecological patterns [25,26], freeway traffic [27], and so on. More applications can be found in the works of Chopard and Droz [20], Deutsch and Norman [19], and Kier, Seybold and Cheng [18].

Such broad range of applications and schemes represents only a little part of what can be found in the literature. Today it is not clear which will be the importance of cellular automata in the future. Will they give some clue about the nature of space and time as Wolfram claims? Is out there something that can be not modeled with any cellular automaton approach? Will they help to unravel the secrets of complexity? Are quantum-dots cellular automata the computers of the future? However, there are no doubts that this modeling paradigm will be used for a long time.

## 1.2 Motivation

### 1.2.1 Molecular systems

The reasons for using cellular automata as a modeling tool for molecular systems can be condensed in one phrase: cellular automata allow to simulate, in a straight and physically meaningful way, discrete entities that interact locally in a parallel fashion.

Cellular automata are an idealization of a physical, chemical or biological system, where the interactions between constituents are coded or embedded in the rule that determines the evolution of the system. For instance, a great variety of chemical processes can be modeled by means of encoding the most important states of the elements of the systems as the states of the cell, and their local interactions by the cellular automaton rule. One simple example: if two cells have the values (1,2) and they are updated to (0,3) in a cellular automata model of a chemical system, it can be the representation of the interaction between a molecule A (1) and a molecule B (2), that react in order to produce a molecule C (2) and leaving a free space (0) where molecule A has been present. As simple as this approach can be, it is capable of reproducing some expected behaviors of simple chemical systems in a qualitative and quantitative way [18]. Of course, more complicated models can be applied to more complicated systems and/or in order to study specific phenomena.

The developing and implementation of parallel software programs is a natural extension of cellular automata models due to their parallel nature. This allows the study of the interaction between a huge number of entities, increase the speed of a particular run or perform a large number of simulations in order to obtain the statistical behavior of the simulated system. The parallel update of the systems also means that the simulated entities evolve at the same time. Although it can appear unnatural or tricky, generally it is not a real problem if the proper rule is implemented and the timestep of the model represents a sufficiently small time interval in the scale of interest of the simulated system.

The spatially discrete nature of cellular automata also helps to represent individual entities in evolutionary models with spatial structure. This is important because real systems are discrete; they are composed of individual atoms, molecules, virus, cells, sand grains, trees, animals, humans and so on, whose interactions depend on their relative position. Local interaction and discrete nature are some of the greatest important features of cellular automata, because these characteristics make them, as Toffoli said, “dynamical systems that play in discrete mathematics a role comparable to that of partial differential equations in the mathematics of the continuum.” It is possible to take advantage of this capability over partial differential equations in two different ways: the first by reproducing the behavior described by partial differential equations by simulating them; and the second, by means of the direct insight and simulation of the system when the solution of the equations is extremely difficult or does not represent the behavior of the system in a feasible fashion. The last feature is the most important because, usually, partial differential equations are based on local mean field approximations, meaning well local mixing of constituents of the systems, neglecting correlation terms from local interactions and their discrete nature. In fact, it is possible that there is a lack of schemes in regard of discrete interactions, probabilistic fluctuations and spatial inhomogeneities.

All the features presented above make cellular automata a valuable modeling paradigm for molecular systems; where the dynamical systems can be composed by large numbers of components interacting in a local (or not so local) fashion. Such components in simulations of materials science systems can be atoms, clusters of atoms, little molecules, proteins or abstract objects representing a family of them. Important fields where microstructure-based cellular automata have been successfully used in the materials sciences are primary static recrystallization and recovery, formation of dendritic grain structures in solidification processes and related nucleation and coarsening phenomena [31]. Some other examples of cellular automata applied to materials science are: excitable media [17, 38], formation of patterns in chemical systems [3], laser dynamics [32], gravity-driven granular flows [33], first-order chemical reactions [2] and more.

Maybe Raabe has expressed one of the most positive and expert-based opinions about the future and importance of cellular automata and related techniques in materials science: “Although the Navier-Stokes framework serves as a long-established basis for predicting fluid behavior, it has still not been possible to resolve some basic questions on the fields of modern materials science and engineering with it... Prominent examples where such limitations occur are the simulation of nano- and microflows in filters, foams, microreactors or otherwise confined geometries;... liquid crystal processing; nanoscale process technology;... liquid phase separation... to name only a few... Lattice gas cellular automata and their more mature (non-Boolean) successors, the Lattice Boltzmann automaton techniques,... seem to be predestined to tackle some of these challenges on the domain of materials-related computational fluid dynamics in a more efficient way than the conventional Navier-Stokes approach” [35].

In this work, several applications of cellular automata to the simulation of molecular systems will be presented. Between the broad range of possibilities, we have selected systems where diffusion of reactive elements or signals are important characteristics. Modeling of diffusion of reactive elements could help to study and explain chemical processes where spatial structure and inhomogeneities are important. As a special case of these systems, it is presented a model of self-assembly. Understanding self-assembly is a fundamental step in order to raise Nanotechnology to the level that is needed for really being the technological revolution that all of us are waiting.

### 1.2.2 Reaction and diffusion in Micro-Scale Systems

Chemical surface reactions produce a large number of different spatio-temporal structures such as oscillations, traveling waves, spiral Turing patterns, etc. It is usual to study the behavior of such structures using a set of  $s$  coupled reaction-

diffusion partial differential equations, that have the general structure:

$$\frac{\partial x_i(\mathbf{r}, \mathbf{t})}{\partial t} = D_i \nabla^2 x_i(\mathbf{r}, \mathbf{t}) + \mathbf{f}_i(\mathbf{x}_1, \mathbf{x}_2, \mathbf{x}_3, \dots, \mathbf{x}_s), \quad (1.1)$$

where  $s$  is the number of different chemical species, the first part of the right hand side represents the diffusion and the last part represents the interaction between the components. In his seminal paper of 1952 [4], A. Turing showed how the spontaneous formation of spatial patterns is possible from almost homogeneous structures where the behavior is dictated by this type of equation and some conditions are satisfied.

Reaction-diffusion equations have been successfully applied to pattern formation and chemical reactions on surfaces. Besides, the majority of physical, chemical, biological and sociological processes can be described in terms of propagating fronts and the most types of propagating fronts can be analyzed in terms of reaction-diffusion systems [37]. However, as has been pointed out above, partial differential equations usually neglect correlation terms from local interactions and discrete nature of the constituents of the system. Therefore, it is a good idea to use cellular automata as a complementary tool, in order to study the effect that discreteness and probabilistic fluctuations have on the behavior of the systems.

However, how good are cellular automata models for this kind of systems? They are good, Adamantzky has stated: “There is little doubt that the most useful way to simulate many excitable media is to use a cellular automata approach” [38]; and “Cellular automata models of reaction-diffusion media exhibit the same spectrum of coherent patterns as numerical simulations of reaction-diffusion equations: traveling waves, spiral waves, stable spots, strips and labyrinths.” [37]. Interesting work on cellular automata and reactive and diffusive systems has been made by Weimar [2].

Thus, it has been shown that reaction and diffusion are fundamental for modeling a broad range of chemical and biological systems and that cellular automata are

a useful and reliable complementary method. Mainly, when spatio-temporal structures, probabilistic fluctuations and spatial inhomogeneities are important.

One of the most important issues in current science where spatio-temporal structures, probabilistic fluctuations and spatial inhomogeneities are important is molecular self-assembly. Molecular self-assembly is defined as a process in which molecules (or parts of molecules) spontaneously form ordered aggregates without direct human intervention; the interactions are usually noncovalent [40]. Self-assembly is recurrent in many fields of science such as Chemistry, Biology and Materials Sciences. The formation of crystals, monolayers, micelles and the replication of DNA helix are only a few examples.

The main characteristics of self-assembly are:

- **Components:** Entities complementary in shape and physico-chemical properties. They go from a disordered state to another of larger order.
- **Interactions:** Generally weak and noncovalent as van der Waals and Coulomb interactions. Attractive and repulsive interactions are almost in balance.
- **Reversibility (or Adjustability):** Balance between attractive and repulsive forces allow to correct errors through the formation of ordered structures.
- **Environment:** Diffusion of components requires a proper medium.
- **Mass transport and agitation:** Energy required in order to make components travel and meet.

Understanding self-assembly is a fundamental goal in current science for several reasons. The first of them is that it is one of the main tools used by living organisms in order to be alive. We can see self-assembly in the formation of micelles, virus capsides, cellular walls, DNA copying, etc. The second is that controlling self-assembly could be the only way to develop and produce new nano-devices and nano-materials in a cheap way and industrial quantities [41]. It is specially important for the computer industry because there the focus is on getting smaller devices

in a denser fashion.

Components in self-assembly can be described as discrete entities that interact in a local fashion, as reactive agents that respond to their environment, as dictated by their physical composition and properties [42]. This response can consist in aggregating to other components or in changing their internal state in response to the state of the neighboring components (conformational switching) [15]. These properties make self-assembly systems good candidates for being studied and modeled through cellular automata methods.

### 1.3 Aims of the work

- To study, model, and simulate chemical and biological systems where spatio-temporal structures, probabilistic fluctuations and/or spatial inhomogeneities can be important for their behavior.
- To study, model, and simulate self-assembly systems, trying to find archetypical self-assembly systems, by means of the abstract representation of components and their internal states and interactions.
- To reinforce the use of cellular automata by performing multidisciplinary studies and modeling of the systems presented above, with cross-over of Biology, Physics, Chemistry and Mathematics.

---

**REFERENCES**

1. M. Gardner, Scientific American, **220** (4), 120 (1970)
2. <http://www.alesdar.org/oldSite/IS/chap3-3.html>
3. S. Wolfram, Theory and Application of Cellular Automata. World Scientific (1986)
4. M. Inoe and M. Nagadome, Journal of the Physical Society of Japan **69**, 1 (2000)
5. T. Toffoli, Physica D **10**, 117 (1984)
6. S. Wolfram, Nature **311**, 419 (1984)
7. F. Bagnoli, R. Rechtman and S. Ruffo, Physics Letters A **172**, 34 (1992)
8. M. V. Medvedev and P. H. Diamond, Phys. Rev E **58**, 6824 (1998)
9. J. Hardy, Y. Pomeau and O. de Pazzis, Phys. Rev. A, **13**, 1949 (1976)
10. U. Frisch, B. Hasslacher and Y. Pomeau, Phys. Rev. Lett. **56**, 1505 (1986)
11. S. Wolfram, A New Kind of Science, Wolfram Media, Inc. (2002)
12. J. Giles, Nature **412**, 216 (2002)
13. C. S. Lent, P. D. Tougaw, W. Porod and G. H. Bernstein, Nanotechnology **4**, 49 (1993)
14. G. L. Snider, A. O. Orlov, I. Amlani, G. H. Bernstein, C. S. Lent, J. L. Merz and W. Porod, Microelectronic Engineering **47**, 261 (1999)
15. C. A. Pérez-Delgado and Donny Cheung, Phys. Rev. A **76**, 032320 (2007)
16. A. Adamantzky and O. Holland, Chaos, Solitons & Fractals **9**, 1233 (1998)
17. T. Szakály, I. Lagzi, F. Izsák, L. Roszol and A. Volford, Central Eur. J. Phys **5**(4), 471 (2007)

18. M. A. Nowak and R. M. May, *Nature* **359**, 826 (1992)
19. M. Sipper, *Artificial Life* **4**, 237 (1998)
20. M. Aubert, M. Badoual, S. Féreol, C. Christov and B. Grammaticos, *Phys. Biol.* **3**, 93 (2006)
21. M. Bartolozzi and A. W. Thomas, *Phys. Rev. E* **69**, 046112 (2004)
22. R. M. Zorzenon dos Santos and S. Coutinho, *Phys. Rev. Lett.* **87**, 168102 (2001)
23. B. Chopard, P. Luthi and M. Droz, *Phys. Rev. Lett.* **72**, 1384 (1994).
24. R. Dewri and N. Chakraborti, *Modelling Simul. Mater. Sci. Eng.* **13**, 173 (2005)
25. J. T. Wootton, *Nature* **413**, 841 (2001)
26. S. Ichinose, *Phys. Rev. E* **64**, 061903 (2001)
27. K. Nagel and M. Schreckenberg, *J. Phys. I France* **2**, 2221 (1992)
28. B. Chopard and M. Droz, *Cellular Automata Modeling of Physical Systems*, Cambridge University Press, New York (1998)
29. A. Deutch and S. Dormann, *Cellular Automaton Modeling of Biological Pattern Formation*, Birkhäuser, Boston (2005)
30. L. B. Kier, P. G. Seybold and C. Cheng, *Modeling Chemical Systems using Cellular Automata*, Springer, The Netherlands (2005)
31. D. Raabe, *Annu. Rev. Mater. Res.* **32**, 53 (2002)
32. J. I. Guisado, F. Jiménez-Morales and J. M. Guerra, *Phys. Rev. E* **67**, 066708 (2003)
33. K. R. LaMarche, S. L. Conway, B. J. Glasser and T. Shinbrot, *Granular Matter* **9**, 219 (2007)

- 
34. P. G. Seybold, L. B. Kier and C. Cheng, *J. Chem. Inf. Comput. Sci.* **37**, 386 (1997)
  35. D. Raabe, *Modelling Simul. Mater. Sci. Eng.* **12**, R13 (2004)
  36. A. M. Turing, *Phil. Trans. R. Soc. Lond. B* **237**, 37 (1952)
  37. A. Adamatzky, *Computing in Nonlinear Media & Automata Collectives*, Taylor & Francis, 1st edition (2001)
  38. A. Adamatzky and O. Holland, *Chaos, Solitons & Fractals* **9**, 1233 (1998)
  39. J. R. Weimar and J. P. Boon, *Phys. Rev. E* **49**, 1749 (1994)
  40. G. M. Whitesides and M. Boncheva, *Proc. Nat. Ac. Sci. U.S.A.* **99**(8), 4769 (2002)
  41. G. M. Whitesides and B. Grzybowski, *Science* **295**, 2418 (2002)
  42. A. Dorin, *Physically Based, Self-Organizing Cellular Automata*, in *Multi-Agent Systems - Theories, Languages and Applications*, C. Zhang and D. Lukose (eds.), *Lecture Notes in Artificial Intelligence* **1544**, Springer-Verlag, pp 74-87 (1998)
  43. R. L. Thompson and N. S. Goel, *J. theor. Biol.* **131**, 351 (1988)

# Chapter 2

## Cellular automata modeling

### 2.1 Definitions and considerations

#### 2.1.1 Cellular automata

The main properties that define a cellular automaton have been already briefly described in the first chapter. Now, we present a formal definition of cellular automata, taken from [20]:

In general, a cellular automaton requires:

- a regular lattice of cells covering a portion of a d-dimensional space;
- a set  $\Phi(\vec{r}, t) = \{\Phi_1(\vec{r}, t), \Phi_2(\vec{r}, t), \dots, \Phi_m(\vec{r}, t)\}$  of Boolean variables attached to each site  $\vec{r}$  of the lattice and giving the local state of each cell at the time  $t = 0, 1, 2, \dots$ ;
- a rule  $R = \{R_1, R_2, \dots, R_m\}$  which specifies the time evolution of the states  $\Phi(\vec{r}, t)$  in the following way

$$\Phi_j(\vec{r}, t+1) = R_j(\Phi(\vec{r}, t), \Phi(\vec{r}+\vec{\delta}_1, t), \Phi(\vec{r}+\vec{\delta}_2, t), \dots, \Phi(\vec{r}+\vec{\delta}_q, t)) \quad (2.1)$$

where  $\vec{r} + \vec{\delta}_k$ ,  $k = 1, 2, \dots, q$  designates the cells belonging to a given neighborhood of cell  $\vec{r}$ .

The regular lattice can be made up of squares or hexagons, as shown in figure 2.1 for a two dimensional grid; or any other geometric form able to cover the selected d-dimensional space, such as cubes, or any other Wigner-Seitz kind of cells resulting from a regular lattice of points. In figure 2.1 it is also shown how different number of states can be used. The type of the grid is selected in order to get the best representation of the system; for instance, a squared grid would be used for magnetic simulations, and a hexagonal grid for simulating rounded cells on a surface. However, it is important preventing, as well as avoiding, to introduce undesirable side effects due to the specific grid selection.

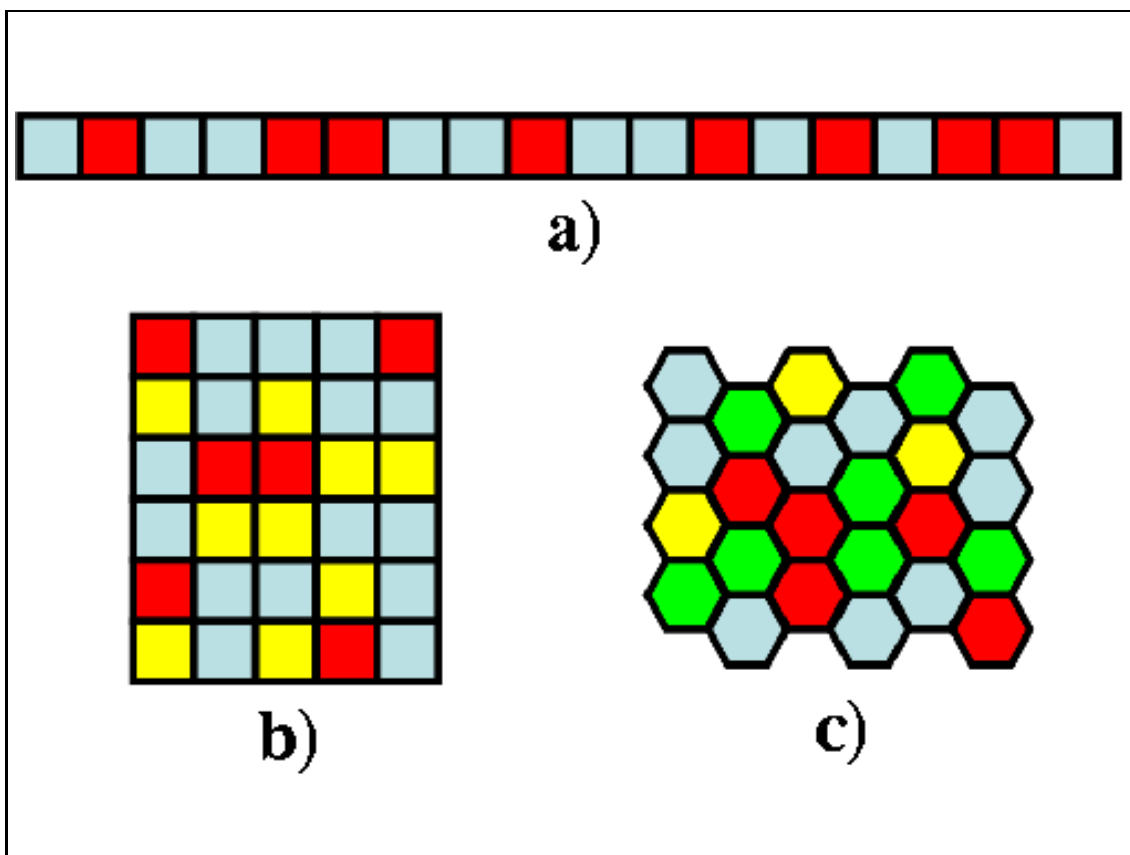


Figure 2.1: Cellular automata grids and cell's states. (a) 1-dimensional grid, 2 states, square cells. (b) 2-dimensional grid, 3 states, square cells. (c) 2-dimensional grid, hexagonal cells, 4 states.

The definition given above, implies that the rule  $R$  is applied in the same way and at the same time to all cells in the grid. In figure 2.2 it is shown Wolfram's rule number 90 and how it is applied. However, if any kind of inhomogeneities are

desired in the application of the rule, it is possible to obtain them by increasing the number of states and using them as markers. Also in the definition, the new state at time  $t + 1$  is only a function of the previous state at time  $t$ . It is possible and in some cases convenient to consider further past states. It is again possible without affecting the definition given above by modifying the set of possible states that a cell can have and coding in them the past states of the cell. The initial conditions at time  $t = 0$  should be determined by the specific purposes of particular simulations.

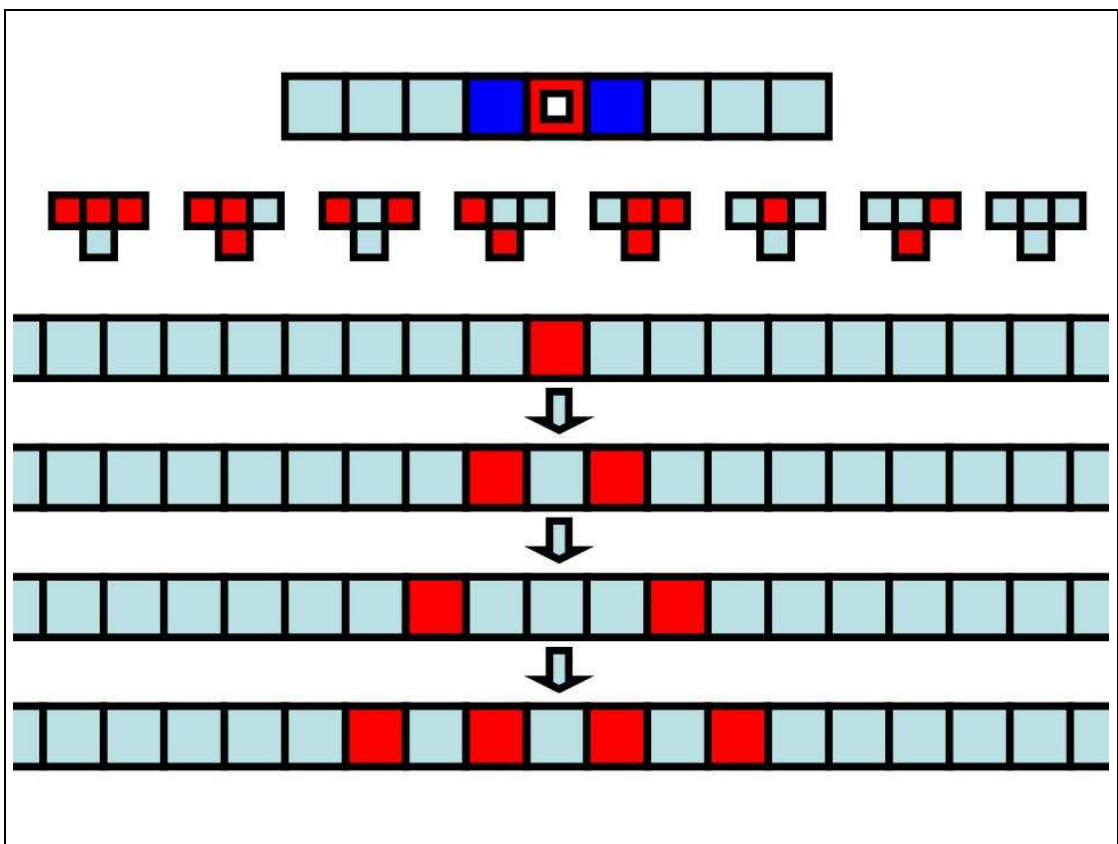


Figure 2.2: Cellular automata rule application. The rule is defined by the action that will be taken in each of the eight possible states of the neighborhood. Four time-steps and three applications of the rule are shown.

### 2.1.2 Neighborhood and boundary conditions

The neighborhood is the set of neighboring cells, considered by the rule, which state will affect the update of a cell. The neighborhood is the same for all cells. One of the most important considerations when designing a cellular automaton model is

to choose the neighborhood that will be regarded by the application of the rule. If the size of the neighborhood is too large, the complexity of the rule could become extreme. If the size is too small, it is possible that some properties will be not obtained from the model. The size is determined by the kind and nature of the system modeled but usually it is enough to consider only the first and/or second neighbors.

For 2-dimensional cellular automata and square grids, two neighborhoods are frequently considered: the von Neumann neighborhood, which consists of the central cell (the one which is to be updated) and its four closest neighbors; and the Moore neighborhood, that contains, in addition, the second nearest neighbors (the diagonal neighbors). Both are depicted in figure 2.3. The selection of neighborhood can be made also in order to reduce computational effort (as the Margolous neighborhood, see [20]) or to increase symmetry.

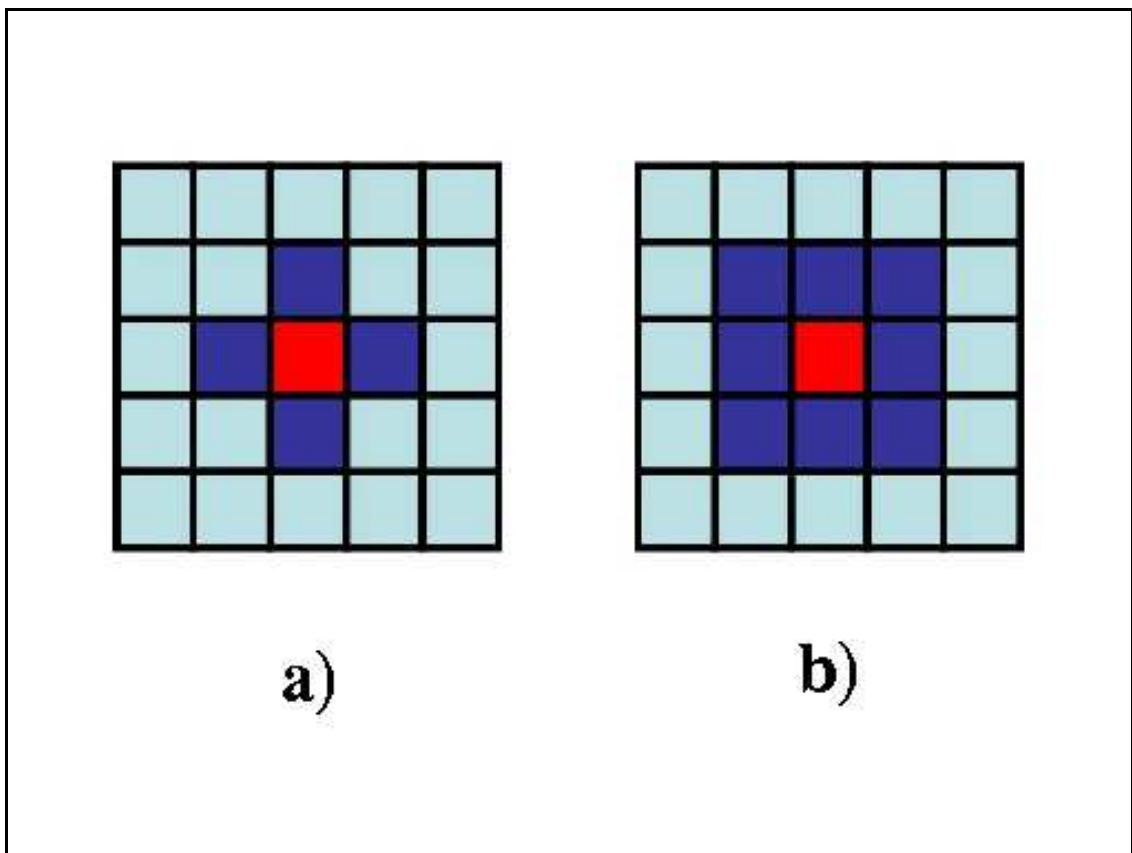


Figure 2.3: (a) Von Neumann neighborhood. (b) Moore neighborhood.

The cellular automata are defined as infinite lattices. Nevertheless, in computer models it is only possible to simulate finite portions of them. Therefore, it is important to select the most proper boundary conditions for the specific system that is being simulated in order to minimize and obtain appropriate finite size effects. One option is to define periodic boundaries, that is to connect the extremes of the grid; for instance, in a square grid it would be to connect the borders, right with left and top with bottom. Another option is to have fixed boundaries, that means that boundary cells have a fixed value, a value that does not change. It can represent walls in a container. The same method can be used if it is desired to simulate walls or restrictions inside the container. One last option is to use reflective boundaries, that means that the values in the boundary cells are copied by their “neighboring cells” outside the simulated range (virtual cells), and apply the rule to the boundary cells considering these values.

It is also possible to assign active properties to boundary cells in order to favor joining, breaking, and reacting between simulated ingredients [18]. Or to code the information directly in the state of the site in order to obtain a different behavior or applying a different rule. As expected, the nature of the simulation will determine the type of boundary conditions that should be used in each case.

### 2.1.3 The rule: options for cellular automata modeling

Cellular automata that follow the definition given at the beginning of the chapter are called deterministic, because their behavior is completely determined by the rule, the boundary conditions and the initial conditions. Their evolution is as deterministic as the most of models in nature, such as those described by coupled sets of ordinary partial differential equations. However, there are systems where a probabilistic approach can be more appropriated: chemical reactants and their rates of conversion, bacterial growth, brownian motion, etc.

In order to insert an amount of randomness in cellular automata models, the

outcome of the rule is selected stochastically between several options. For each configuration of the neighborhood there are several outcomes, and to each of them it is assigned a probability of being selected. This kind of cellular automata are called probabilistic (cellular automata). They are a useful generalization because they allow to adjust some parameters in a continuous fashion despite the discrete nature of cellular automata. Besides, using such stochastic scheme gives as a result that each run is an independent “experiment” and statistical analysis can be performed. Probabilistic cellular automata can be the most important extension of cellular automata. However, it is possible to think of other kinds of cellular automata, as the asynchronous update of the cells, which can be achieved by the stochastic selection of the cell that would be updated.

It is a mistake to think that any numerical scheme with discrete space and time is a cellular automaton. Coupled maps are not cellular automata, for instance. Most important, part of the richness of cellular automata comes from the microscopic and direct description of the cell interactions that can be achieved with the rule. This is not possible by the simple discretization of partial differential equations. Nevertheless, it is important to underline that cellular automata approach is not a rigid framework, and it is more important to obtain an effective numerical model that conserve limitations. “It is rather a philosophy of modeling which should be considered with some pragmatism” [20].

## 2.2 A simple model: Directed percolation

Directed percolation is a well studied problem and can be described as follows: imagine a square lattice as shown in figure 2.4, any node can be present with a probability  $p$  or absent with probability  $(1 - p)$ . Similarly, any bond may be present with probability  $q$  or absent with probability  $(1 - q)$ . It is assumed that only one site is “wet” at time  $t = 0$ . The conduction of water is made from one wet node to another existing node below it if they are connected by an existing bond. Then, each level can

be related with one timestep. Given the values of  $p$  and  $q$  (between 0 and 1), it is interesting to ask for the probability of finding wet sites at (time) level  $t$  and for the typical size of the wet cluster. It is found that there are critical values  $(p_c, q_c)$ , called the percolation thresholds, where a “geometrical phase transition” occurs and the wet cluster spans the whole system.

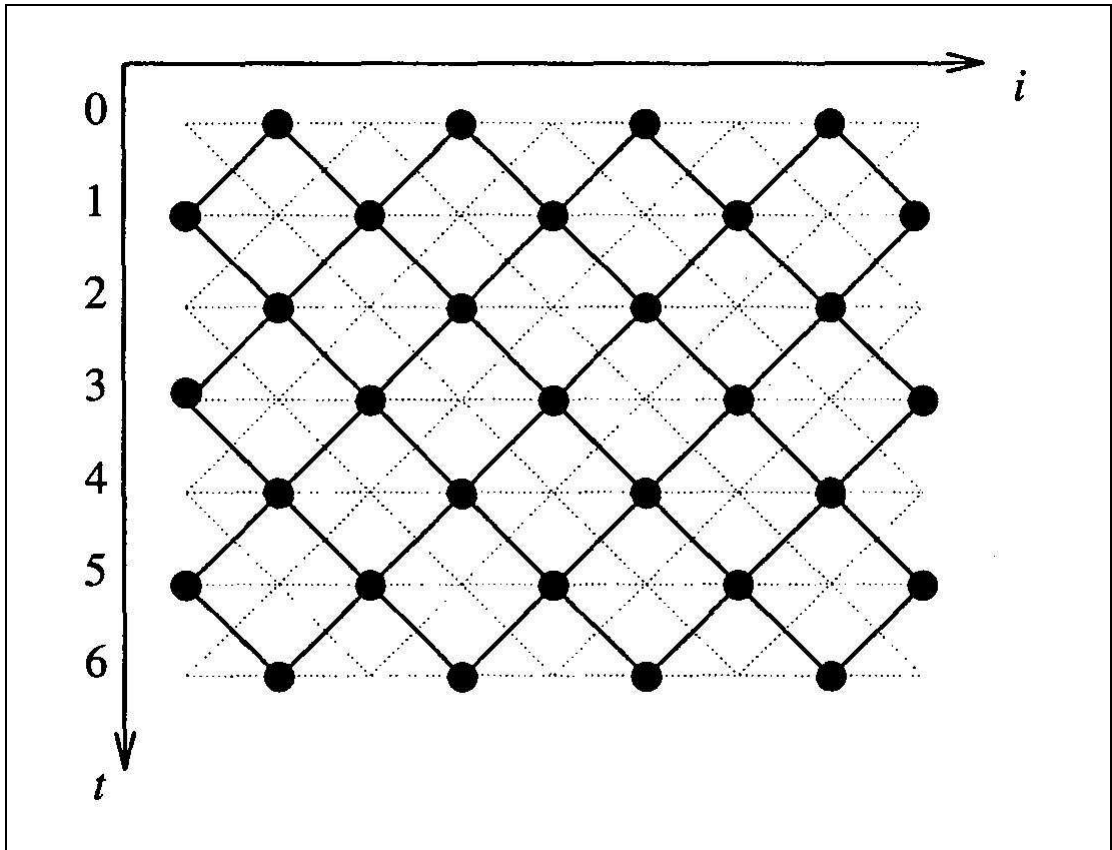


Figure 2.4: Directed percolation problem in two dimensions and square lattice. The dots represent the nodes and the lines represent the bonds. The vertical axis corresponds to lattice level (or time). Figure from [20]

This problem can be studied by means of a probabilistic cellular automaton. Consider a 1-dimensional cellular automata with periodic boundary conditions. Each site is associated with a variable  $\psi_i(t) = 0$  or  $1$ . At odd (even) times, odd (even) indexed sites change their state according to a probabilistic rule, and even (odd) indexed sites stay in the same state. The evolution of the automata can be represented by a diagram as figure 2.4. The rule is defined by conditional probabilities of the kind  $P(\psi_i(t+1)|\psi_{i-1}(t)\psi_{i+1}(t))$ , that is, the new state of a cell depends on

the state of its two neighbors, but it is independent of the self state. Such equations are:

$$P(1|00) = 0, \quad y \equiv P(1|11) = pq, \quad z \equiv P(1|01) = P(1|10) = pq(2-q), \quad (2.2)$$

where it is considered that for the new time step it is the same if a neighboring node “does not exist” in the last step or if it does not has water. The parameter space is presented in figure 2.5. This simple cellular automaton leads to a behavior with complex structure and reproduces the behavior expected for directed percolation and the geometrical phase transition.

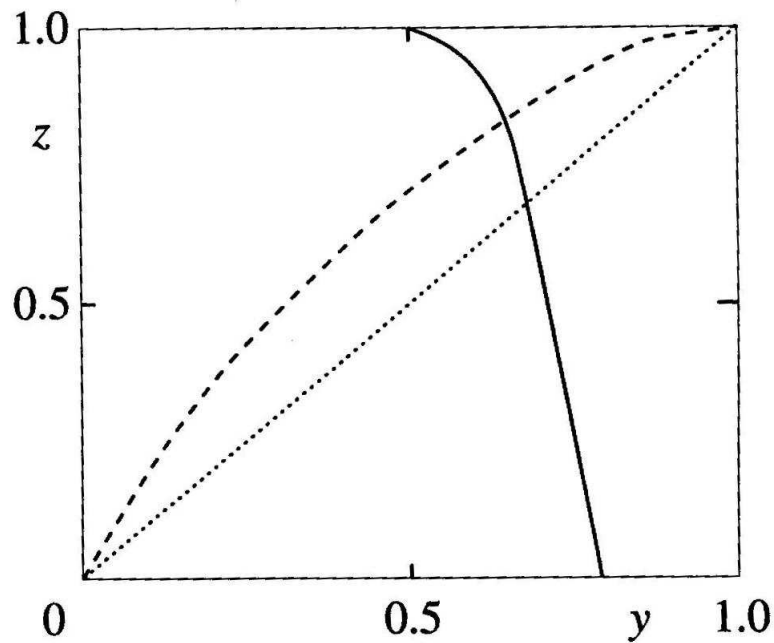


Figure 2.5: Parameter space  $y = pq$ ;  $z = pq(2 - q)$  defining the cellular automata rule for generalized directed percolation. The dashed and dotted lines correspond to the bond and site percolation, respectively. The system percolates to the right of the (solid) transition line. Figure from [20]

## 2.3 Lattice gas CA Models

### 2.3.1 The HPP rule

In the 1970's Hardy, Pomeau and de Pazzis developed the HPP lattice gas model [4]. It was recognized that this model was in fact a cellular automata, and was termed Lattice Gas Automata (LGA). The purpose of this model is to simulate a gas of particles moving and colliding in a 2-dimensional square lattice, in such a way that momentum and particle number are conserved locally, giving real microscopic features to the model. The HPP rule is the first of an important class of cellular automata models, that are used for the study of hydrodynamic systems.

Since the HPP model relies on a 2-dimensional square lattice, particles can move along the main four symmetry directions of the grid, as shown in figure 2.6. However, at most one particle can be in a given direction with a given velocity in a cell, resulting in an exclusion principle. The position (or the absence) of a particle in a cell is represented by the state of that cell. It is done using four bits; for instance, if at iteration  $t$  site  $\vec{r}$  has the following state  $s(\vec{r}, t) = (\mathbf{1011})$ , it means that three particles are entering the site along direction 1, 3 and 4, respectively.

The evolution of this model usually is split in two stages: collision and propagation. The rule of collision specify the way the particles entering in the same node interact. The collision between particles must conserve particle number and momentum. This can be achieved by setting the following rule (using the bit representation):

$$(\mathbf{1010}) \rightarrow (\mathbf{0101}) \quad (\mathbf{0101}) \rightarrow (\mathbf{1010}) \quad (2.3)$$

all other possible configurations being unchanged (see figure 2.7). This rule promotes the equal distribution of energy in all the degrees of freedom, at the same time the total momentum is conserved. The other phase is called propagation, and consists in the simple motion of all particles towards the next node according to their individual direction of motion. The exclusion principle will be conserved by

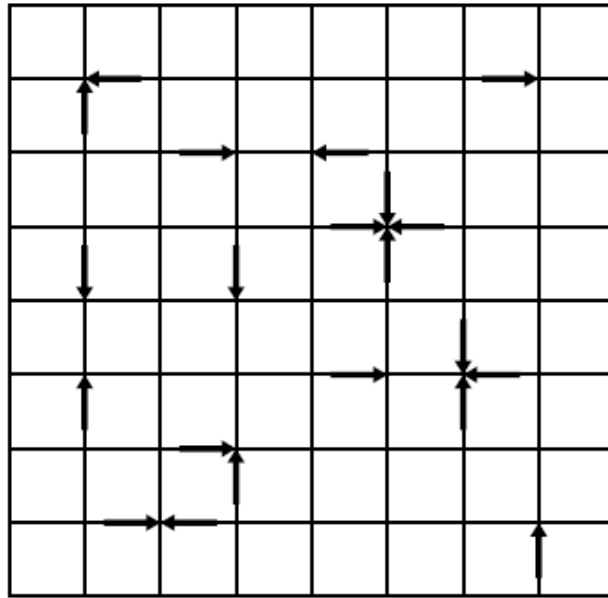


Figure 2.6: Illustration of the HPP model. Arrows represent the presence and direction of movement of the particles. Nodes in the grid are the points of interaction. Figure from [3].

these steps once it was provided at  $t = 0$ .

Another property of real microscopic nature that is obtained by the HPP model is invariance under time reversal. Each configuration comes from exactly one configuration and therefore each configuration goes to exactly one specific configuration. Then, the past history of one configuration of the automaton can be completely determined. Besides, no numerical errors are introduced due to the discrete nature of the model.

### 2.3.2 The FHP model

In 1986, U. Frisch, B. Hasslacher and Y. Pomeau developed a similar model, now called FHP [16]. The main difference is that, for isotropy reasons, a hexagonal grid is used. This leads to six directions and at most six particles per node. Due to the improve of the symmetry, this model reproduces, in some appropriate limits, the behavior prescribed by the Navier-Stokes equation of hydrodynamics.

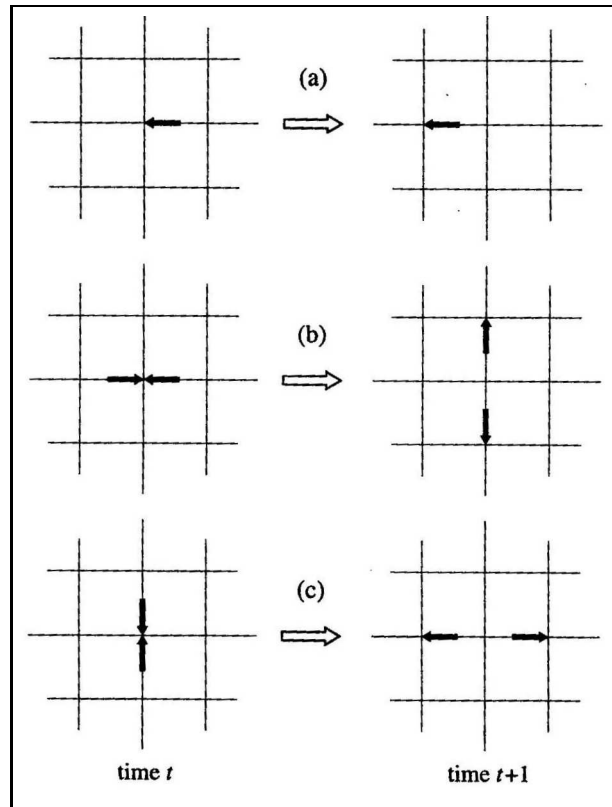


Figure 2.7: Collision in the HPP Model. Momentum and particle number are conserved by collision in the nodes. Figure from [20].

It is known that the Navier-Stokes equations of hydrodynamics are a result of the local conservation of mass and momentum in a fluid. In addition, there is also implicitly considered some (spherical) symmetries. Therefore, the FHP model includes all the ingredients needed in order to reproduce the behavior predicted by the Navier-Stokes equation. An interesting point is that the HPP model can not reproduce this behavior and the seemingly slight difference between four and six directions is enough to achieve it.

In order to conserve the particle number and momentum in collisions in the FHP model one has to determine the result for the collision of some configurations of two or three particles. When exactly two particles enter the same site with opposite velocities, both of them are deflected by 60 degrees as seen in figure 2.8. As two outputs are possible, a random number can be generated in order to choose the

deflection. It is also possible to assign an extra bit to the site, in such a way that a clockwise change is made when the bit has the value 0, and a counter clockwise change is made in the other case. This bit can change each time step in order to have the same rate for each possibility. In addition, this last choice has the advantage of being time-reversible, which is a fundamental symmetry of microscopic physics. When exactly three particles collide with an angle of 120 degrees between each other, then the particles are bounced back as seen in figure 2.8. In all other cases, the particles are considered as transparent to each other (no collision) in order to conserve momentum. The propagation step is as in the HPP model, each particle moves in the direction of its movement towards the next node.

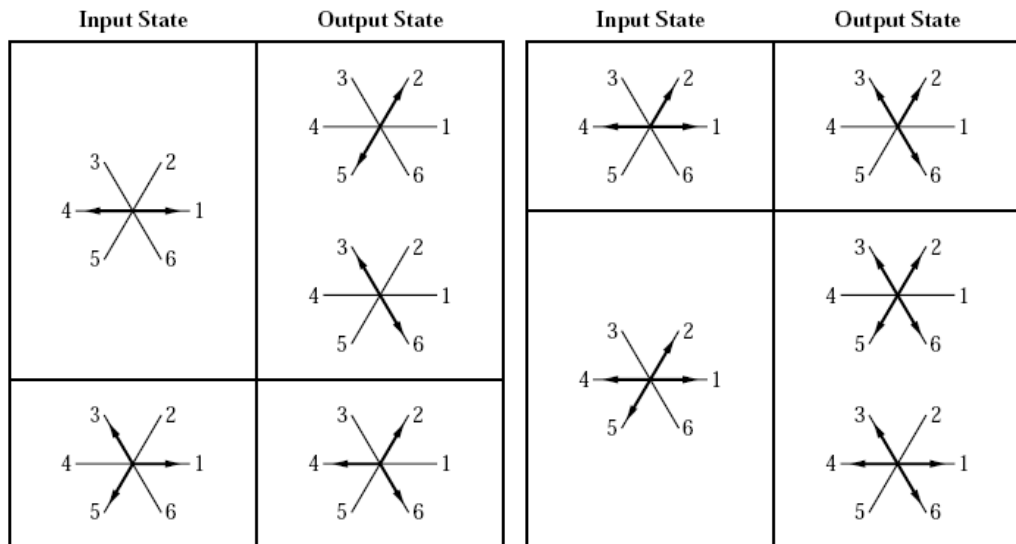


Figure 2.8: Types of collisions in the FHP model. Figure from [18]

Although LGAs show difficulties in simulating high Reynolds number flows, they have been successfully applied in complex situations where traditional computer techniques are not already applicable, such as [20]: Flows in porous media, immiscible flows and instabilities, spreading of a liquid droplet and wetting phenomena, microemulsion erosion and transport problems. They also have been successfully used in the simulations of pattern formation and biological systems as shown by Deutsch and Dormann [19]. In addition, LGA methods can be a proper tool for studying physical systems which are not described by appropriate macroscopic equations, e.

g.: granular media, some types of rheological media, complex flows and microscopic flows, and so on [18].

## 2.4 Why CA and LGCA Simulations?

### 2.4.1 Modeling Nature

“It is the role, and the privilege, of a scientist to study Nature and to seek to unlock her secrets.” [18]

When scientists try to understand, explain or simply see how nature works, they divide what they are studying in systems, identifiable sections of the world with form and/or function recognizable through time. These systems can be also made up by parts, with their own form and function, but interacting between them in such a way that they look integrated in a whole.

In order to describe and understand what is happening in the system, scientists create hypotheses, theories and models. Hypotheses are guessings about what is happening in the system; theories are formal theoretical explanations of what is happening in the system and are constructed, improved or wiped out from the testing of hypotheses and analysis of models derived from them. Finally, models are general constructions in which the parts and interactions of the system are described and identified.

A model is a simplification of the system itself. It must contain the most important features of the system in order to reproduce the behavior that is being studied, but trying to avoid the features that are not important. The models must capture the essence of the system behavior without becoming too complicated. If the model does not reproduce the behavior of the real system, it means that some hypotheses are wrong, that some important feature was not included, or that the theory that supports the model must be corrected (assuming that the model was conceived

without errors).

The scientific importance of models resides in giving us a tool for testing our knowledge and ideas. Besides, if the model has been successful in reproducing results consistently with reality, they can be used for studying related systems, and even to found and/or predict new phenomena in nature. This makes a virtuous cycle between hypotheses, theories and models.

Most models of physical systems take the form of mathematical relationships, coupled equations that describe rates of change, interactions between components, forces, fields, etc. Such mathematical approach has been extremely successful in representing nature in all fields of knowledge, becoming the most popular and powerful method for formalizing science. However, sometimes the exact solutions of the equations that describe a system are too difficult to obtain in an exact analytic way. In such cases, the value of the set of equations is diminished because they are not anymore useful. Nevertheless, approximations of such equations are possible, and the study of the evolution of a system can be made by means of computational algorithms and models.

Over the past two decades there has been a really huge growth in the creation and use of computer models for natural phenomena. Molecular dynamics, Monte-Carlo methods and magnetic Ising type systems are only several examples of the techniques and systems that are typically studied by means of computer simulations. Such approach allows the study of systems under conditions that would be extremely difficult in real experiments: controlled parameters, special forms or structures, homogeneity of components, and so on. Computer simulations also permits to easily study the effect of changing only one parameter, adding or deleting only one feature of the model or to observe how the model could behave at scales that are not possible for real experiments as can be femtoseconds, nanometers, or individual behavior of atoms.

### 2.4.2 Cellular automata as a modeling tool

Cellular automata are an idealization of a physical, chemical or biological system, where the interactions between constituents are coded or embedded in the rule that determines the evolution of the system. As mentioned and shown in chapter one: “cellular automata allow to simulate, in a straight and physically meaningful way, discrete entities that interact locally in a parallel fashion”, making them a proper method for simulating molecular systems. However, they have properties that make them an efficient tool for simulating many other kinds of systems.

All models are simplifications, and cellular automata are simple tools that have all the elements for representing almost any kind of systems with spatial structure. There are only cells in a grid, states of the cells and a local rule for changing the states. Cells can represent any scale of space depending on the rule. States can represent any kind of things: ants, cars, flowers, people, atoms, molecules, grains, etc. The rule can represent a myriad of different interactions between the components. Then, cellular automata have the properties of simplicity of concept and flexibility, although specific implementations can be as complex as in any other modeling paradigm.

The parallel scheme of cellular automata leads in a natural way to the development of parallel software, resulting in comparatively fast run-time implementations. Even if high performance computing is not used, the implementations can be faster than other approaches due to the use of states represented by integer numbers. This opens the option of performing larger computational experiments, a large number of them, using a large number of interacting components, scan how change in parameters affect behavior or performing studies using rather modest computational resources. Then, statistical analysis are allowed and favored as well as the search and study of particular cases.

In addition, cellular automata are spatially extended systems. Such kind of tools are very important for studying and understanding systems where non-trivial

collective behavior arises. The latter effect can be understood as an unexpected behavior of some macroscopic quantities. A typical example is the periodic or quasi-periodic behavior of the total density (total sum of state over the whole grid), in complete disagreement with equilibrium statistical mechanics or mean-field calculations. Besides, as mentioned previously, the spatial nature of cellular automata is an important feature for simulating systems where discrete interactions, probabilistic fluctuations and spatial inhomogeneities are fundamental, even when collective behavior is “trivial”.

On the other hand, sometimes the collective behavior depends in a non significant way on particular configurations of local behavior or specific kind of interactions. Navier-Stokes equations are the result of conservation of momentum and mass, without considering the specific potential or interaction between particles. The particular form of interactions affect the coefficients, but not the algebraic structure. This leads us to consider several levels or scales of reality in physical systems. In those cases, cellular automata also provide a useful framework, by means of the representation of the microscopic interactions, that results in the correct physics where macroscopic phenomena are being observed. This capability of cellular automata and its use are very close in spirit to Ising models, where the fundamental features are retained in the model in the simplified form of the effective spin interaction, which is of quantum nature but is represented by a simple numerical interaction. However, this is enough to produce magnetic domains and phase transitions, that are macroscopic features.

In fact, the cellular automata approach is especially appropriate when the specific nature of interactions at the microscopic level are not relevant at the macroscopic scale of observation and the simplification of real interactions is a great advantage. This is a common case, due to the fact that the complexity usually comes from collective behavior rather than the specific form of microscopic interactions. However, the physical interpretation of the simplified interactions must be still clear and intuitive without being oversimplified, as Einstein said:

“Everything should be made as simple as possible but not simpler”

There are more properties that make cellular automata appropriate for modeling, as the capacity to implement different geometries, simulate walls, or the exact evolution due to their Boolean nature (so no truncation occurs!). Nevertheless, the important point is that the simulated system must be faithfully represented, without forgetting that models are for being used and not for being blindly believed. With this warning, cellular automata models provide a very powerful tool in fundamental research, real problems, and pedagogical applications.

---

*REFERENCES*

1. B. Chopard and M. Droz, Cellular Automata Modeling of Physical Systems, Cambridge University Press, New York (1998)
2. L. B. Kier, P. G. Seybold and C. Cheng, Modeling Chemical Systems using Cellular Automata, Springer, The Netherlands (2005)
3. B. Chopard, A. Dupuis, A. Masselot and P. Luthi, Cellular Automata and Lattice Boltzmann Techniques: an Approach to model and Simulate Complex Systems, Computer Science Department, University of Geneva, Geneva, Switzerland.
4. J. Hardy, Y. Pomeau and O. de Pazzis, Phys. Rev. A, **13**, 1949 (1976)
5. U. Frisch, B. Hasslacher and Y. Pomeau, Phys. Rev. Lett. **56**, 1505 (1986)
6. L.-S. Luo, “The Lattice-Gas and Lattice Boltzmann Methods: Past, Present and Future”, in Proceedings of the International Conference on Applied Computational Fluid Dynamics, Beijing, 2000, edited by J.-H. Wu and Z.-J. Zhu (Beijing, China, 2000), p. 52. Available at <http://www.lions.odu.edu/~lluo/>
7. A. Deutsch and S. Dormann, Cellular Automata Modeling of Biological Pattern Formation, Birkhäuser (2005)

# Chapter 3

## Continuous Stirred Tank Reactor CA model

### 3.1 Models in Chemistry

Molecular Dynamics and Monte Carlo methods are among the most wide spread computational approaches that have been developed for chemical investigations. In most cases these techniques rely on the classical view of atoms and molecules interacting via “force fields”, that are represented by a set of mathematical equations that describe the attractions or repulsions between atomic species or groups of atoms, due to their charges, relative distances, and specific geometrical configurations [1]. More features can be added and the molecular and atomic interactions can be made more complex in order to achieve better accuracy representing the studied system. However, these improvements usually imply greater computational effort, so that a compromise between sophistication and practicality is required.

The molecular dynamics approach is normally based on the numerical solution of classical equations of motion (Newton, Lagrange or Hamilton), although quantum effects can be taken into account. In the beginning of simulation it is set an initial configuration of atoms in the space and then it evolves according to the force fields equations, solved in discrete time steps, usually in the scale of femtoseconds ( $10^{-15}$ s) in order to work on the scale of studied phenomena and keep numerical and

energetic stability. The evolution is followed over a very large number of time steps. However, the calculations demand a large computational effort, so that the time spent performing the simulation is orders of magnitude larger than the simulated time, that is usually on the scale of few tens of nanoseconds due this computational restriction. Therefore, Molecular Dynamics is an appropriate method for studying many phenomena of chemical and biochemical interest, but it is not convenient for larger time scales.

The Monte Carlo methods for molecular simulations consider a large number of possible configurations of the system, that result from moving the chemical constituents by random (but limited) amounts in each step. The configurations are evaluated according to their energies: those lowering the system's energy are accepted, and those raising the energy are "weighted" and proportionately accepted, according to their potential energies. The weighting is normally proportional to  $e^{-\delta V/kT}$ , where  $\delta V$  is the potential energy change,  $k$  is the Boltzmann constant, and  $T$  is the absolute temperature. In order to calculate thermodynamical and structural features of the system it is made a statistical analysis from a large and weighted sample ("ensemble") of such configurations.

Both, Molecular Dynamics and Monte Carlo approaches, have demonstrated to be very worthy for the study of chemical systems, giving insight on the behavior and properties. However, their elaborate models for representing and calculating interactions, made them excessively demanding on computational effort for many interesting research level calculations, making necessary the use of supercomputers or powerful clusters.

An option is the use of different schemes with simplified representations of atomic and molecular interactions. The option we are interested in is cellular automata methods. Each cell state can be interpreted as a completely different chemical species, or perhaps as chemical reactants that only differ in minimal features as orientation or distance to a catalytic surface. The states and the evolution rule are

intended as to represent in the most basic way the most important features of the chemical system that is under study. This simplified kind of schemes can be able of reproduce the behaviors and phenomena of interest.

The relative simplicity of CA methods allow to play with the basic features of constituents in such a way that it could be easier to identify which of them are fundamental for the studied phenomena. Besides, CA usually need less computational effort than Molecular Dynamics methods, although rules can be made as complex as required and so they could be as complex as Molecular Dynamics equations. If large number of constituents are needed, the CA schemes can be adapted in order to fit to high performance computation.

Nowadays, there is a significant amount of scientific work on CA as a means to simulate chemical systems. These schemes are not unified but they apply and create different approaches in order to better represent the studied system. There are simulations of simple first order chemical reactions [2], generation of Liesegang patterns considering moving reactants and nucleated products [3], approaches to chemical signaling and morphogenesis [19], and studies on reaction-diffusion systems [2], just to mention a few but significant examples. Therefore, the CA methods are well fitted for the research and representation of many interesting and important chemical systems.

## 3.2 The CA model for CSTR

In this chapter, the classical dynamical systems model of continuous stirred tank reactors (CSTR) in which a first order chemical reaction takes place is reformulated in terms of the stochastic cellular automata procedure developed in the works of Seyborg [2] and Neuforth [6], which is extended by including the feed flow of chemical reactants. We show that this cellular automata model is able to simulate the dilution rate and the mixing process in the CSTR, as well as the details of the heat removal

due to the jacket. It is discussed its reliability as a model, its advantages over ordinary differential equation for performing studies when spatial inhomogeneities are present and its use as a discrete method for modeling nanoreactors. The cellular automata approach is expected to be of considerable applicability at any industrial scales and especially for any type of microchemical systems.

The work in this section has been published in the Korean Journal of Chemical Engineering, under the title “Cellular Automata Modeling of Continuous Stirred Tank Reactors”. This work was developed in collaboration with Ph.D. Vrani Ibarra-Junquera and Ph.D Haret Rosu [7].

### 3.2.1 Introduction

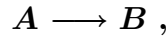
A chemical reactor could be any vessel containing chemical reactions. In general, a reactor is designed such as to maximize the yield of some particular products while requiring the least amount of money to purchase and operate. Normal operating expenses include energy input, energy removal, raw material costs, labor, etc. Energy changes can occur in the form of heating or cooling, or agitation. The latter is quite important because an appropriate mixing has a large influence on the yield. Therefore, the design and operation of mixing devices often determines the profitability of the whole plant.

In particular, in the widely developed continuous stirred tank reactors (CSTR) one or more fluid reagents are introduced into a tank equipped with an impeller while the reactor effluent is removed [8]. The impeller stirs the reagents to ensure proper mixing. Classical CSTR dynamical models, based on coupled deterministic ordinary differential equations (ODEs), are the usual approach to chemical systems at the macroscopic scale. It has been demonstrated to have considerable usefulness but it should be mentioned that they are based on the common assumption that spatial inhomogeneities may be neglected. Thus ODEs are a mean field approach and the analytical solutions of the ordinary differential equations (ODEs) provide

an accurate model only in this case. When the system is not homogeneous, application of the above assumption often yields a model that does not accurately represent the system. This is the case, for example, of CSTRs with a highly viscous medium where spatial heterogeneities exist in species concentrations, temperature, etc. Of course, the application of partial differential equations (PDEs) to model spatial inhomogeneities such as diffusion and hydrodynamic turbulence may produce accurate models. However, their solution requires advanced numerical techniques such as finite element methods. Moreover, the numerical techniques for solving the PDEs could be computationally expensive and do not account for localized stochastic phenomena. In particular, chemical systems are discrete from the microstructure till the molecular level and statistical fluctuations in concentration and temperature occur at these local scales. Cellular automata are an attractive alternative to PDEs to model complex systems with inhomogeneities of this type. A cellular automata lattice is comprised of discrete cells whose states are functions of the previous state of the cell and its neighbors. Rules are used to update each cell by scanning the value of the cells in the neighborhood. Seyborg [2] and Neuforth [6] have shown that stochastic cellular automata models can be successfully applied to simulate first order chemical reactions. In their papers, they worked on a squared lattice of cells, each of them having a chemical reactant. The reactions are performed by considering a probability of change, from reactant A to product B, proportional to the kinetics constant that defines the chemical equation. However, this type of calculation does not apply directly to the CSTR case, where a chemical feed flow is present. In this chapter, it is extended the stochastic cellular automata (CA) model to CSTRs by simulating the feed flow flux by means of a random selection of a subset of cells to which the flux conditions with respect to chemical concentration and temperature are imposed. We would like to remark that mixing in a stirred tank is complicated and not well described despite the extensive usage of dimensionless numbers and models based on ODEs [9]. Therefore, more accurate models are essential for developing and testing control strategies or even to explore new reactor geometries.

### 3.2.2 The ODE-based model of jacketed CSTR

As already mentioned, we consider an ideal jacketed CSTR where the following exothermic and irreversible first-order reaction is taking place:



The CSTR modeling equations in dimensionless form are the following [10]

$$\frac{d \mathbf{X}_1}{d \tau} = -\phi \mathbf{X}_1 k(\mathbf{X}_2) + q (\mathbf{X}_{1f} - \mathbf{X}_1) \quad (3.1)$$

$$\frac{d \mathbf{X}_2}{d \tau} = \beta \phi \mathbf{X}_1 k(\mathbf{X}_2) - (q + \delta) \mathbf{X}_2 + \delta \mathbf{X}_3 + q \mathbf{X}_{2f} \quad (3.2)$$

$$\frac{d \mathbf{X}_3}{d \tau} = \frac{q_c}{\delta_1} (\mathbf{X}_{3f} - \mathbf{X}_3) + \frac{\delta}{\delta_1 \delta_2} (\mathbf{X}_2 - \mathbf{X}_3) , \quad (3.3)$$

where  $\mathbf{X}_1$ ,  $\mathbf{X}_2$ , and  $\mathbf{X}_3$  are the dimensionless concentration of reactant A, temperature, and cooling jacket temperature, respectively. We note that it is possible to use the dimensionless coolant flow rate,  $q_c$ , to manipulate  $\mathbf{X}_2$ .

The relationships between the dimensionless parameters and variables and the physical variables are the following:

$$\begin{aligned} k(\mathbf{X}_2) &= \exp\left(\frac{\mathbf{X}_2}{1 + \mathbf{X}_2 \gamma^{-1}}\right), \quad \gamma = \frac{E}{R T_{f_0}}, \quad \mathbf{X}_3 = \frac{T_c - T_{f_0}}{T_{f_0}} \gamma, \quad \mathbf{X}_2 = \frac{T - T_{f_0}}{T_{f_0}} \gamma \\ \beta &= \frac{(-\Delta H) C_f}{\rho C_p t_{f_0}}, \quad \delta = \frac{U A}{\rho C_p Q_0}, \quad \phi = \frac{V}{Q_0} k_0 e^{-r}, \quad \mathbf{X}_1 = \frac{C}{C_{f_0}}, \quad \mathbf{X}_{1f} = \frac{C_f}{C_{f_0}}, \\ \mathbf{X}_{2f} &= \frac{T_f - T_{f_0}}{T_{f_0}} \gamma, \quad \delta_1 = \frac{V_c}{C}, \quad \tau = \frac{Q_0}{V} t, \quad \mathbf{X}_{3f} = \frac{T_{c_f} - T_{f_0}}{T_{f_0}} \gamma, \quad \delta_2 = \frac{\rho_c C_{p_c}}{\rho C_p} \end{aligned}$$

where the meaning and the nominal values of these parameters are given in Table 1. In the rest of the chapter we shall use the solution of this ODE model as the theoretical case with which the CA simulations will be compared.

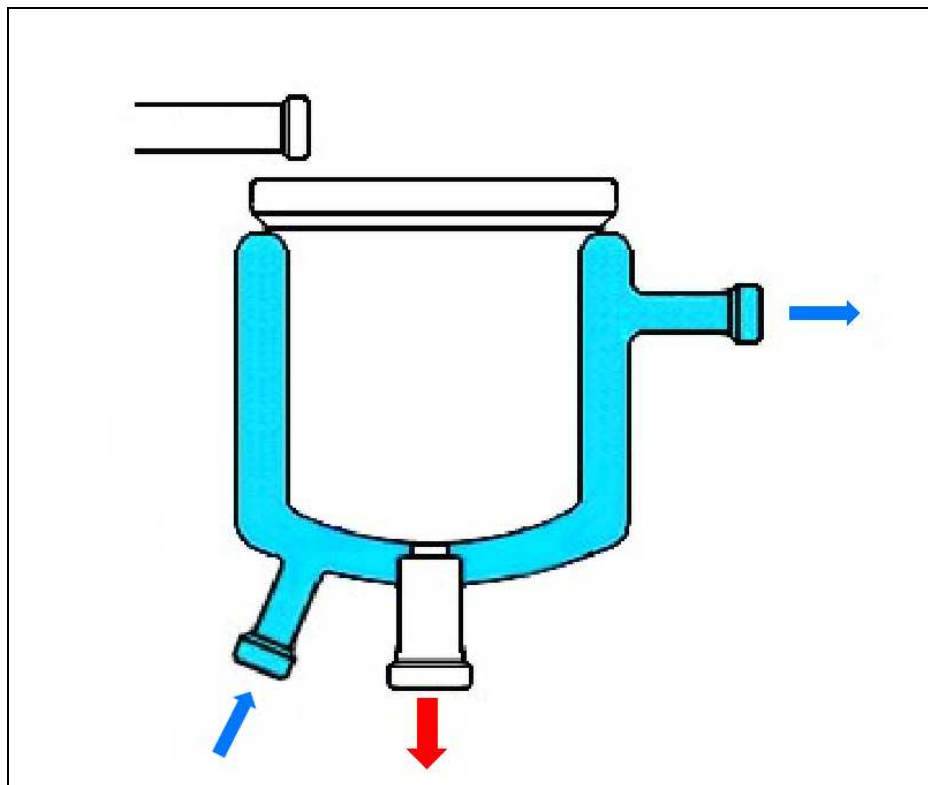


Figure 3.1: Schematic representation of the jacketed CSTR.

### 3.2.3 Stochastic CA model for Jacketed CSTR

The process simulated in this work is the exothermic reaction that converts a chemical A into a product B in a jacketed CSTR. Our model is composed of three squared lattices of cells, all of the same size. The first lattice that we call the chemical lattice is for chemicals A and B and provides the chemical distribution in the tank reactor. This distribution is given as follows: in each cell there is only one unit of reactant A or one unit of product B (not necessary representing a single molecule), under the condition that all cells are occupied. The second lattice is the tank temperature lattice. It contains the temperatures  $T_{ij}$  in real-numbered values. The chemical lattice and the temperature lattice are of the same dimension and their cells are in one-to-one correspondence. The third lattice represents the coolant system. This lattice is of the same dimension as the previous ones and therefore each temperature tank cell is in “contact” with a coolant jacket cell.

In our model the first process in each time step is the irreversible conversion of

Table 3.1: Parameters of the model

Symbol	Meaning	Value (arb. units)
$C$	Reactor composition	<b>0.001</b>
$C_f$	Feed composition	<b>1.0</b>
$q$	Dimensionless reactor feed flow rate	<b>1.0</b>
$q_c$	Dimensionless coolant flow rate	<b>1.65</b>
$q_{cs}$	Steady-state value of $Q$	<b>1.0</b>
$T$	Reactor temperature	<b>1.0</b>
$T_c$	Coolant temperature	<b>1.0</b>
$UA$	Heat transfer coefficient times the heat transfer area	<b>1.0</b>
$V$	Reactor volume	<b>1.0</b>
$V_c$	Cooling jacket volume	<b>1.0</b>
$X_{1f}$	Dimensionless feed concentration	<b>1.0</b>
$X_{2f}$	Dimensionless feed temperature	<b>0.0</b>
$X_{3f}$	Dimensionless coolant feed temperature	<b>1.0</b>
$\beta$	Dimensionless heat of reaction	<b>8.0</b>
$\delta_1$	Dimensionless volume ratio	<b>0.1</b>
$\delta_2$	Dimensionless density multiplied by the heat capacity of coolant	<b>1.0</b>
$\phi$	Hill's threshold parameter	<b>0.072</b>
$\gamma$	Dimensionless activation energy	<b>20.0</b>
$\rho_c C_{pc}$	Density multiplied by the heat capacity of coolant	<b>1.0</b>
$\tau$	Dimensionless time	—

chemical A into product B. The conversion rate is determined by  $\phi k(\mathbf{X2})$  as in [10], where  $\mathbf{X2}$  is the average temperature of the tank temperature lattice. This first order kinetics “constant” is multiplied by the time step in order to get the proportion of the reactant A that is expected to be converted into product B in each evolution step. If the time step is small enough this number could be also considered as the probability that a molecule of chemical A is converted in product B. Such proportion is compared with a randomly generated number, one different random number for each cell in the lattice containing reactant A. If the random number is less than the proportion, the reactant A is changed for product B in the cell. Since the reaction is exothermic, the temperature value in the temperature array is increased by  $\beta$  (according to Eq. (2)) in the corresponding cell.

The second simulated process is the tank temperature diffusion that can be con-

sidered as an energy diffusion. It can be performed by means of finite differences, but in order to obtain an almost ODE-independent model we have implemented a moving average method, where the value of the temperature in a cell at the next time step is the average temperature of its neighborhood. This procedure gives similar results to those of finite differences, as shown by Weimar for reaction-diffusion systems simulated by cellular automata [11] (see Appendix A). We used a square neighborhood formed by  $(2R + 1)^2$  cells, where  $R$  is the number of steps that we have to walk from the center of the cell in order to reach the most far horizontal (vertical) cell in the neighborhood.

The third simulated process is the tank feed flow. We have simulated the feed flow rate  $q$  in a stochastic way. In order to get an approximation to the proportion of the tank that must be replaced by the incoming flow,  $q$  is multiplied by the time step and by the total number of cells in the lattice. This gives us a real number  $x$ . Then, following Weimar [11], we used a probabilistic minimal noise rule, i.e., we define the probability  $p = x - [x]$  (where  $[x]$  is the maximal integer number  $x$ ) in order to decide if  $[x]$  or  $[x] + 1$  cells will be replaced by the flow. We choose  $[x]$  with probability  $1 - p$  and  $[x] + 1$  with probability  $p$ . This method conserves the proportion  $x$  in a statistical way. Subsequently, a cell is selected in a random way, by means of two random numbers which are used to select a row and a column, in such a way that all cells has the same probability of being selected. If the cell has been selected in the same time step, a new selection is made. This is repeated until we have reached the number of cells that must be replaced. Finally, the selected cells are changed in the temperature lattice by the feed flow temperature  $X_2 f$ , and in the reactive lattice it is put a unit of reactant A with probability  $X_1 f$ , that represent the concentration of chemical A in the feed flow. In the simulations presented in this work we used  $X_1 f = 1$ . This method of flow simulation could be improved in several ways, in order to simulate different tank geometries or for showing the flow direction. However, in this work we want only to show that the CA method could fit the CSTR behavior in a very good approximation, with the advantage of spatial analysis.

The fourth simulated process is the energy interchange between the tank and the jacket. This has been done by directly calculating the energy/temperature interchange between each tank temperature cell and its corresponding jacket temperature cell. This interchange is dictated by the difference between the two temperatures and it is weighted by  $\delta$ ,  $\delta_1$ , and  $\delta_2$  as in Eqs. (1) and (2).

The fifth and the sixth simulated processes are the coolant flow and the coolant temperature diffusion, respectively. Both of them are performed in a similar way as for the concentration and temperature tank.

### 3.2.4 Simulations

In this section we first present the comparison between the curves obtained by differential equations and those obtained from the implemented cellular automata model (see 3.2). It is clear that cellular automata simulations resemble with excellent agreement the values for the concentration of chemical A, the tank temperature and the jacket temperature at all times. Using a time step of 0.001 it is shown that the curves coincide at the initial time, transient time and for stable state. We have found that we can maintain this remarkable fitness by properly adjusting the time step to a sufficiently small value.

When a kinetic constant based on the average temperature is used, it is implicitly assumed that the mixing in the CSTR is perfect, vanishing any temperature inhomogeneities. One could ask what could be the change in the tank behavior if the mixing is almost perfect. It could be studied by using a model that consider the spatial distribution of temperature. We studied this effect by calculating the kinetic constant in a local manner by taking the temperature from each cell in the temperature lattice. The effect for a 1000 x 1000 cells array and a time step of 0.001 is shown in Fig. 3.3. It could be observed that the tank temperature curve for the perfect mixing and the one for the locally calculated kinetic constant are the same

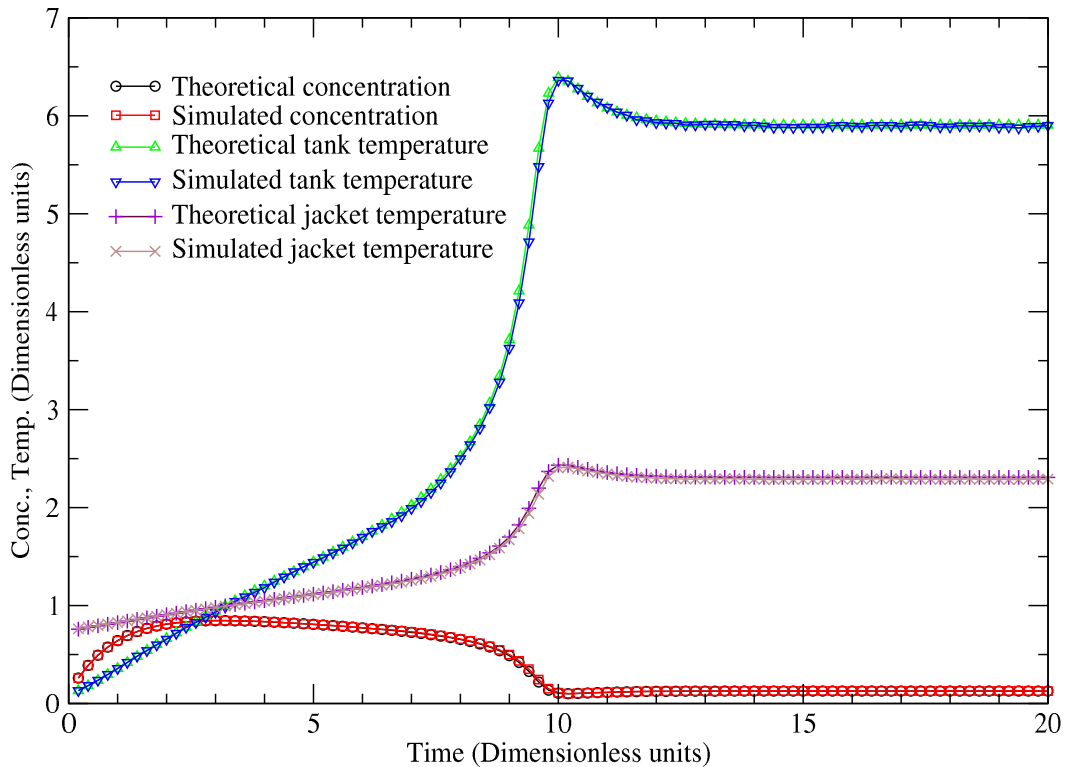


Figure 3.2: Comparison between the curves from the differential equations and the curves obtained from simulations with the CA approach. Initial values are:  $X_1=0.1$ ,  $X_2=0.1$ ,  $X_3=0.1$ . For the six curves: 37 points separated by a dimensionless time of 0.4 were taken from 20000-point simulations with a dimensionless time step of 0.001.

for almost all times. However, they separate during the transient period, leading to a reduction in the magnitude of the peak and a little delay in its appearance. The curve was calculated with a tank temperature diffusion process per time step with a  $\mathbf{R} = \mathbf{1}$  neighborhood. If more diffusion steps are used per time step the curves obtained tend to the theoretical one as is expected. Besides, it could be also interpreted as the effect of a perfect mixed tank, but with material where each component tends to maintain its energy.

The ODEs generally represent the characteristics of the global system, where it has enough number of elements such that the statistical fluctuations are of small amplitude. However, when the system size and the quantity of elements are dimin-

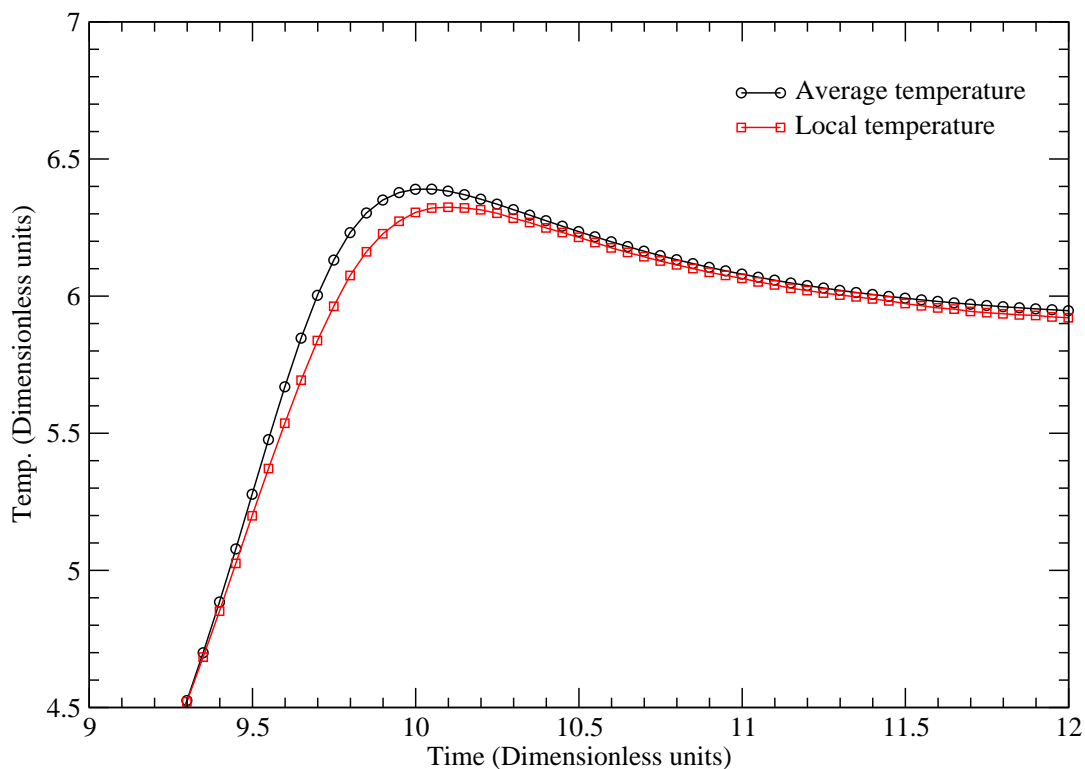


Figure 3.3: Comparison between the tank temperature evolution curves for a kinetic constant based on average temperature and for kinetics constant calculated on the base of the local temperature. Initial values are:  $\mathbf{X1}=0.1$ ,  $\mathbf{X2}=0.1$ ,  $\mathbf{X3}=0.1$ . The array is of 1000 x 1000 cells and the dimensionless time step is of 0.001; one temperature diffusion step per time step.

ished, the statistical fluctuations could be of increasing importance. In this way, another advantages of the cellular automata method proposed here is its flexibility with respect to the reactor size, and its stochastic nature, that allows to study how much the system could be affected by the initial conditions and by the stochastic features of the process. We have performed several simulations applying the parameters presented above in lattices of very small dimensions,  $N \times N$  with  $N$  less than 20, in which case we can think of the CA stochastic model as a good description of a catalytic surface dividing two regions, one carrying the chemical A and the other as a temperature reservoir. Our model is a simple approach, useful as a first approximation, in the analysis and study of microreactors or even nanoreactors. We recall that

the usage of microreactors for *in situ* and on-demand chemical production is gaining increasing importance as the field of microreaction engineering has already demonstrated potential to impact a wide spectrum of chemical, biological, and process system applications [12]. There are already many successfully developed microreactors for chemical applications such as partial oxidation reactions [13], phosgene synthesis [14], multiphase processing [15], and (bio)chemical detection [16]. Figure 3.4 displays the variability that could be found in CSTR systems at small scales. It is clear evidence that the statistical fluctuations are a primordial issue at this scale. In addition, one could notice that the dynamical behavior could be totally different to the expected behavior of a larger system e.g., 1000 x 1000 cells lattice.

Finally, the study of small systems by direct simulation using stochastic simulations could give us insight in how an open CSTR system could behave when the statistical fluctuations and the initial configuration are important. In Fig. 3.5 one can see that the possible behaviors of a system of size 20 x 20 have large deviations from the average and the theoretical values.

This kind of variability is not provided by pure ODEs (without a stochastic term). Moreover, the discreteness of the CA procedure adds an important contribution to these differences. Both the stochastic part and the discreteness part are intrinsic features of small scales. We think that this stochastic CA approach could be an important simulating tool for this small scale variability and for testing control strategies in reduced environments. This is due to the fact that CA approaches could be seen as an intermediate step between the ODEs models and the specific experimental situation.

### 3.2.5 Concluding Remarks

A cellular automata approach for the CSTR with cooling jacket has been presented. It is able to reproduce the CSTR dynamical behavior calculated by ODE's with a good approximation and in an easy way. The presented stochastic model allow us

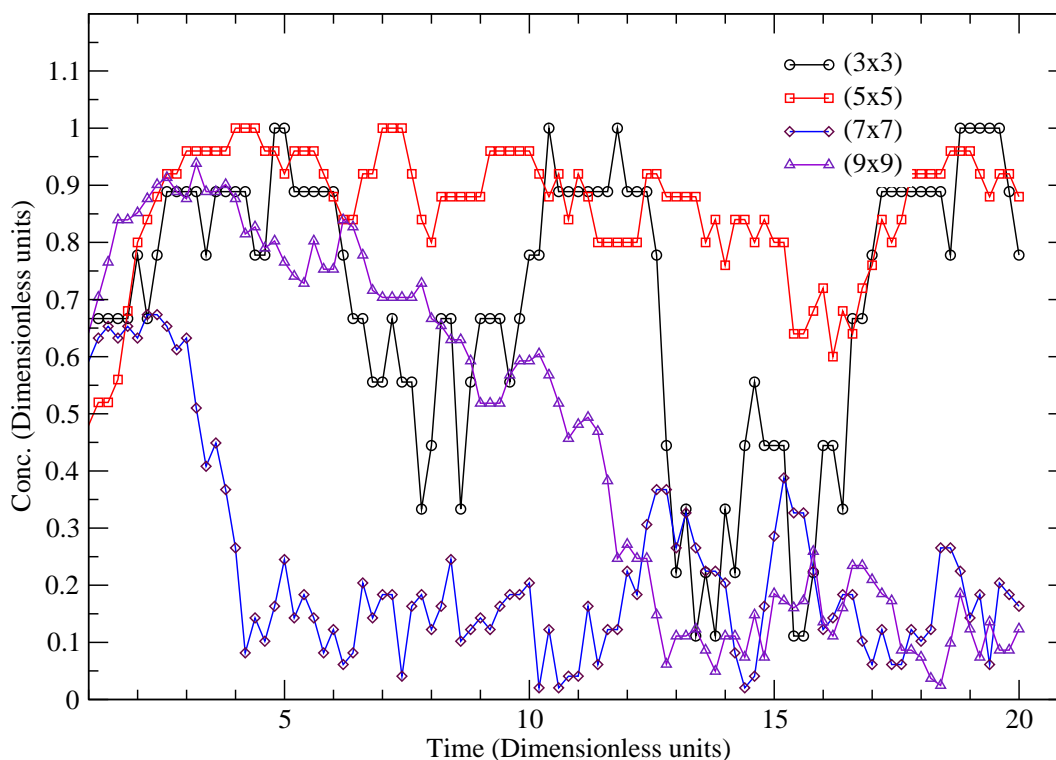


Figure 3.4: Behaviors that could be found in systems with small number of elements (cells for the CAs and clusters of molecules in the real case). These behaviors are different from the expected one for systems with a large number of elements. The initial values are  $\mathbf{X1}=0.1$ ,  $\mathbf{X2}=0.1$ ,  $\mathbf{X3}=0.1$ . The employed time step is 0.001. One hundred points separated by a time lag of 0.2 were taken from 20000-point simulations with a time step of 0.001; one temperature diffusion step per time step.

to study what could be the behavior of the variables of the tank when the reaction probability depends on the local temperature. It also give us an approach to study systems with few elements, such as micro and nanoreactors, for example catalytic membranes separating two phases. The main advantages of the CA approach presented here are its stochastic nature and the direct involvement of a spatial structure. This also represents a tool for studying the role of initial configuration and stochastic fluctuations in systems with few elements. Additionally, the CA approach is a clear improvement of the CSTR modeling and moreover can be applied to different reactor and jacket geometries, as well as for considering in more detail the real mass flow in the tank reactor-geometry.

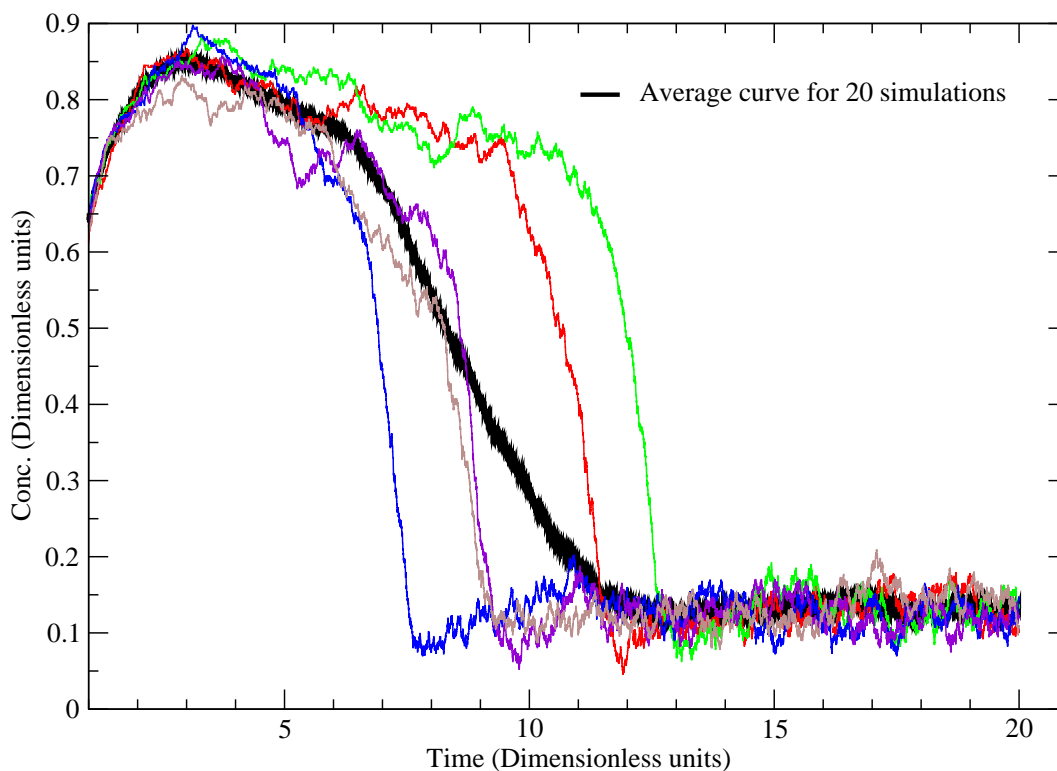


Figure 3.5: Different concentration behaviors of chemical A for systems of the same size (20 x 20) that are treated by the same method and could be the underlying dynamic characteristic of microreactors. Two individual simulations corresponding to two different initial distributions of the chemical A over the cells are displayed together with the average curve of 400 individual simulations as well as the theoretical curve corresponding to the ODE-based model. The initial configuration and the stochasticity and discreteness introduced in the model lead to a time-distributed behavior. The initial values are:  $X_1=0.1$ ,  $X_2=0.1$ ,  $X_3=0.1$ . The time step is 0.001; one temperature diffusion step per time step.

We have found that in our CA implementation at lattice dimensions beyond 400x400 and below time steps of 0.001 the ODE-based solutions (curves) are very well reproduced thus indicating that for those values the stochastic noise is very small. On the other hand, at small lattice dimensions the CA procedure gives strong fluctuations which are due to the CA discretization that sometimes could match the discretization of Nature at those scales.

Finally, we mention that CA-type models can be used to analyze local microorganism densities which are directly related to the production yields of important fermentation products, such as bacterial cellulose obtained in generalized stirring reactors [17].

---

**REFERENCES**

1. D. C. Rapaport, "The Art of Molecular Dynamics Simulation". Cambridge University Press, Cambridge (1995.)
2. Seybold P.G, Kier L.B., Cheng C.-K., "Simulation of first-order chemical kinetics using cellular automata", J. Chem. Inf. Comput. Sci., **37**, 386 (1997).
3. B. Chopard, P. Luthi and M. Droz, Phys. Rev. Lett. **72**, 1384 (1994.)
4. A. Deutch and S. Dormann, Cellular Automaton Modeling of Biological Pattern Formation, Birkhäuser, Boston (2005)
5. J. R. Weimar and J. P. Boon, Phys. Rev. E **49**, 1749 (1994)
6. Neuforth A., Seybold P.G., Kier L.B., Cheng C.-K., "Cellular automata models of kinetically and thermodynamically controlled reactions", Int. J. Chem. Kinetic **32**, 529 (2000).
7. J.E. Pérez-Terrazas, V. Ibarra-Junquera and H.C. Rosu, Korean J. Chem. Eng. **25**(3),461 (2008)
8. Epstein, I.R., Pojman, J.A., An Introduction to Nonlinear Chemical Dynamics, Oxford University Press, Oxford, (1998).
9. Chakraborty S., Balakotaiah V., "A novel approach for describing mixing effects in homogeneous reactors", Chemical Engineering Science **58**, 1053 (2003).
10. Silva, R.G., Kwong, W.H., "Nonlinear model predictive control of chemical processes", Brazilian J. Chem. Eng. **16**, 83 (1999).
11. Weimar, J.R., "Cellular automata for reaction-diffusion systems", Parallel Computing **23**, 1699 (1997).
12. Jensen, K.F., "Microreaction engineering -is small better?", Chemical Engineering Science **56**, 293 (2001).

13. Hsing, I.M., Srinivasan, R., Jensen, K.F., Schmidt, M.A., "Simulation of micro-machined chemical reactors for heterogeneous partial oxidation reactions", *Chemical Engineering Science* **55**, 3 (2000).
14. Ajmera, S.K., Losey, M.W., Jensen, K.F., "Microfabricated packed-bed reactor for phosgene synthesis", *AIChE J.* **47**, 1639 (2001).
15. de Mas, N., Gnther, A., Schmidt, M.A., Jensen, K.F., "Microfabricated multiphase reactors for the selective direct fluorination of aromatics", *Ind. Eng. Chem. Res.* **42**, 698 (2003).
16. Koh, W.-G., Pishko M., "Immobilization of multi-enzyme microreactors inside microfluidic devices", *Sensors and Actuators B: Chemical* **106**, 335 (2005).
17. Jung, J.Y., Khan T., Park, J.K., Chang H.N., "Production of bacterial cellulose by *Gluconacetobacter hansenii* using a novel bioreactor equipped with a spin filter", *Korean J. Chem. Eng.* **24**, 265 (2007).
18. L. B. Kier, P. G. Seybold and C. Cheng, *Modeling Chemical Systems using Cellular Automata*, Springer, The Netherlands (2005)

# Chapter 4

## A Biological System

In this chapter it is presented a mathematical analysis for diffusion of excitations at the brain scale (corticothalamic system) and on microtubule walls (after polymerization occurs). This work was developed in collaboration between PH.D. O. Cornejo Pérez, Ph.D Haret Rosu and M.Sc. Jaime Pérez Terrazas, and was published as a chapter of the book “Physics of Emergence and Organization”, with the title “Supersymmetric Methods in the Traveling Variable: Inside Neurons and at the Brain Scale” [1].

### **4.1 Supersymmetric methods in the traveling variable: inside neurons and at the brain scale**

We apply the mathematical technique of factorization of differential operators to two different problems. After a brief overview on microtubules, we review previous results related to the supersymmetry of the Montroll kinks moving onto the microtubule walls as well as mentioning the sine-Gordon model for the microtubule non-linear excitations. Second, we find analytic expressions for a class of one-parameter solutions of a sort of diffusion equation of Bessel type that is obtained by supersymmetry from the homogeneous form of a simple damped wave equations derived in the works of P.A. Robinson and collaborators for the corticothalamic system. We also present a possible interpretation of the diffusion equation in the brain context.

### 4.1.1 Microtubule structure and dynamics, brief overview

The following information comes from references [2–4].

Microtubule are cytoskeletal polymers that perform a variety of essential functions for the survival of all eukaryotes at the cellular level as the transport of some substances and organelles, cell motility, cell division and morphogenesis, etc. Microtubules are flexible polymers whose mechanical properties are an important factor in the determination of cell architecture and are the main components of some cell regions as the axonemal structures found in cilia and flagella. It have been even suggested that MTs are also implicated in higher neuronal functions, including memory and the emergence of “consciousness” [9]. Microtubule are made of repeating  $\alpha$ ,  $\beta$ -tubulin heterodimers with a molecular weight of 110 kDa. These heterodimers bind head to tail to form linear protofilaments, and about 13 protofilaments associate in parallel to make the microtubule wall. The heterodimers have a defined polarity and so the protofilaments and the resulting polymer has also a defined polarity, with two ends that are structurally and functionally distinct. In the cell, the minus end ( $\alpha$ -tubulin side) is often attached at microtubule organizing centers (MTOCs) such as the centrosome, whereas the plus end ( $\beta$ -tubulin side) is free in the cytoplasm or attached to a specific target such as kinetochore.

Essential to the function of microtubules is their dynamic character. Microtubules can “move” on an unidirectional flux in a steady state by means of the polymerization on the plus end and depolymerization on the minus end. If the net rates are closely the same, the effect is that the structure is moving in one direction, although the tubulin dimers that compose it have not the same preferential direction of movement. This property is known as treadmilling and recent studies have shown its importance in the cell, both for interface and mitosis. A more general property of microtubules is known as “dynamical instability ” and consists on switching stochastically between growing and shrinking phases. These dynamic properties of microtubules have their origin on the binding and hydrolysis of guanosine 5'-triphosphate (GTP) by tubulin. There is a molecule of GTP at each

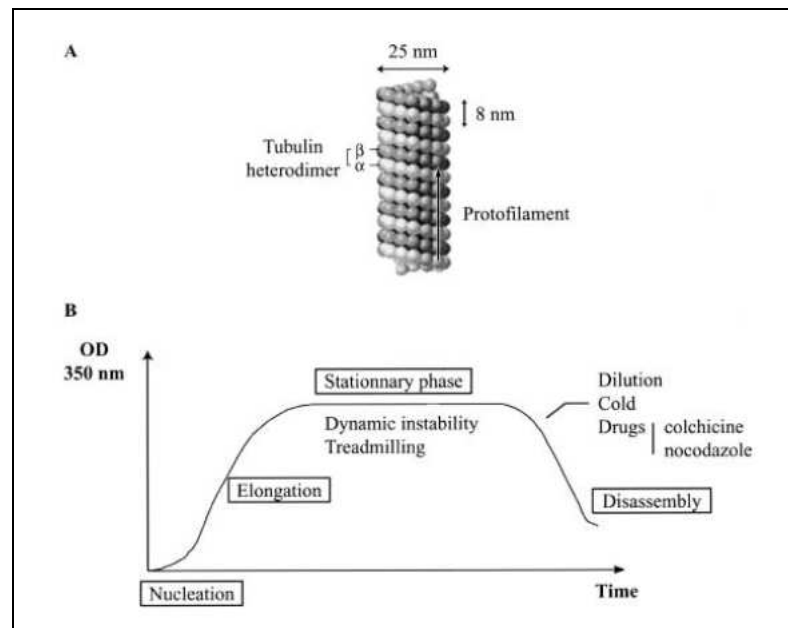


Figure 4.1: Microtubule structure and assembly. A) Schematic representation of microtubule structure. B) Various phases of microtubule assembly. Figure from [4].

monomer in the tubulin heterodimer. Exactly after polymerization of a tubulin dimer, the GTP molecule attached to the  $\beta$ -tubulin directly involved in the union is hydrolyzed. Then microtubule is made of dimers with GTP molecules attached to the  $\alpha$ -tubulin monomers and guanosine 5'-diphosphate (GDP) molecules attached to the  $\beta$ -tubulin monomers; excepting maybe those on the plus end where next polymerization steps will occur. This cap of GTP-tubulin stabilizes the microtubule but, if the GTPs at the plus end are hydrolyzed the microtubule rapidly depolymerizes, resulting on the shrinking phase. Most of the energy that is released by GTP hydrolysis is stored in the microtubule lattice, where it is suggested that have important functions on microtubule dynamics and interactions with other molecules.

The regulation of the microtubule system includes the interaction with numerous microtubule-associated proteins (MAPs) that are themselves regulated. This regulatory system produces precise temporal and spatial patterns of microtubules throughout all the cell cycle. It is also an important factor that tubulin sequence and structure contain the information required for the self-assembly of protofilaments onto dynamic microtubules. Some computational approaches for understanding the dynamic of microtubules systems include Montecarlo simulations [6, 7], nonequilib-

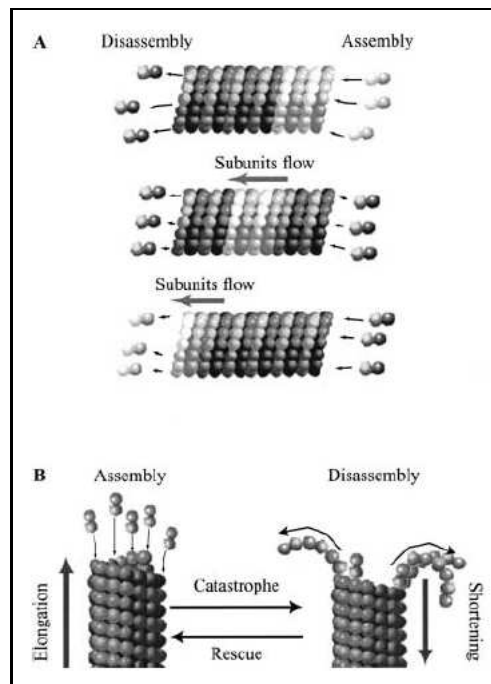


Figure 4.2: Schematic diagram of microtubule behavior at steady state. A) Treadmilling. The length is constant by the exchange of dimers between microtubule and free tubulin in the environment. B) Dynamical Instability. Individual polymers show length fluctuations due to phases of catastrophe, rescue and regrowth. Figure from [4].

rium system self-organization theory [8] and reaction-diffusion schemes [9,10], and stochastic CA models [11]

#### 4.1.2 Nonlinear biological excitations

The possibility of soliton excitations in biological structures has been first pointed out by Englander et al [12] in 1980 who speculated that the so-called ‘open states’ units made of approximately ten adjacent open pairs in long polynucleotide double helices could be thermally induced solitons of the double helix due to a coherence of the twist deformation energy. Since then a substantial amount of literature has been accumulating on the biological significance of DNA nonlinear excitations (for a recent paper, see [13]). On the other hand, the idea of nonlinear excitations has emerged in 1993 in the context of the microtubules (MTs) [14], the dimeric tubular polymers that contribute the main part of the eukaryotic cytoskeleton. In the case of neurons, MTs are critical for the growth and maintenance of axons. It is known

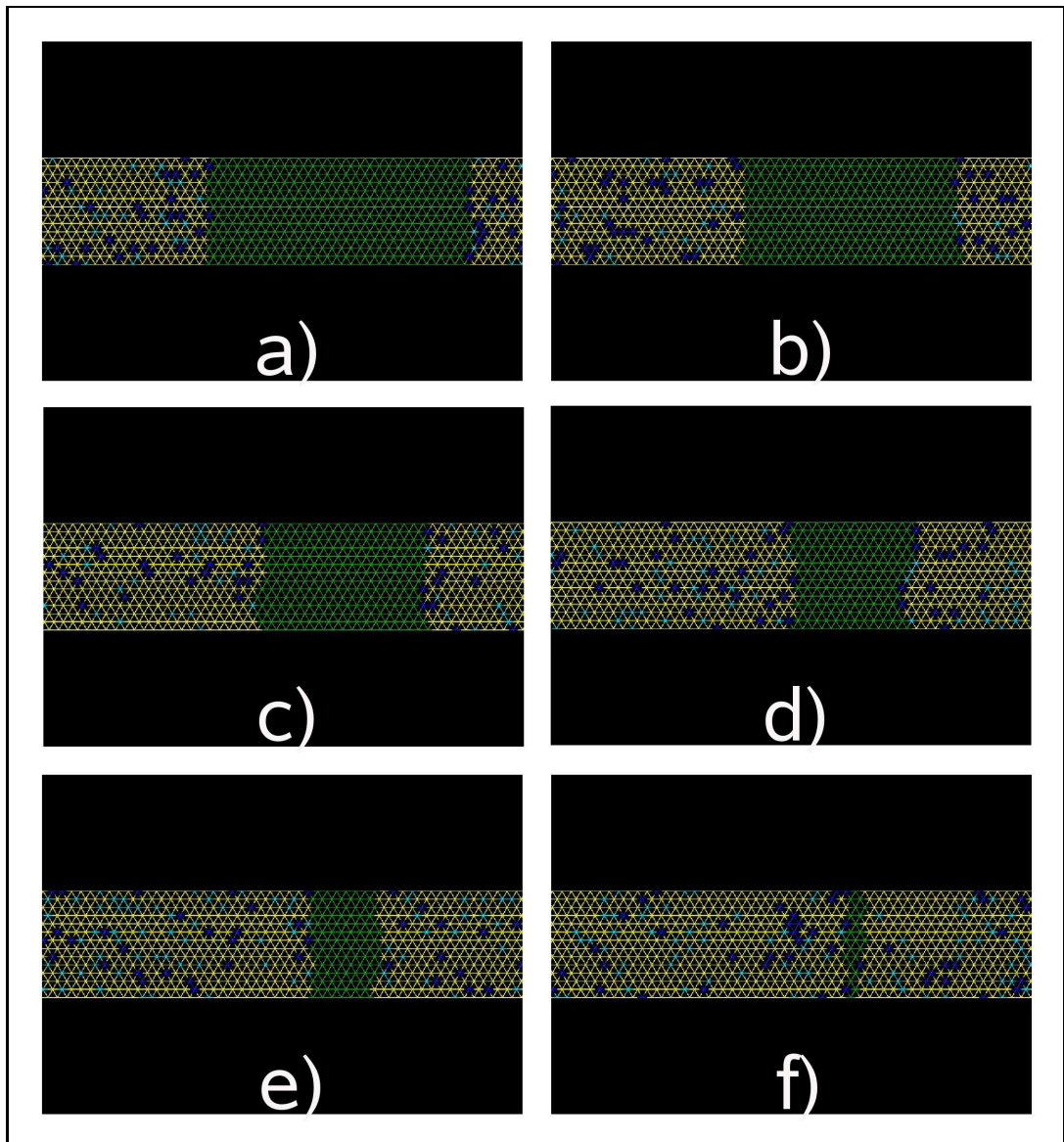


Figure 4.3: Stochastic Cellular Automata Model of Microtubule Assembly/Disassembly. GTP polymerized dimers are in green, GTP dimers are in dark blue and GDP dimers are in light blue. Microtubule is shown as a flat structure for better visualization. Simulation at a) beginning, b) 20 timesteps, c) 40 timesteps, d) 60 timesteps, e) 80 timesteps and f) 100 timesteps. Simulation for disassembly based on the model presented in [11]

that axonal MTs are spatially organized but are not under the influence of a MT-organizing center as in other cells. We also remind that in 1995 Das and Schwarz have used a two-dimensional smectic liquid crystal model to show the possibility of electrical solitary wave propagation in cell membranes [15]. Nevertheless, there is no clear experimental evidence at the moment of any of these biological solitons and kinks.

### 4.1.3 Supersymmetric MT Kinks

Based on well-established results of Collins, Blumen, Currie and Ross [16] regarding the dynamics of domain walls in ferrodistorive materials, Tuszyński and collaborators [14, 17] considered MTs to be ferrodistorive and studied kinks of the Montroll type [18] as excitations responsible for the energy transfer within this highly interesting biological context.

The Euler-Lagrange dimensionless equation of motion of ferrodistorive domain walls as derived in [16] from a Ginzburg-Landau free energy with driven field and dissipation included is of the travelling reaction-diffusion type

$$\psi'' + \rho\psi' - \psi^3 + \psi + \sigma = 0 , \quad (4.1)$$

where the primes are derivatives with respect to a travelling coordinate  $\xi = x - vt$ ,  $\rho$  is a friction coefficient and  $\sigma$  is related to the driven field [16].

There may be ferrodistorive domain walls that can be identified with the Montroll kink solution of Eq. (4.1)

$$M(\xi) = \alpha_1 + \frac{\sqrt{2}\beta}{1 + \exp(\beta\xi)} , \quad (4.2)$$

where  $\beta = (\alpha_2 - \alpha_1)/\sqrt{2}$  and the parameters  $\alpha_1$  and  $\alpha_2$  are two nonequal solutions of the cubic equation

$$(\psi - \alpha_1)(\psi - \alpha_2)(\psi - \alpha_3) = \psi^3 - \psi - \sigma . \quad (4.3)$$

Rosu has noted that Montroll's kink can be written as a typical **tanh** kink [19]

$$M(\xi) = \gamma - \tanh\left(\frac{\beta\xi}{2}\right) , \quad (4.4)$$

where  $\gamma \equiv \alpha_1 + \alpha_2 = 1 + \frac{\alpha_1\sqrt{2}}{\beta}$ . The latter relationship allows one to use a simple construction method of exactly soluble double-well potentials in the Schrödinger equation proposed by Caticha [20]. The scheme is a non-standard application of Witten's supersymmetric quantum mechanics [21] having as the essential assumption

the idea of considering the  $M$  kink as the switching function between the two lowest eigenstates of the Schrödinger equation with a double-well potential. Thus

$$\phi_1 = M\phi_0 , \quad (4.5)$$

where  $\phi_{0,1}$  are solutions of  $\phi_{0,1}'' + [\epsilon_{0,1} - u(\xi)]\phi_{0,1}(\xi) = 0$ , and  $u(\xi)$  is the double-well potential to be found.

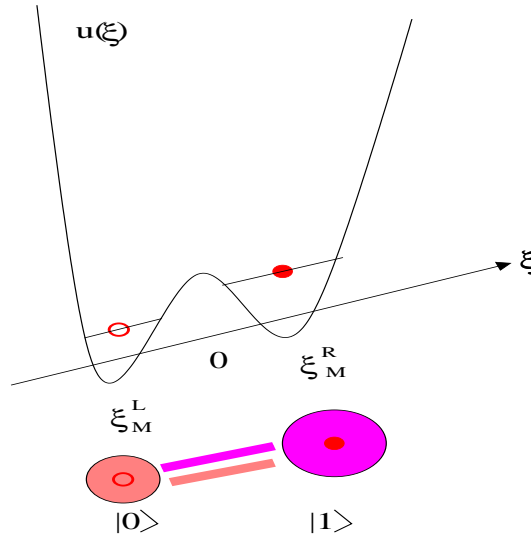


Figure 4.4: Single electron within the traveling double-well potential  $u(\xi)$  as a qubit. The electron can switch from one wall to another by tunneling and the relation between the wavefunctions in the two wells is given by Eq. (4.5).

Substituting Eq. (4.5) into the Schrödinger equation for the subscript 1 and subtracting the same equation multiplied by the switching function for the subscript 0, one obtains

$$\phi_0' + R_M\phi_0 = 0 , \quad (4.6)$$

where  $R_M$  is given by

$$R_M = \frac{M'' + \epsilon M}{2M'} , \quad (4.7)$$

and  $\epsilon = \epsilon_1 - \epsilon_0$  is the lowest energy splitting in the double-well Schrödinger equation. In addition, notice that Eq. (4.6) is the basic equation introducing the superpotential  $R$  in Witten's supersymmetric quantum mechanics, i.e., the Riccati

solution. For Montroll's kink the corresponding Riccati solution reads

$$R_M(\xi) = -\frac{\beta}{2} \tanh\left(\frac{\beta}{2}\xi\right) + \frac{\epsilon}{2\beta} \left[ \sinh(\beta\xi) + 2\gamma \cosh^2\left(\frac{\beta}{2}\xi\right) \right] \quad (4.8)$$

and the ground-state Schrödinger function is found by means of Eq. (4.6)

$$\begin{aligned} \phi_{0,M}(\xi) = \phi_0(0) \cosh\left(\frac{\beta}{2}\xi\right) \exp\left(\frac{\epsilon}{2\beta^2}\right) \exp\left(-\frac{\epsilon}{2\beta^2} \left[ \cosh(\beta\xi) \right. \right. \\ \left. \left. - \gamma\beta\xi - \gamma \sinh(\beta\xi) \right] \right), \end{aligned} \quad (4.9)$$

while  $\phi_1$  is obtained by switching the ground-state wave function by means of  $M$ . This ground-state wave function is of supersymmetric type

$$\phi_{0,M}(\xi) = \phi_{0,M}(0) \exp\left[-\int_0^\xi R_M(y) dy\right], \quad (4.10)$$

where  $\phi_{0,M}(0)$  is a normalization constant.

The Montroll double well potential is determined up to the additive constant  $\epsilon_0$  by the 'bosonic' Riccati equation

$$\begin{aligned} u_M(\xi) = R_M^2 - R_M' + \epsilon_0 = \frac{\beta^2}{4} + \frac{(\gamma^2 - 1)\epsilon^2}{4\beta^2} + \frac{\epsilon}{2} + \epsilon_0 \\ + \frac{\epsilon}{8\beta^2} \left[ (4\gamma^2\epsilon + 2(\gamma^2 + 1)\epsilon \cosh(\beta\xi) - 8\beta^2) \cosh(\beta\xi) \right. \\ \left. - 4\gamma(\epsilon + \epsilon \cosh(\beta\xi) - 2\beta^2) \sinh(\beta\xi) \right]. \end{aligned} \quad (4.11)$$

If, as suggested by Caticha, one chooses the ground state energy to be

$$\epsilon_0 = -\frac{\beta^2}{4} - \frac{\epsilon}{2} + \frac{\epsilon^2}{4\beta^2} (1 - \gamma^2), \quad (4.12)$$

then  $u_M(\xi)$  turns into a travelling, asymmetric Morse double-well potential of depths depending on the Montroll parameters  $\beta$  and  $\gamma$  and the splitting  $\epsilon$

$$U_{0,m}^{L,R} = \beta^2 \left[ 1 \pm \frac{2\epsilon\gamma}{(2\beta)^2} \right], \quad (4.13)$$

where the subscript  $m$  stands for Morse and the superscripts  $L$  and  $R$  for left and right well, respectively. The difference in depth, the bias, is  $\Delta_m \equiv U_0^L - U_0^R = 2\epsilon\gamma$ , while the location of the potential minima on the traveling axis is at

$$\xi_m^{L,R} = \mp \frac{1}{\beta} \ln \left[ \frac{(2\beta)^2 \pm 2\epsilon\gamma}{\epsilon(\gamma \mp 1)} \right], \quad (4.14)$$

that shows that  $\gamma \neq \pm 1$ .

An extension of the previous results is possible if one notices that  $R_M$  in Eq. (4.8) is only the particular solution of Eq. (4.11). The general solution is a one-parameter function of the form

$$R_M(\xi; \lambda) = R_M(\xi) + \frac{d}{d\xi} \left[ \ln(I_M(\xi) + \lambda) \right] \quad (4.15)$$

and the corresponding one-parameter Montroll potential is given by

$$u_M(\xi; \lambda) = u_M(\xi) - 2 \frac{d^2}{d\xi^2} \left[ \ln(I_M(\xi) + \lambda) \right]. \quad (4.16)$$

In these formulas,  $I_M(\xi) = \int^\xi \phi_{0,M}^2(\xi) d\xi$  and  $\lambda$  is an integration constant that is used as a deforming parameter of the potential and is related to the irregular zero mode. The one-parameter Darboux-deformed ground state wave function can be shown to be

$$\phi_{0,M}(\xi; \lambda) = \sqrt{\lambda(\lambda + 1)} \frac{\phi_{0,M}}{I_M(\xi) + \lambda}, \quad (4.17)$$

where  $\sqrt{\lambda(\lambda + 1)}$  is the normalization factor implying that  $\lambda \notin [0, -1]$ . Moreover, the one-parameter potentials and wave functions display singularities at  $\lambda_s = -I_M(\xi_s)$ . For large values of  $\pm\lambda$  the singularity moves towards  $\mp\infty$  and the potential and ground state wave function recover the shapes of the non-parametric potential and wave function. The one-parameter Morse case corresponds formally to the change of subscript  $M \rightarrow m$  in Eqs. (4.15) and (4.16). For the single well Morse potential the one-parameter procedure has been studied by Filho [23] and Bentaiba et al [24].

The one-parameter extension leads to singularities in the double-well potential

and the corresponding wave functions. If the parameter  $\lambda$  is positive the singularity is to be found on the negative  $\xi$  axis, while for negative  $\lambda$  it is on the positive side. Potentials and wave functions with singularities are not so strange as it seems [25] and could be quite relevant even in nanotechnology where quantum singular interactions of the contact type are appropriate for describing nanoscale quantum devices. We interpret the singularity as representing the effect of an impurity moving along the MT in one direction or the other depending on the sign of the parameter  $\lambda$ . The impurity may represent a protein attached to the MT or a structural discontinuity in the arrangement of the tubulin molecules. This interpretation of impurities has been given by Trpišová and Tuszyński in non-supersymmetric models of nonlinear MT excitations [26].

#### 4.1.4 The sine-Gordon MT solitons

Almost simultaneously with Sataric, Tuszyński and Zakula, there was another group, Chou, Zhang and Maggiora [27], who published a paper on the possibility of kinklike excitations of sine-Gordon type in MTs but in a biological journal. Even more, they assumed that the kink is excited by the energy released in the hydrolysis of GTP  $\rightarrow$  GDP in microtubular solutions. As the kink moves forward, the individual tubulin molecules involved in the kink undergo motion that can be likened to the dislocation of atoms within the crystal lattice.

They performed an energy estimation showing that a kink in the system possesses about 0.36 - 0.44 eV, which is quite close to the 0.49 eV of energy released from the hydrolysis of GTP.

Moreover, they assumed that the interaction energy  $U(\mathbf{r})$  between two neighboring tubulin molecules along a protofilament is harmonic:

$$U(\mathbf{r}) \approx \frac{1}{2} \mathbf{k} (\mathbf{r} - \mathbf{a}_0)^2, \quad (4.18)$$

where  $\mathbf{k} = \frac{d^2U(\mathbf{a}_0)}{d\mathbf{r}^2}$  and  $\mathbf{r} = \mathbf{x}_i - \mathbf{x}_{i-1}$ . In addition to this kind of nearest neighbor interaction, a tubulin molecule is also subjected to interactions with the remaining tubulin molecules of the MT, i.e., those in the same protofilament but not nearest

neighbor to it.

Chou et al cite pages 425-427 in the book of R.K. Dodd et al (Solitons and Non-linear Wave Equations, Academic Press 1982) for the claiming that this interaction for the  $i$ th tubulin molecule of a protofilament can be approximated by the following periodic effective potential

$$U_i = U_0 \left( 1 - \cos \frac{2\pi \xi_i}{a_0} \right), \quad (4.19)$$

where  $U_0$  is the half-height of the potential energy barrier and  $\xi_i$  is the displacement of the  $i$ th tubulin molecule from the equilibrium position within a particular protofilament.

Introducing the new variable  $\phi_i = \frac{2\pi}{a_0} \xi_i$  the following sine-Gordon equation is obtained

$$m \frac{\partial^2 \phi}{\partial t^2} = k a_0^2 \frac{\partial^2 \phi}{\partial x^2} - \left( \frac{2\pi}{a_0} \right)^2 U_0 \sin \phi \quad (4.20)$$

that can be reduced to the standard form of the sine-Gordon equation

$$\frac{\partial^2 \phi}{\partial x^2} - \frac{1}{c^2} \frac{\partial^2 \phi}{\partial t^2} = \frac{1}{l^2} \sin \phi \quad (4.21)$$

if one sets  $c^2 = \frac{k a_0^2}{m}$  and  $l^{-2} = \frac{4\pi^2 U_0}{k a_0^4}$ . Now, it is well known that the sine-Gordon equation has the famous inverse tangent kink solution

$$\phi = \tan^{-1} \left( \exp \left[ \pm \frac{\gamma}{l} (x - vt) \right] \right), \quad (4.22)$$

where  $\gamma = \frac{1}{\sqrt{1 - \frac{v^2}{c^2}}}$  is an acoustic Lorentz factor and  $w = \frac{\gamma}{l}$  is the kink width.

Most interestingly, the momentum of a tubulin dimer is strongly localized:

$$p = \frac{d(m\xi)}{dt} = \frac{m a_0}{\pi} \frac{\gamma v}{l} \operatorname{sech} \left[ - \frac{\gamma}{l} (x - vt) \right]. \quad (4.23)$$

This momentum function possesses a very high and narrow peak at the center of the kink width implying that the corresponding tubulin molecule will have maximum momentum when it is at the top of the periodic potential. According to Chou et al this remarkable feature occurs only in nonlinear wave mechanics.

Interestingly, for purposes of illustration, these authors have assumed the width of a kink  $w \approx 3a_0$ . Therefore, with the kink moving forward, the affected region always involves three tubulin molecules. For a general case, however, the width  $w$  of a kink can be calculated from

$$w = \frac{a_0}{2\pi} \sqrt{\frac{ka_0^2}{U_0}}, \quad (4.24)$$

if the force constant  $k$  between two neighboring tubulin molecules along a protofilament, the distance  $a_0$  of their centers, and the energy barrier  $2U_0$  of the periodic, effective potential are known. Then the number of tubulin molecules involved in a kink is given by

$$\frac{w}{a_0} = (2\pi)^{-1} \sqrt{ka_0^2/U_0}. \quad (4.25)$$

It is further known that the tubulin molecules in a MT are held by noncovalent bonds, therefore the interaction among them might involve hydrogen bonds, van der Waals contact, salt bridges, and hydrophobic interactions.

It was found by Israelachvili and Pashley [28] that the hydrophobic force law over the distance range 0-10 nm at 21°C is well described by

$$\frac{F_H}{R} = Ce^{-D/D_0} N/m, \quad (4.26)$$

where  $D$  is the distance between tubulin molecules,  $D_0$  is a decay length, and  $R = \frac{R_1 R_2}{R_1 + R_2}$  is a harmonic mean radius for two hydrophobic solute molecules, all in nm.  $R$  is 4 nm in the case of tubulin.

#### 4.1.5 More on the hydrolysis and solitary waves in MTs

Inside the cell, the MTs exist in an unstable dynamic state characterized by a continuous addition and dissociation of the molecules of tubulin. The polypeptides  $\alpha$  and  $\beta$  tubulin each bind one molecule of guanine nucleotide with high affinity. The nucleotide binding site on  $\alpha$  tubulin binds GTP *nonexchangeably* and is referred to as the N site. The binding site on  $\beta$  tubulin *exchanges* rapidly with free nucleotide in the tubulin heterodimer and is referred to as the E site.

Thus, the addition of each tubulin is accompanied by the hydrolysis of GTP 5' bound to the  $\beta$  monomer. In this reaction an amount of energy of  $6.25 \times 10^{-21}$  J is freed that can travel along MTs as a kinklike solitary wave.

The exchangeable GTP hydrolyses very soon after the tubulin binds to the MT. At  $pH = 7$  this reaction takes place according to the formula:



The last mathematical formulation of the manner in which the energy  $\Delta_H E$  is turned into a kink excitation claims that the hydrolysis causes a dynamical transition in the structure of tubulin [29].

## 4.2 Quantum information in the MT walls

Biological information processing, storage, and transduction occurring by computer-like transfer and resonance among the dimer units of MTs have been first suggested by Hameroff and Watt [30] and enjoys much speculative activity [31].

For the case of sine-Gordon solitons, the information transport has been investigated by Abdalla et al [32].

Recently Shi and collaborators [33] worked out a processing scheme of quantum information along the MT walls by using previous hints of Lloyd for two-level pseudospin systems [34]. The MT wall is treated as a chain of three types of two pseudospin-state dimers. A set of appropriate resonant frequencies has been given. They conclude that specific frequencies of laser pulse excitations can be applied in order to generate quantum information processing.

Lloyd's scheme uses the driving of a quantum computer by means of a sequence of laser pulses. He assumes a 1-dimensional arrangement of atoms of two types (A and B) that could be each of them in one of two states and are affected only by nearest neighbors. Then, information processing could be performed by laser pulses of specific frequencies  $\omega_{K\alpha,\beta}$ , that change the state of the atom of the K kind (A or B type) if in a pair of atoms AB, A is in  $\alpha$  state and B is in state  $\beta$ .

### 4.2.1 Supersymmetry at the Brain Scale

Neuronal activity is the result of the propagation of impulses generated at the neuron cell body and transmitted along axons to other neurons. Recently, Robinson and collaborators [36] obtained simple damped wave equations for the axonal pulse fields propagating at speed  $\mathbf{v}_a$  between two populations,  $\mathbf{a}$  and  $\mathbf{b}$ , of neurons in the thalamocortical region of the brain. The explicit form of their equation is

$$\hat{O}_R \phi_a(t) = S[\mathbf{V}_a(t)] , \quad (4.28)$$

where

$$\hat{O}_R = \left( \frac{1}{\nu_a^2} \frac{d^2}{dt^2} + \frac{2}{\nu_a} \frac{d}{dt} + 1 - r_a^2 \nabla^2 \right) , \quad (4.29)$$

where  $\nu_a = \mathbf{v}_a / r_a$ ,  $r_a$  is the mean range of axons  $\mathbf{a}$ , and  $\mathbf{V}_a = \sum_b \mathbf{V}_{ab}$  is a so-called cell body potential which results from the filtered dendritic tree inputs. Robinson has used the experimental parameters in this equation for the processing of the experimental data. In the following we concentrate on a particular mathematical aspect of this equation and refer the reader to the works of Robinson's group for more details concerning this equation.

#### The homogeneous equation

We treat first the homogeneous case, i.e.,  $\mathbf{S} = \mathbf{0}$  and we discard the subindexes as being related to the phenomenology not to the mathematics. Let us employ the change of variable  $\mathbf{z} = \mathbf{a}\mathbf{x} + \mathbf{b}\mathbf{y} - \mathbf{c}\mathbf{t}$  (see, e.g., [37]), which is a traveling coordinate in 2+1 dimensions. This is justified because it was noticed by Wilson and Cowan [35] that distinct anatomical regions of cerebral cortex and of thalamic nuclei are functionally two-dimensional although extending to three spatial coordinates is trivial. We have the following rescalings of functions:  $\phi_t = -\mathbf{c}\phi_z$ ,  $\phi_{tt} = \mathbf{v}^2\phi_{zz}$ ,  $\phi_{xx} = \mathbf{a}^2\phi_{zz}$ ,  $\phi_{yy} = \mathbf{b}^2\phi_{zz}$ . Then, we get the ordinary differential equation corresponding to the damped wave equation in the following form

$$\hat{O}_{R,z} \phi \equiv \left( \frac{d^2}{dz^2} - 2\mu \frac{d}{dz} + \mu^2 \right) \phi = \alpha^2 \phi , \quad (4.30)$$

where

$$\mu = \frac{\nu c}{c^2 - \nu^2 r^2 (a^2 + b^2)}, \quad \alpha^2 = \frac{\nu^4 r^2 (a^2 + b^2)}{[c^2 - \nu^2 r^2 (a^2 + b^2)]^2}. \quad (4.31)$$

The simple damped oscillator equation (4.30) can be easily factorized

$$L_\mu^2 \phi \equiv \left( \frac{d}{dz} - \mu \right) \left( \frac{d}{dz} - \mu \right) \phi = \alpha^2 \phi. \quad (4.32)$$

The case  $c^2 < \nu^2 r^2 (a^2 + b^2)$  implies  $\mu < 0$  and the general solution of (4.30) can be written

$$\phi(z) = e^{\mu z} (A e^{\alpha z} + B e^{-\alpha z}). \quad (4.33)$$

The opposite case  $c^2 > \nu^2 r^2 (a^2 + b^2)$  will lead to only a change of sign in front of  $\mu$  in all formulas henceforth, whereas the case  $c^2 = \nu^2 r^2 (a^2 + b^2)$  will be considered as nonphysical. The non-uniqueness of the factorization of second-order differential operators has been exploited in a previous paper [38] on the example of the Newton classical damped oscillator, i.e.,

$$\hat{N} \mathbf{y} \equiv \left( \frac{d^2}{dt^2} + 2\beta \frac{d}{dt} + \omega_0^2 \right) \mathbf{y} = \mathbf{0}, \quad (4.34)$$

which is similar to the equation (4.30), unless the coefficient  $2\beta$  is the friction constant per unit mass,  $\omega_0$  is the natural frequency of the oscillator, and the independent variable is just time not the traveling variable. Proceeding along the lines of [38], one can search for the most general isospectral factorization

$$(D_z + f(z))(D_z + g(z))\phi = \alpha^2 \phi. \quad (4.35)$$

After simple algebraic manipulations one finds the conditions  $f + g = -2\mu$  and  $dg/dz + fg = \mu^2$  having as general solution  $f_\lambda = \frac{\lambda}{\lambda z + 1} - \mu$ , whereas  $f_0 = -\mu$  is only a particular solution. Using the general solution  $f_\lambda$  we get

$$\hat{A}_{+\lambda} \hat{A}_{-\lambda} \phi \equiv \left( D_z + \frac{\lambda}{\lambda z + 1} - \mu \right) \left( D_z - \frac{\lambda}{\lambda z + 1} - \mu \right) \phi = \alpha^2 \phi. \quad (4.36)$$

This equation does not provide anything new since it is just equation (4.31). However, a different operator, which is a supersymmetric partner of (4.36) is obtained by applying the factorizing  $\lambda$ -dependent operators in reversed order

$$\hat{A}_{-\lambda}\hat{A}_{+\lambda}\tilde{\phi} \equiv \left(D_z - \frac{\lambda}{\lambda z + 1} - \mu\right) \left(D_z + \frac{\lambda}{\lambda z + 1} - \mu\right) \tilde{\phi} = \alpha^2 \tilde{\phi}. \quad (4.37)$$

The latter equation can be written as follows

$$\hat{O}_\lambda \tilde{\phi} \equiv \left(\frac{d^2}{dz^2} - 2\mu\frac{d}{dz} + \mu^2 - \alpha^2 - \frac{\lambda^2}{(\lambda z + 1)^2}\right) \tilde{\phi} = 0, \quad (4.38)$$

or

$$\left(\frac{d^2}{dz^2} - 2\mu\frac{d}{dz} + \omega^2(z)\right) \tilde{\phi} = 0, \quad (4.39)$$

where

$$\omega^2(z) = \mu^2 - \alpha^2 - \frac{\lambda^2}{(\lambda z + 1)^2} \quad (4.40)$$

is a sort of parametric angular frequency with respect to the traveling coordinate.

This new second-order linear damping equation contains the additional last term with respect to its initial partner, which may be thought of as the Darboux transform part of the frequency [39].  $Z_\lambda = 1/\lambda$  occurs as a new traveling scale in the damped wave problem and acts as a modulation scale. If this traveling scale is infinite, the ordinary damped wave problem is recovered. The  $\tilde{\phi}$  modes can be obtained from the  $\phi$  modes by operatorial means [38].

Eliminating the first derivative term in the parametric damped oscillator equation (4.39) one can get the following Bessel equation

$$\frac{d^2 u}{dx^2} - \left(\frac{n^2 - \frac{1}{4}}{x^2} + \beta^2\right) u = 0, \quad (4.41)$$

where  $x = z + 1/\lambda$ ,  $n^2 = 5/4$ , and  $\beta = i\alpha$ . Using the latter equation, the general solution of equation (4.39) can be written in terms of the modified Bessel functions

$$\tilde{\phi} = (z + 1/\lambda)^{1/2} [C_1 I_{\sqrt{5}/2}(\alpha(z + 1/\lambda)) + C_2 I_{-\sqrt{5}/2}(\alpha(z + 1/\lambda))] e^{\mu z}. \quad (4.42)$$

What could be a right interpretation of the supersymmetric partner equation (4.37)? Since the solutions are modified Bessel functions, we consider this equation as a diffusion equation with a diffusion coefficient depending on the traveling coordinate. Noticing that the velocity in the traveling variable of this diffusion is the same as the velocity of the neuronal pulses we identify it with the diffusion of various molecules, mostly hormones, in the extracellular space (ECS) of the brain, which is known to be necessary for chemical signaling and for neurons and glia to access nutrients and therapeutics occupying as much as 20 % of total brain volume *in vivo* [40].

### The nonhomogeneous equation

The source term  $\mathbf{S}$  in Robinson's equation (4.28) is a sigmoidal firing function, which despite corresponding to a realistic case led him to work out extensive numerical analyses. Analytic results have been obtained recently by Troy and Shusterman [41] by using a source term comprising a combination of discontinuous exponential coupling rate functions and Heaviside firing rate functions. In addition, Brackley and Turner [42] incorporated fluctuating firing thresholds about a mean value as a source of noisy behavior [42].

The procedure of Troy and Shusterman can be applied for the parametric damped oscillator equation as well as for the Bessel diffusion equation obtained herein in the realm of Robinson's brain wave equation with the difference that the method of variation of parameters should be employed. The detailed mathematical analysis is left for a future work.

**REFERENCES**

1. H. C. Rosu, O. Cornejo-Pérez and J. E. Pérez-Terrazas, Supersymmetric Methods in the Traveling Variable: Inside Neurons and at the Brain Scale, pp. 253-265, published in the book *Physics of Emergence and Organization*, edited by Ignazio Licata and Ammar Sakaji, World Scientific Publishing Co. Pte. Ltd., 2008.
2. E. Nogales, *Cell Mol. Life Sci* **56**, 133 (1999)
3. E. Nogales, *Annu. Rev. Biochem.* **69**, 277 (2000)
4. O. Valiron, N. Caudron and D. Job, *Cell Mol. Life Sci* **58**, 2069 (2001)
5. R. Penrose, *Shadows of the Mind: A Search for the Missing Science of Consciousness*, Oxford University Press (1994)
6. V. VanBuren, D. J. Odde and L. Cassimeris, *Proc. Natl. Acad. Sci. U.S.A.* **99**, 6035 (2002)
7. P. A. Deymier, Y. Yang and J. Hoying, *Phys. Rev. E* **72**, 021906 (2005)
8. K. A. Katrukha and G. T. Guriya, *Cell Biophysics* **51**, 781 (2006)
9. N. Glade, J. Demongeot and J. Tabony, *C. R. Biologies* **325**, 283 (2002)
10. N. Glade, J. Demongeot and J. Tabony, *Cell Biology* **5**, 23 (2004)
11. H. Hotani, R. Lahoz-Beltra, B. Combs, S. Hameroff and S. Rasmussen, *Nanobiology* **1**, 61 (1992)
12. S.W. Englander, N.R. Kallenbach, A.J. Heeger, J.A. Krumhansl, and S. Litwin, *Proc. Natl. Acad. Sci. U.S.A.* **77**, 7222 (1980).
13. J.D. Bashford, *J. Biol. Phys.* **32**, 27 (2006).
14. M.V. Satarčić, J. A. Tuszyński and R.B. Żakula, *Phys. Rev. E* **48**, 589 (1993).
15. P. Das and W.H. Schwarz, *Phys. Rev. E* **51**, 3588 (1995).

16. M.A. Collins, A. Blumen, J.F. Currie, and J. Ross, *Phys. Rev. B* **19**, 3630 (1979).
17. J.A. Tuszyński, S. Hameroff, M.V. Sataric, B. Trpišová, and M.L.A. Nip, *J. Theor. Biol.* **174**, 371 (1995).
18. E.W. Montroll, in *Statistical Mechanics*, ed. by S.A. Rice, K.F. Freed, and J.C. Light (Univ. of Chicago, Chicago, 1972).
19. H.C. Rosu, *Phys. Rev. E* **55**, 2038 (1997).
20. A. Caticha, *Phys. Rev. A* **51**, 4264 (1995).
21. E. Witten, *Nucl. Phys. B* **185**, 513 (1981).
22. B. Mielnik, *J. Math. Phys.* **25**, 3387 (1984); D.J. Fernandez, *Lett. Math. Phys.* **8**, 337 (1984); M.M. Nieto, *Phys. Lett. B* **145**, 208 (1984). For review see H.C. Rosu, *Symmetries in Quantum Mechanics and Quantum Optics*, eds. A. Ballesteros et al (Serv. de Publ. Univ. Burgos, Burgos, Spain, 1999) pp. 301-315, quant-ph/9809056.
23. E.D. Filho, *J. Phys. A* **21**, L1025 (1988).
24. M. Bentaiba, L. Chetouni, T.F. Hammann, *Phys. Lett. A* **189**, 433 (1994).
25. T. Cheon and T. Shigehara, *Phys. Lett. A* **243**, 111 (1998).
26. B. Trpišová and J.A. Tuszyński, *Phys. Rev. E* **55**, 3288 (1997).
27. K.-C. Chou, C.-T. Zhang, and G.M. Maggiora, *Biopolymers* **34**, 143 (1994).
28. J. Israelachvili and R. Pashley, *Nature* **300**, 341 (1982).
29. M.V. Sataric and J.A. Tuszyński, *J. Biol. Phys.* **31**, 487 (2005).
30. S. Hameroff and R.C. Watt, *J. Theor. Biol.* **98**, 549 (1982).
31. See e.g., J. Faber, R. Portugal, L. Pinguelli Rosa, *Information processing in brain MTs*, contribution at the Quantum Mind 2003 Conference, q-bio.SC/0404007.

32. E. Abdalla, B. Maroufi, B. Cuadros Melgar, and M. Brahim Sedra, *Physica A* **301**, 169 (2001).
33. C. Shi, X. Qiu, T. Wu, R. Li, *J. Biol. Phys.* **32**, 413 (2006).
34. S. Lloyd, *Science* **261**, 1569 (1993).
35. H.R. Wilson and J.D. Cowan, *Biol. Cybernetics* **13**, 55 (1973).
36. P.A. Robinson, C.J. Rennie, D.L. Rowe, S.C. Connor, *Human Brain Mapping* **23**, 53 (2004); H. Wu and P.A. Robinson, *J. Theor. Biol.* **244**, 1 (2007); P.A. Robinson, *Phys. Rev. E* **72**, 011904 (2005).
37. P.G. Estévez, Ş. Kuru, J. Negro, L.M. Nieto, *J. Phys. A* **39**, 11441 (2006).
38. H.C. Rosu and M. Reyes, *Phys. Rev. E* **57**, 2850 (1998).
39. G. Darboux, *C.R. Acad. Sci.* **94**, 1456 (1882).
40. R.G. Thorne and C. Nicholson, *Proc. Natl. Acad. Sci. U.S.A.* **103**, 5567 (2006) and references therein.
41. W.C. Troy and V. Shusterman, *SIAM J. Applied Dynamical Systems* **6**, 263 (2007).
42. C.A. Brackley and M.S. Turner, *Phys. Rev. E* **75**, 041913 (2007).

# Chapter 5

## A CA model for Self-Assembling

### 5.1 Self-assembly: an overview

#### 5.1.1 What is self-assembly?

Molecular self-assembly is the spontaneous association of molecules, under equilibrium conditions, in structurally well defined aggregates that are bound by non-covalent bonds [1]: hydrogen bonds, ionic bonds (electrostatic interactions), hydrophobic interactions, van der Waals interactions and hydrogen bonds mediated by water [2].

Self-assembly can be classified in the following way [3]:

- Static self-assembly: Systems that are in a global or local minimum energy state and does not have energy dissipation, as molecular crystals and folded globular proteins.
- Dynamic self-assembly: Structures and patterns occurs if the system is dissipating energy, as Belousov-Zhabotinsky chemical systems for instance.
- Self-assembly using templates: Interactions between components and the environment determine the final structure. Crystallization on surfaces is an example.
- Biological self-assembly: This is a superset that contains all previous classes.

These systems are characterized by the variety and complexity of the functions of the produced structures.

Self-assembly is ubiquitous in biological and chemical systems as can be assessed in crystallization, micelles, viruses, functional protein complexes, etc. Understanding self-assembly and discovering how to take advantage from it is one of the most important issues in Nanotechnology and biologically inspired technologies (Biomimetics), because this knowledge could lead to industrial production of all kinds of nanodevices and new materials, with high reliability at remarkable low costs [3].

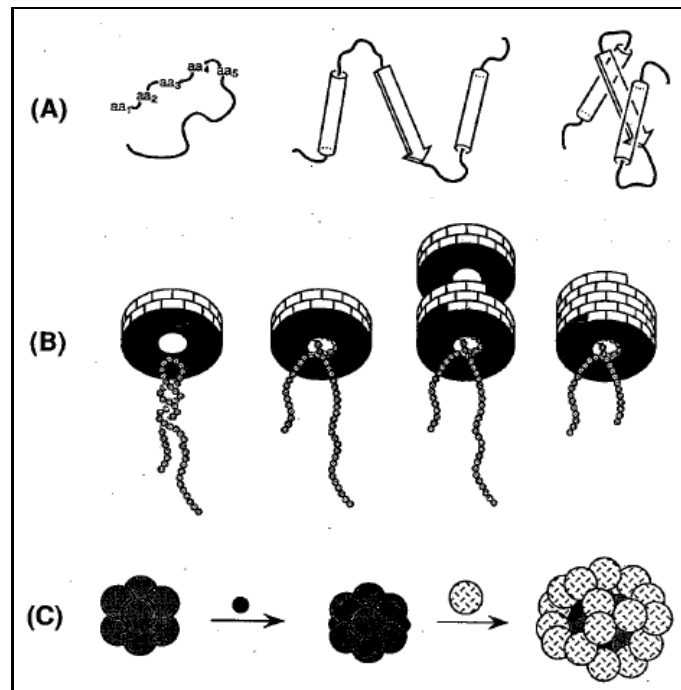


Figure 5.1: Self-assembly: biological examples. a) Protein folding. b) Tobacco virus assembling. c) Piruvata dehydrogenase complex formation. Figure from [3]

The main characteristics of self-assembly are [4]:

- *Components.* They are the pieces or elements that go from a disordered state to a state with some degree of order (system level).
- *Interactions.* Interactions are normally non-covalent, as hydrogen bridges, induced dipoles, coordination bonds, etc. For self-assembling, it is required a balance between attractive and repulsion forces in the formation stage.

- *Adjustment capability.* Components must have some degree of freedom in order to be able to find the minimal energy state.
- *Environment.* It is always required an environment that allows the diffusion of the components.
- *Mass transport and agitation.* Energy is needed to promote the diffusion motion of each component.

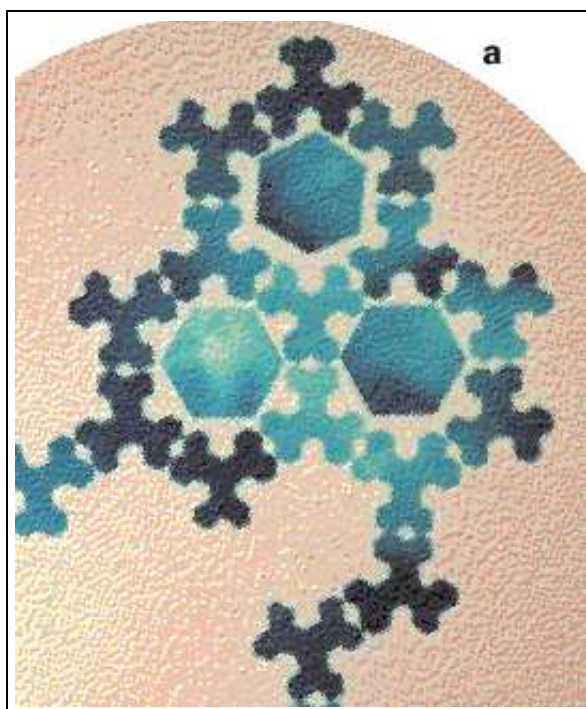


Figure 5.2: Ordered structure made up by components that are complementary in form and molecular interactions. Figure from [5]

Therefore, self-assembly is the formation of an ordered structure from a disordered system of components. The components must be complementary in physical and chemical interactions such as form, surface properties, magnetic dipoles, electrostatic characteristics, etc. Besides, it must occur without direct human intervention in the assembling of pieces. The ordered structure is reached by local corrections and is dictated by the information embedded in the components, for instance their form and electrostatic interactions. However, it is also possible to have conformational changes, *i.e.*, the state or properties of components can change in response to the conditions of its near environment (density, pH, etc.).

Learning how to design components and environments for self-assembling of well defined structures with desired functions is the main key for turning into reality many nanotechnology dreams.

### 5.1.2 Self-assembly research revisited

There have been a growing interest in self-assembling in the last twenty years due to the impact of several works. Bowden reported the assembling of systems made up of designed hexagons with hydrophobic and hydrophilic sides [6]. The hexagonal pieces are immersed in a mixture of water and perfluorodecane (PDF). The attraction and repulsion interaction between the pieces are capable of producing crystalline patterns. This kind of approach became later more popular in the self-assembly research, and several works began to use capilar forces (see [7] for instance). These kind of structures are manly achieved at the microscopic and mesoscopic scale and usually there is lack of control in the global form of the system, although the local structure is well assembled.

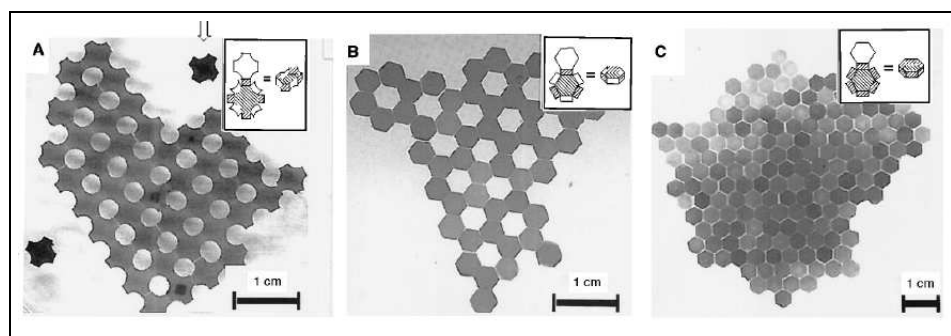


Figure 5.3: Crystalline aggregates made by self-assembly of (A) crosses, (B) hexagons in a open lattice and (C) closed packed hexagons. Figure from [6].

In the area of self-assembling at the molecular level particularly interesting is the work of Padilla *et. al.* [8], where one can find ideas for nanomaterials fabrication by combining naturally symmetric protein components. As a first step, a database search is performed looking for proteins that polymerize in their native form, conforming structures with 2-fold, 3-fold, ... n-fold symmetry. Once two of such proteins

are identified a genetic manipulation is applied in order to create a protein that is the union of those two proteins. In this way, it is obtained (sometimes) a piece which extremes tries to polymerize in a given  $n$ -fold symmetry. Fig. 5.4 depicts these ideas in a clearer way, and show how two proteins that polymerize with different  $n$ -fold symmetry can be used for producing different structures if angles are manipulated. In this work initial experimental trials are reported using influenza virus protein, carboxylesterase and trimeric bromoperoxidase.

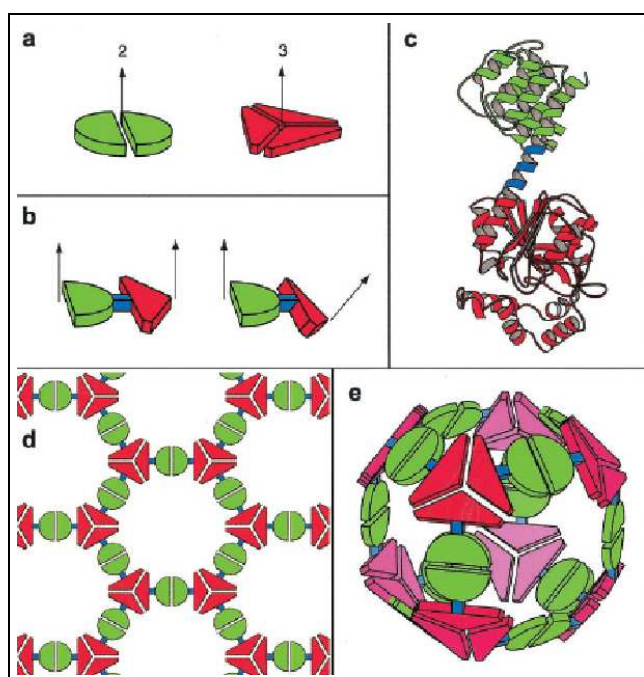


Figure 5.4: General molecular method for producing self-assembling pieces with symmetry. a) Green circle represents a dimeric molecule and the red triangle represents a trimeric molecule. b) By genetic manipulation it is created a molecule that join both molecules. c) Schematic representation of the real structure. d) and e) Possible self-assembled structures. Figure from [8]

An impressive work has been done by the group of Paul Rothermund [9], where a general method is developed for the folding of a long DNA strand in any given 2-dimensional array. As a first step the 2-dimensional array is decomposed in an even number of parallel lines. Then, a long single line is created such that all parallel lines are included. The thickness of this long line represents the thickness of a double chain helix of DNA (approximately 2 nanometers). With the help of a computational algorithm, union points and crossing areas for better resistance are

identified. Finally, the design is divided in a long strand that follows all the structure and several complementary and short strands. In the experiment the long strand folds slowly in the desired structure in a coordinated way with the assembly of short DNA strands. Some of the structures that were successfully assembled are displayed in Fig. 5.5

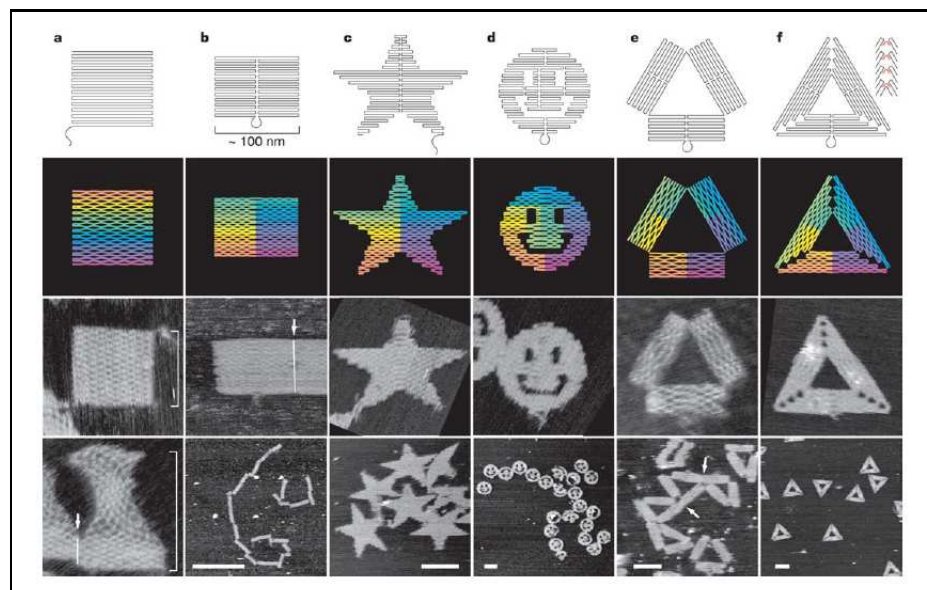


Figure 5.5: Structures assembled with DNA strands. Figure from [9]

In order to understand self-assembling it is important to simulate it and use different computational approaches: molecular dynamics, multiagent systems and cellular automata. Rapaport simulated the self-assembly of the capsides of some viruses by molecular dynamics simulations [11]. He designed molecular structures and appropriate atomic interaction potentials for keeping molecular aggregates of atoms as pieces with defined forms. Such pieces had complementary form and the resulting interaction potential between pieces was attractive. In his model, Rapaport found a high formation rate with a very low rate of assembly errors.

Troisi *et. al.* modeled self-assembly by a multiagents approach [12]. Translational and rotational movement was determined by energy considerations and a random numbers generator. They made comparisons between the energy of several structures of  $n$  pieces and decided if the new structure was conserved or disaggrega-

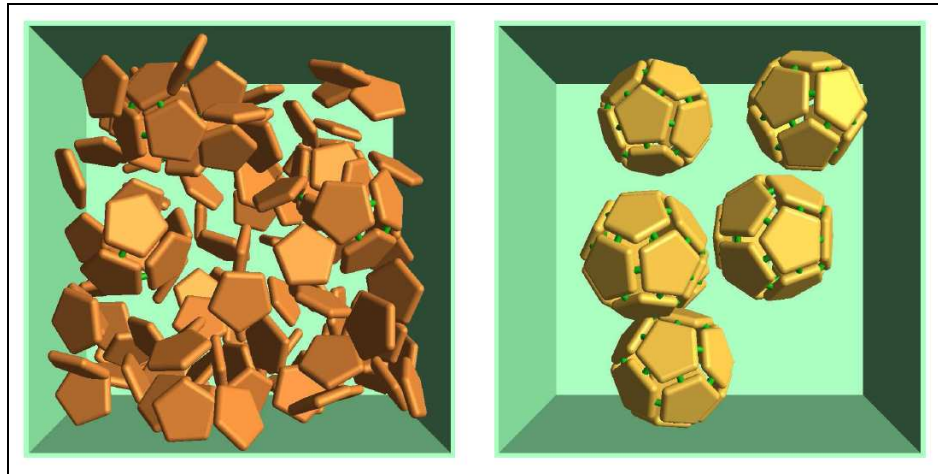


Figure 5.6: Formation of virus capsids in a molecular dynamics model. Figure from [11].

tion of some pieces occurs. They studied systems that would produce closed packed structures (by design) and made comparisons employing the Monte Carlo method. Their method was superior in speed for reaching optimal structures.

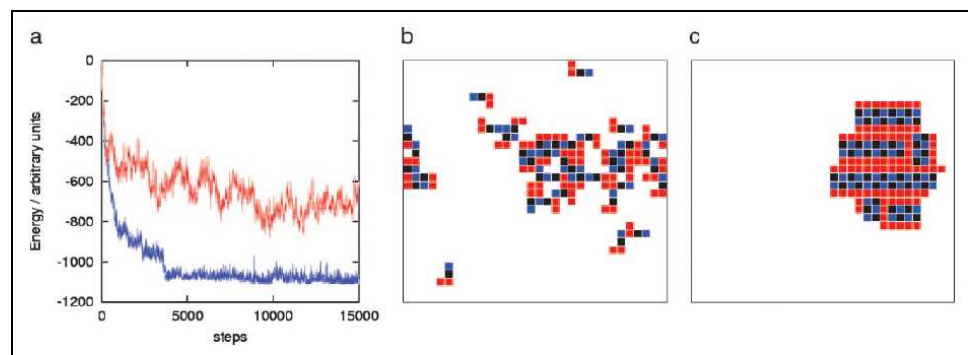


Figure 5.7: Comparison between a multiagent model for self-assembly and Monte Carlo method. a) Energy decrement: red line for Monte Carlo and blue line for Multi-agent system. b) Final result after 15000 Monte Carlo iterations. c) Final result after 15000 iterations with Multiagents. Figure from [12].

There are more works on self-assembly simulations: Nilsson and Rasmussen used Lattice Gas Cellular Automata (LGCA) for mycelle formation in aqueous system [13], Schulman and Winfree [14] studied the relationship between energy gains and losses when an aggregate grows, and Thompson and Goel [15] studied how to take advantage of conformational changes in order to create a well defined structure with function.

## 5.2 Description of the proposed LGCA model

In this work results from the simulation of self-assembly by Lattice Gas Cellular Automata (LGCA) method are presented. This method has been chosen over traditional Cellular Automata procedures because it has been proven that LGCA methods are useful and reliable for fluid simulation, taking into account elastic collisions and momentum and mass conservation.

The model presented in this work is a LGCA system in a square lattice with periodic boundary conditions. Each node has four channels, and each channel can have at most one particle at a time, resulting in an exclusion principle. A main difference with other LGCA models is that particles are not only points, they correspond to pieces with the form of a cross. The ends of different crosses can be attached between them, representing, in a first approach, covalent bonding in real self-assembly systems. Each piece has a set of indicators that define the type of piece and contain information about its current state. The first four indicators give information about what kind of ends has the cross. By means of a general interaction matrix one can define the types of ends that are able to attach to each other. The following four indicators are attaching permissions for the respective extreme, and can be used for conformational changes. Other indicators are used for defining the current orientation of the piece and the direction of its momentum.

The collision step is implemented mainly as in a traditional LGCA: the translational momentum is conserved and the energy is distributed after some time in all the degrees of freedom. However, in the model presented here, when collisions occur a probability is assigned for a change in orientation (rotation) of the involved pieces. Propagation step is implemented as usually in a LGCA system unless the propagation can not happen in a node where a clustered piece is found.

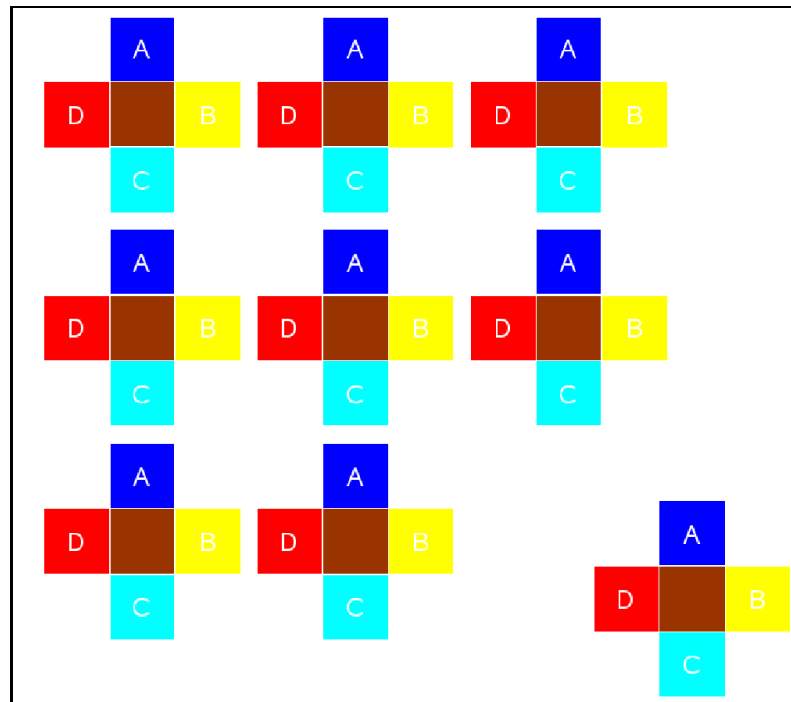


Figure 5.8: Pieces assembled in a ordered structure, square lattice. Extreme A kind can attach with extreme kind C, in the same way extremes B and D are able to stick between them.

As initial conditions all pieces are put in the channels of the nodes of the lattice in a random way, but following the restriction of the exclusion principle. Only one piece is put as a seed in the central node and is the trigger for the aggregate formation. This piece has permission for being stuck with other pieces. All other pieces have permission for attaching to any clustered piece and become themselves clustered pieces. So, if sticky ends are correspondent, free pieces can only attach with pieces already clustered.

The conditions for a free piece to be attached with a clustered piece are:

- it must be the only piece in the node.
- there must be a clustered piece in the neighboring node, in the direction of movement of the free piece.
- the extremes between the free piece and the clustered piece must be able to stick according to the interaction matrix.

The results presented here are based on this set of conditions. The first condition imposes a restriction on the maximum number of pieces that can be present in a node when a piece will become clustered. It is typically used in Diffusion Limited Aggregation (DLA) models [20]. The second one represents a need for some kinetic energy, or more interaction time, in order to allow the attachment between pieces. The third is a characteristic of the model proposed here that specify the interactions between pieces. It allows the construction of very specific structures by creating very specific pieces, although a small increase in the size or complexity of the modeled structure could require a major increase in the number of defined interactions. Of course these restrictions can be modified and tuned for creating an enhanced set of conditions for specific systems. It is part of the richness of LGCA models. However, the results presented here are based on this basic set of conditions and the discussion is made under these assumptions.

## 5.3 Self-assembly model in action

### 5.3.1 Tests

The following results were made in order to verify the algorithm functionality as well as to analyze self-assembly in a square lattice.

The evolution of a cluster or aggregate is depicted in Fig. 5.9. All pieces have their four extremes belonging to the same extreme kind, so the expected structure is a closed packed arrangement of pieces in a square fashion. It is observed that the resulting structure is not perfect but it has multiple structural defects, which are due to the fact that the local correction probability is zero in this test and holes are easily formed in the structure.

The rate of conversion is shown for different systems in Fig. 5.10. The first system is composed by pieces that can attach any of their four extremes with any extreme of a piece already in the cluster. It is observed that at the beginning the

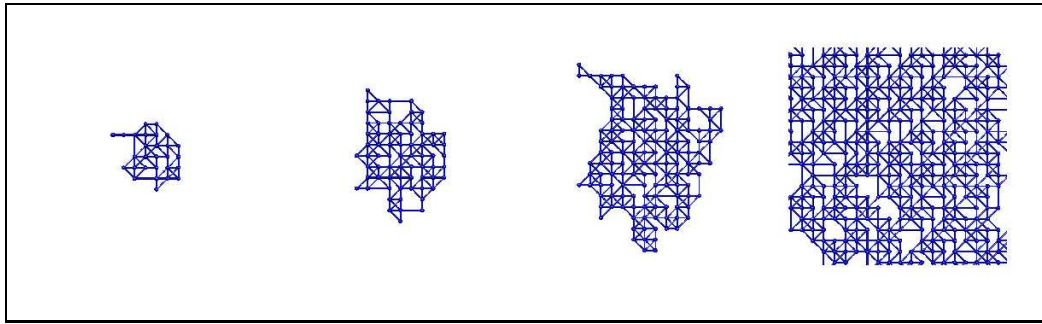


Figure 5.9: Evolution of an aggregate: test try. a) 100 time steps, b) 150 time steps, c) 200 time steps, d) 400 time steps (detail). Density used: 0.7 pieces per node.

conversion is slow because the surface of the aggregate is still small. As this surface grows the conversion speed also grows until the number of free pieces is enough depleted and the conversion is therefore reduced. This behavior is observed for the three systems, although for different time.

In addition, the data for a system that is intended to assemble in a compact arrangement of pieces but that is formed by two different kind of pieces that will arrange in a chess-like fashion: any of the extremes of a “black” piece can only attach with extremes of a “white” piece. The formation speed of the last structure is slower than the former, because in the latter case there is the possibility that a free piece can not attach with a neighboring clustered piece. This occurs where two “black” or two “white” pieces hold together.

Finally, the evolution for a third system, where all pieces are identical but the rules of attachment of extremes are defined as: “The north attach with the south, and the east attach with the west”. This means that the pieces have four different kinds of extremes and each of them has a complementary extreme. This promotes a crystal structure with all their pieces oriented in a particular direction. Such restriction makes even slower the transformation from free pieces to clustered pieces due to the fact that there are more “wrong” relative positions between pieces.

The maximum in the first system is reached at 831 time steps, at 1947 time steps in the second and close to 3000 time steps in the third. Although the relation

between the first two could at first sight be expected to be close to 1:2, there is not a direct relation because the system is not linear. In all cases the accumulation of clustered pieces is sigmoid-like. The plotted results are averages after 20 different simulations for each one of the three different systems, using a grid of 400 x 400 nodes, a density of 0.1 pieces per node and counting new clustered pieces each 40 time steps.

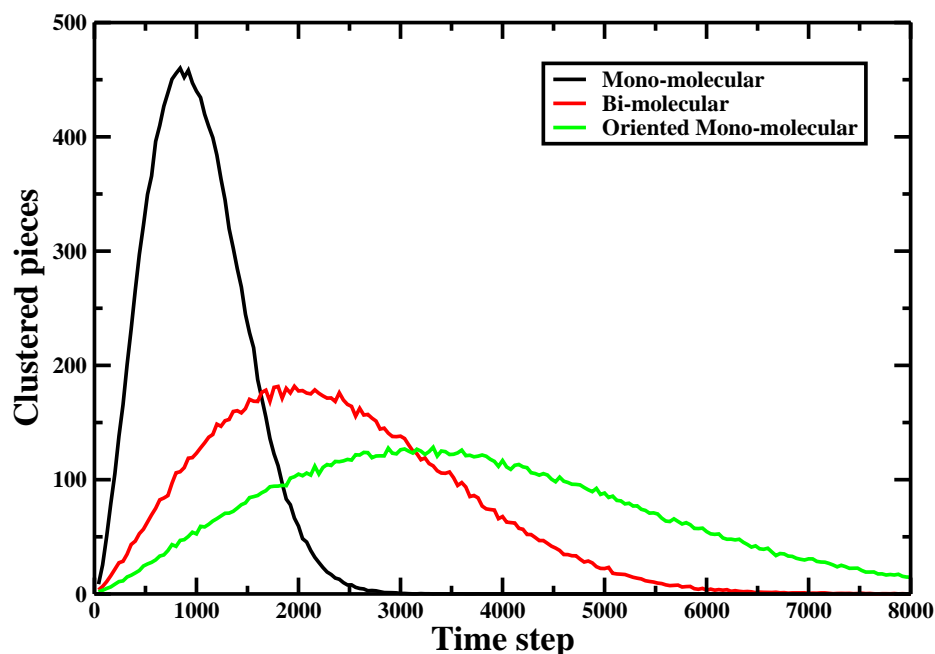


Figure 5.10: Conversion speed for the three systems under discussion. Black is for the one piece system, red is for the system with two pieces, and green is for a system with oriented pieces.

### 5.3.2 Density effects

Some tests for studying the effect of changes of density were performed using the same kind of simple pieces. For the compact designed crystal structure it is observed that the largest conversion rate (clustered pieces / total pieces), just after the peak of conversion, is obtained when a density of 0.7 pieces per node is used. If the density

is reduced the probability for free pieces for getting in contact with the clustered pieces is also reduced. If the density increases, the probability for a piece to be alone in a node (condition for attachment) is diminished. Thus, 0.7 pieces per node is the density value where these two phenomena allow a maximum conversion rate, at least at short times. For longer times, the conversion rates for higher densities are severely affected by the restriction that only one piece can be clustered if it is alone in the node. For low densities, the final conversion rate depends not only on the density value but also on stochasticity, because the last free pieces can finish in a situation where they can not collide with other pieces and besides without a chance of touching the central cluster.

But, which density value could be appropriate for modeling self-assembly? With a high density, the pieces would be practically confined inside a certain zone, propagating and colliding with a notable stochastic but still physical nature until they got stuck in the cluster. Several tests indicated that, when the density is relatively high (over 0.2 pieces per node) the resulting clusters are quite dense, instead of the expected dendritic arrangement. For densities close to 0.2 pieces per node a two stage process growth develops (see figure 5.11). The first is a fast increase of the cluster in a compact way, where there are several holes inside the structure that can be considered as defects in a crystalline lattice. The second stage shows a slower growth, with a gradual development of branches in the cluster in a dendritic fashion.

This two-stage growth suggests that manipulation on the growth process can be performed in order to create clusters at the nanoscale and at the microscale with a controlled proportion (in areas) between a central dense section and an external branched section with lower density. What is needed is to maintain the density over a threshold value by adding pieces or by having a reservoir big enough to maintain the density value high for a desired time. After that, it is possible to add pieces at a density low enough for maintaining a constant growing of the branches. It is important to stress that the value of 0.2 pieces per node is a value that corresponds to the model presented here, where the entire system is composed of pieces that can

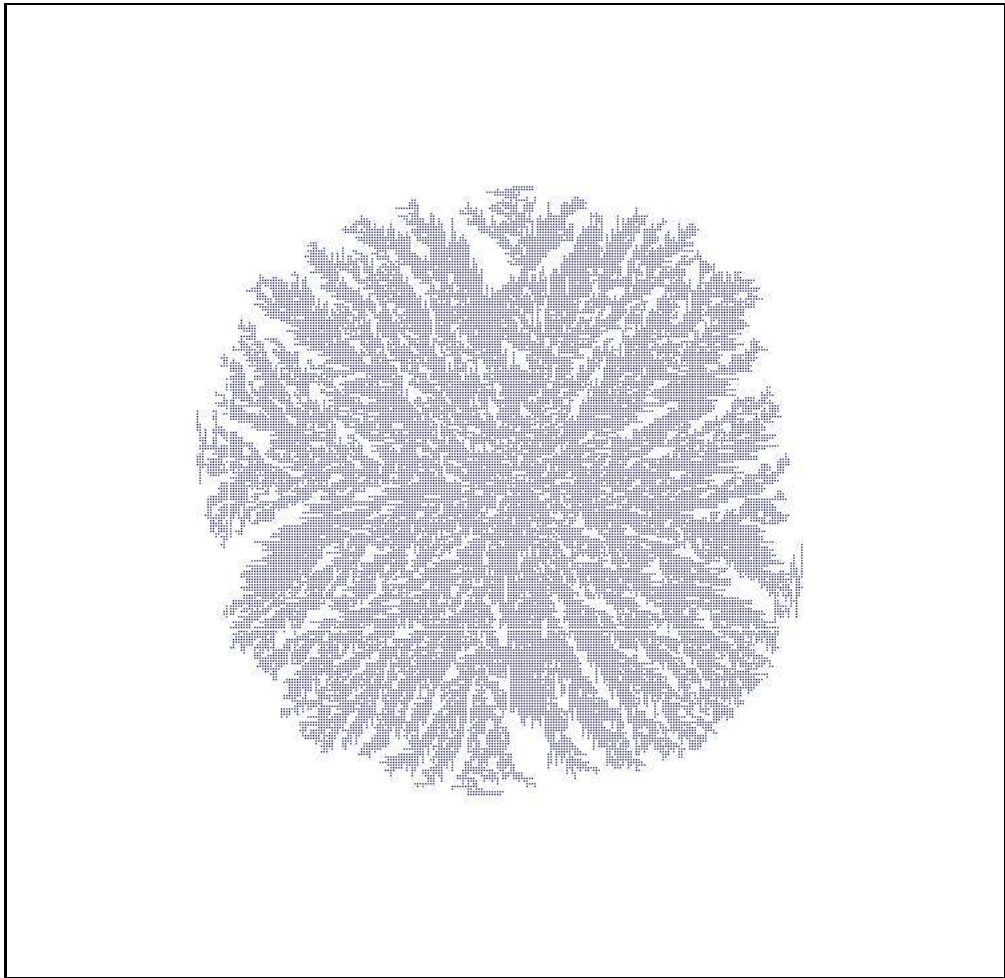


Figure 5.11: Cluster formed at an initial density of 0.2 pieces per node after 8000 time steps. A dense little center is noticed together with a gradual development of branches at the outsides. (Horizontal and vertical lines in the picture are an artifact from the program used for visualization).

clusterize. However, in a real system this value could be severely affected by the fact that the pieces are immersed in an environment made by non-sticky molecules that would slow the growth process. So, higher densities would be required in real systems in order to obtain the same dense structures.

In figure 5.12 we display the conversion rate from free pieces to clustered pieces for five different densities under 0.1 pieces per node. The growth of the contour of the cluster is self-promoted: more perimeter favors the attachment of new pieces, and new pieces means (almost always) more perimeter. This explains why the peak of conversion is displaced to the right as the density is reduced as a consequence

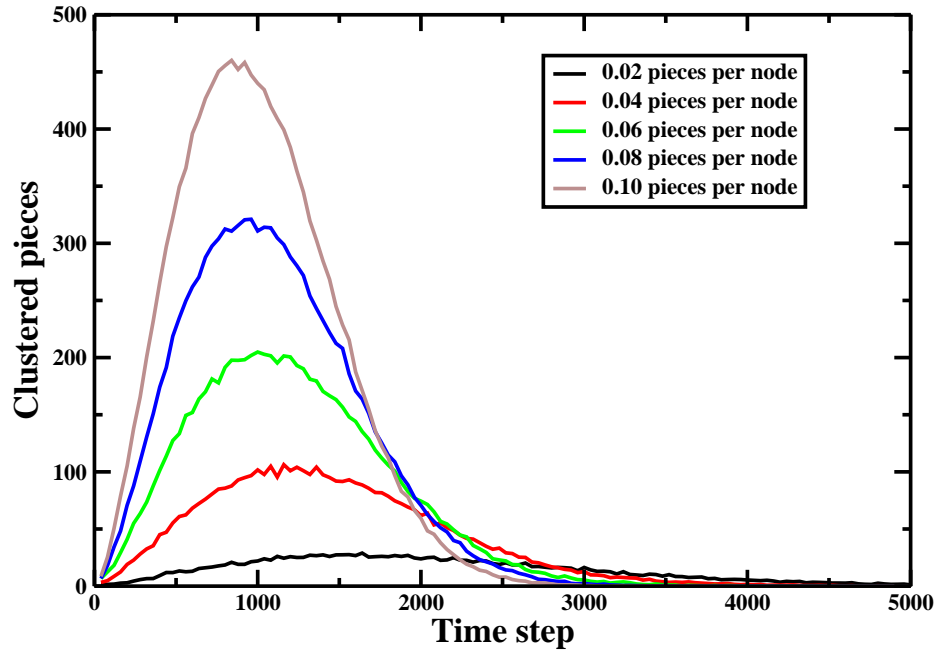


Figure 5.12: Conversion speed for five different densities, all of them below 0.1 pieces per node, in a grid of 400 x 400 nodes.

of the slower growth of the contour of the cluster. Of course, the right side of the graphics corresponds to the depletion of the number of free pieces. For a density of 0.02 pieces per node the peak of conversion has practically disappeared, indicating that the velocity of conversion is comparatively constant for this combination of density and grid size. However, this behavior indicates that this system is close to the lower cluster density that can be reached for this model. A measure for this is discussed in the following.

We can use several quantities for characterizing the clusters that results from simulations. In this work we have used two. The first of them is to calculate the rate between the perimeter of the cluster to the total number of pieces in the cluster. This is a direct analog of the surface to volume rate that is so important at nanoscales. It is clear that its maximum value in two dimension is four, where all sides of all pieces are exposed so they are the perimeter, although it is also obvious

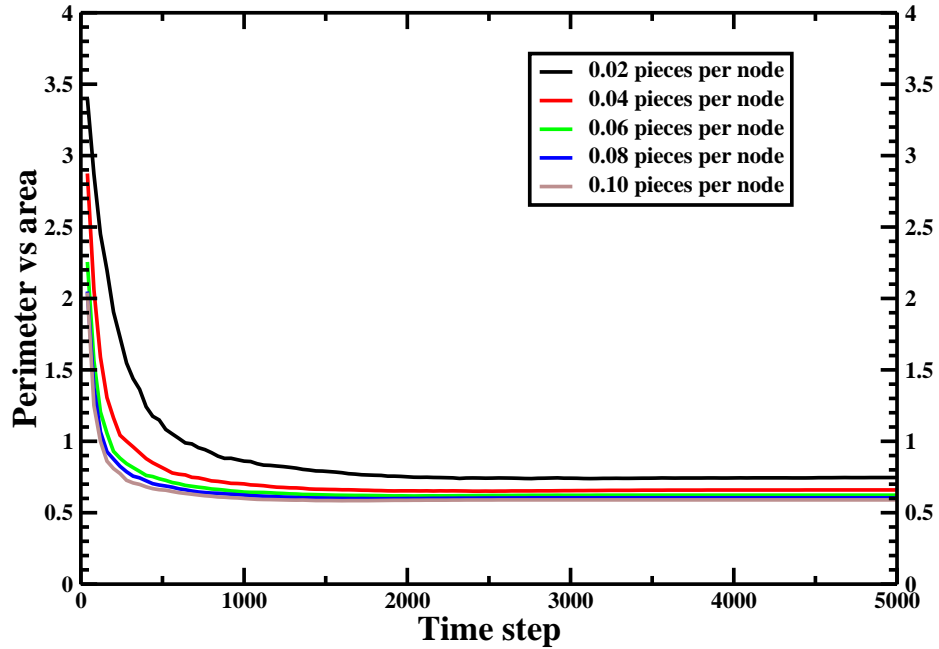


Figure 5.13: Relation between perimeter and area for five different densities.

that this value is not possible for a cluster with more than one piece. An estimate of the minimum value is also easy to calculate. For a completely dense and squared arrangement of  $N \times N$  pieces the area is  $N^2$  and the perimeter is  $4N$ , so the rate contour vs area is  $4/N$ . This number could be as close to zero as desired if  $N$  can be as large as needed if a perfect squared arrangement without holes is formed. In our simulations the values for this measure were between 0.56 and 0.40 for densities between 0.2 and 0.7 pieces per node. In figure 5.13 the behavior for this measure for densities under 0.1 pieces per node is plotted. The measures are between 0.6 and 0.75, with the higher value corresponding to the lower density. This is less than one side exposed per clustered piece. This is in agreement with the formation of a clustered structure with a lower density and more perimeter that is related with the branched nature of the final structure. However, for lower densities this value has a limiting value related with structure, determined by the nature of DLA systems, and the specific value depends on the conditions imposed to the model presented.

The second measure that we have considered is related to the “counting box method”. The dimension  $D$  calculated by this method sometimes coincide with the Hausdorff exponent, a measure used for systems with fractal properties, such as DLA structures and the Sierpinski triangle. This is expressed as:

$$D = \lim_{\epsilon \rightarrow 0} \frac{\ln(N)}{\ln(1/\epsilon)}, \quad (5.1)$$

where  $N$  is the minimum number of squared boxes of side  $\epsilon$  needed to cover the structure. This measure assumes that the side of the smallest square box that covers the whole structure has a length of one unit. For the clusters that result from our simulations we propose a measure  $F$  (from “false fractality measure”), that is defined as:

$$F = \frac{\ln(N)}{\ln(1/SideLength)}, \quad (5.2)$$

where  $N$  is the number of clustered pieces, and “*SideLength*” is the length of the side of the smallest square box that covers completely the cluster. The measure  $F$  assumes that the length of a node (or a piece) is the unity.

It is worth noting that no finite algorithm can perform the computation of the Hausdorff exponent in its formal mathematical definition. On the other hand, the dimension  $D$  calculated from the counting box method can be identified in some systems as a numerical approximation to the value expected if self-similarities would exist at all length scales. From this point of view, our measure  $F$  can be considered as the real measure of the structure obtained by the simulation, in the sense that it does not discard its finite number of pieces and scales involved. However, it is expected that the value of  $F$  would be as close as desired to an “ideal” dimension  $D$  for a given set of parameters if the grid size is as large as needed and the initial density of pieces is inside a window of appropriated values.

In figure 5.14 the evolution of measure  $F$  for several densities is displayed. For densities over 0.1 pieces per node, the measure  $F$ , for a same initial density, shows

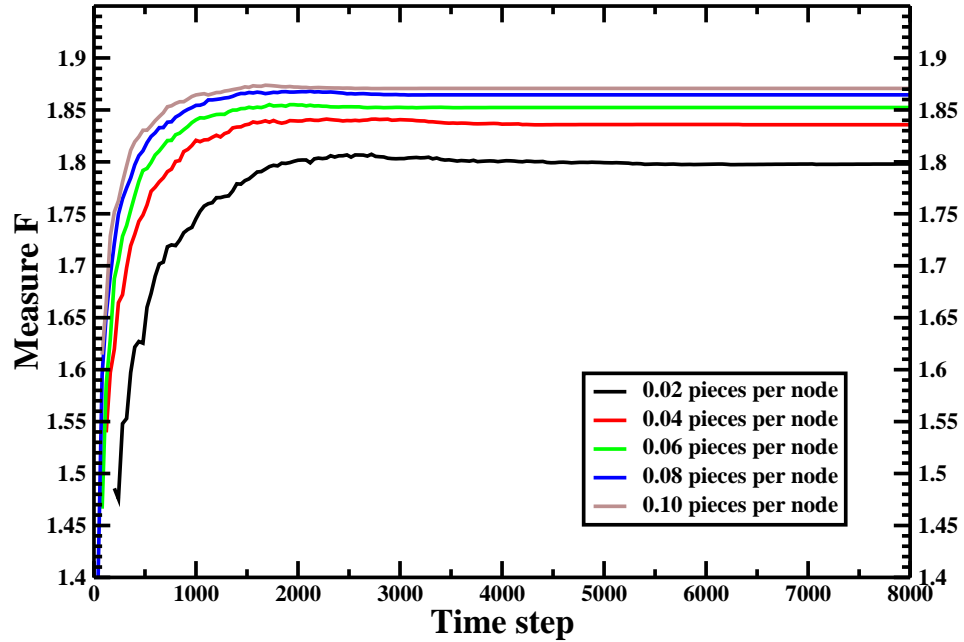


Figure 5.14: Time evolution of the measure  $F$  for different initial densities.

differences between the minimum and the maximum values of less than 0.03, with a reduction in the difference related with an increase in density. For lower densities the difference is higher, with a value of 0.08 for a density of 0.02 pieces per node (20 simulations, a grid of 400 x 400 nodes). For simulations using larger grids, such differences are reduced. The behavior of the measure  $F$  is in agreement with the presence of branches in the structure substituting the dense core of the cluster.

### 5.3.3 Systems with pieces with induced defects

We studied several systems that have “normal” pieces as well as “mutant” pieces. Normal pieces are defined as having all their extremes of the same kind, all of them being sticky. Mutant pieces are similar to the normal pieces but with defects: some of their extremes are not capable of forming a bond with any other extreme. This can be the result of a loss of the sticking ability due to chemical or physical changes. However, we consider in our simulations that such defects have been introduced

intentionally, with the purpose of inducing changes in the growth of the cluster structure. A normal piece can be considered as a piece without defects.

The mutant pieces considered are the following:

- One defective extreme (M1)
- Two defective extremes (North and East) (M2L)
- Two defective extremes (North and South) (M2I)
- Three defective extremes (M3)
- Four defective extremes (M4)

In order to study systems where defective pieces are introduced several simulations were performed using grids of 400 x 400 nodes, with a mixture of 50 percent of normal pieces and 50 percent of mutant pieces of only one kind. In addition, we have made simulations with a 100 percent of normal pieces as a control test, useful for comparisons. The total initial density considering both kinds of pieces was 0.1 pieces per node.

When all the pieces are normal the aggregate has the general appearance of a “traditional” DLA system, with a branched growth, although with a higher density at the core. This is the expected result, since this kind of pieces have no practical difference with pieces that were point-like instead of crosses.

When there are a half of normal pieces and a half of mutant M1 pieces the formed structures have a more defined branching growth, related with a lower structure density. The clusters appear to have a major global tendency to be rounded with respect to those in systems without mutant pieces. It could be that a more homogeneous distribution of pieces is promoted by the lower chance for attaching between pieces because of defects.

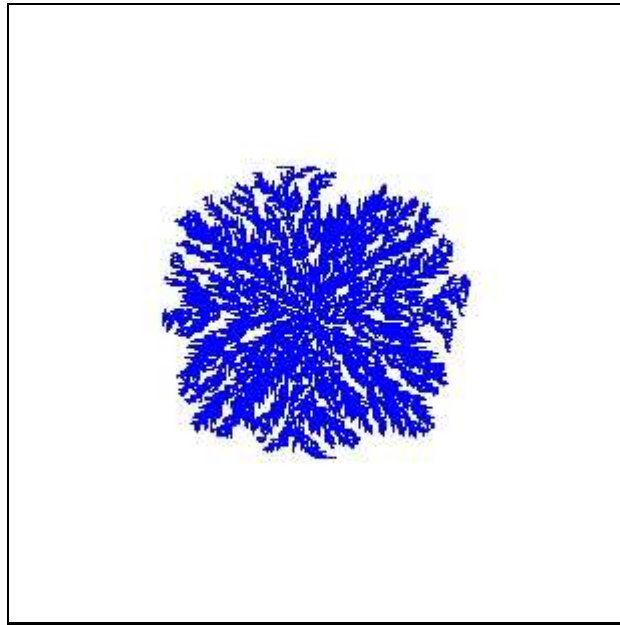


Figure 5.15: Cluster formed by pieces without defects. The initial density is 0.1 pieces per node and the grid is 400 x 400 nodes, 4000 time steps.

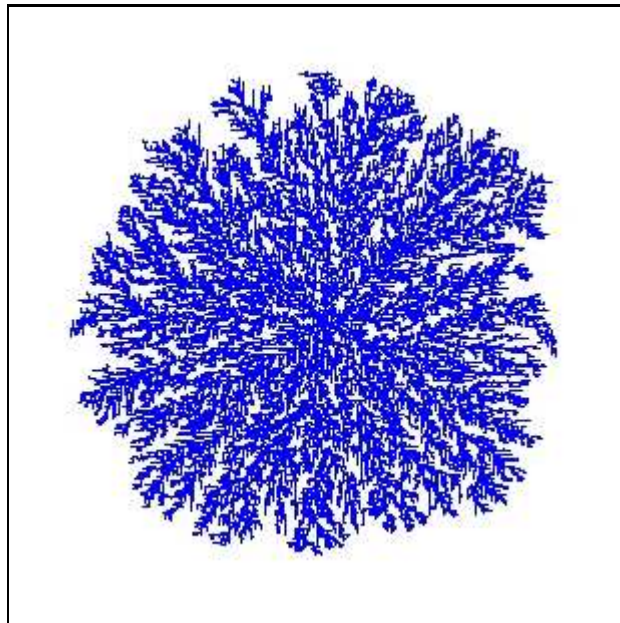


Figure 5.16: Cluster formed by normal pieces and M1 mutant pieces. The initial density is 0.1 pieces per node for a grid of 400 x 400 nodes, 8000 time steps.

Systems made up from an initial soup with half of M2L mutant pieces show even less denser structures, with branches with more internal curves. In some way, they make one to think about some branched systems in nature as some desertic or marine plants. The growth in the number of curves in the structure is obviously promoted by the kind of mutant pieces, that have their bonding extremes in a L fashion.

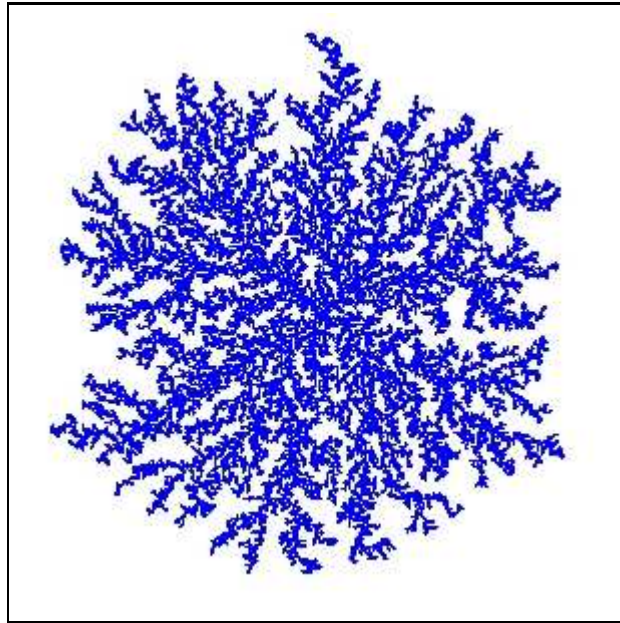


Figure 5.17: Cluster formed by normal pieces and M2L mutant pieces. The initial density is 0.1 pieces per node for a grid of 400 x 400 nodes, 8000 time steps.

When M2I mutant pieces are involved the aggregates show characteristics at different scales. At the smallest scale, the growth of vertical and horizontal stripes is promoted, as expected for the distribution of defects in the mutant pieces that favor the growth only along a line. However, at small scale the presence of normal pieces allows the formation of little orthogonal branches. This generates structures that resemble the smallest branches in a snowflake. At the global scale one can notice big branches but they are not well defined, instead they look diffuse due to the linear branches at the small scale. Those branches can grow in a radial fashion from the core or they can grow in a spiral fashion. The latter characteristic of the structure is global.

Structures made up from the mixing of normal and M3 pieces show two different densities at different scales. At small scale, the density of the branches is high, while at the global scale the density is lower. The mutant pieces M3 are strong inhibitors of growth because they have only one extreme able to establish bonding. Once they are attached to the cluster they close a direction of growth at the small scale. On the other hand normal pieces promote growth. So the structure is formed under a

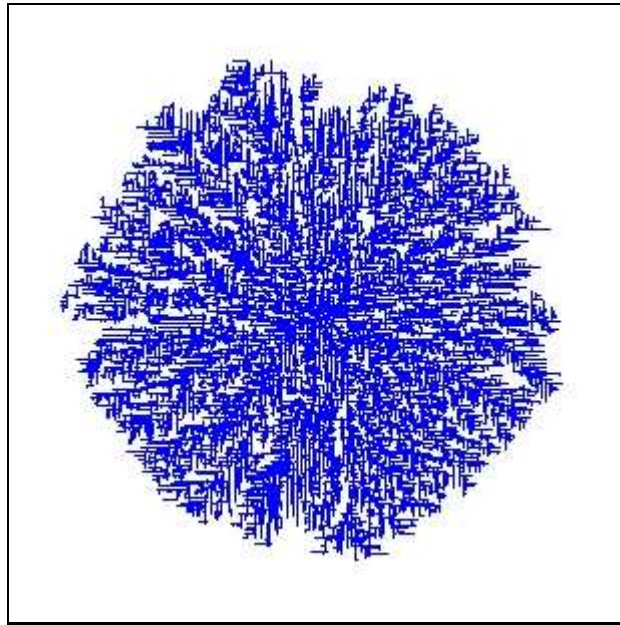


Figure 5.18: Cluster formed by normal pieces and M2I mutant pieces. The initial density of 0.1 pieces per node, same size and time steps as previous figures.

struggle between growth promoter (normal) pieces and growth inhibitor (M3) pieces. In this way, the structure is formed of dense but isolated branches.

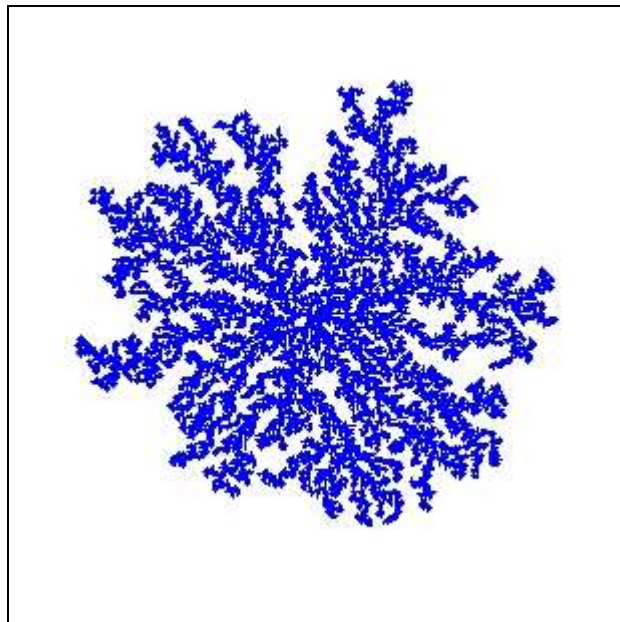


Figure 5.19: Cluster formed by normal pieces and M3 mutant pieces. Same conditions as in previous figures.

Combining normal pieces with M4 pieces is comparable to adding a molecular

environment rather than having pieces with defects. The global effect is a reduction in the rate of growth of the structure. This environment has an effect on the structure similar to reducing the initial density and therefore the resulting aggregates are closer to typical DLA systems. The structures are smaller than in the systems discussed above because the number of pieces that can be part of the cluster has been reduced to one half.

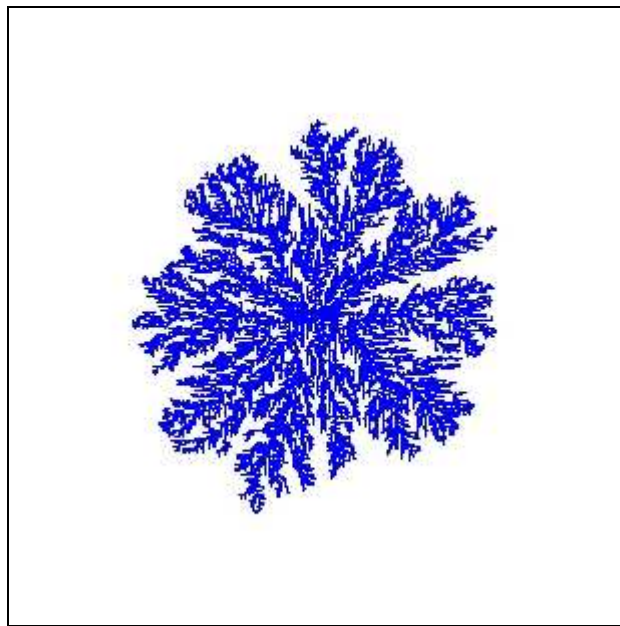


Figure 5.20: Cluster formed by normal pieces and M4 mutant pieces. The initial density is 0.1 pieces per node for a grid of 400 x 400 nodes, 8000 time steps.

In figure 5.21 the conversion rates for the systems discussed above are displayed. The initial total density is 0.1 pieces per node and a mixture of 50 percent of normal pieces and 50 percent of mutant pieces was used. The simulation with only normal pieces is also shown for reference. One notices that the conversion rate has a peak that is displaced to larger times and lower values as the attachment between pieces becomes more difficult. It is directly related with the number of non sticky extremes of the mutant pieces. However, the difference between the systems with the M2L and M2I mutant pieces is provoked not by the number of non sticky extremes per mutant piece but by the distribution of these non sticky ends all over the contour of the aggregate. The M2L pieces close the directions of growth locally and turn up the direction of growth by 90 degrees. The M2I pieces also close directions of

growth locally but they promote linear growth in a preferential direction.

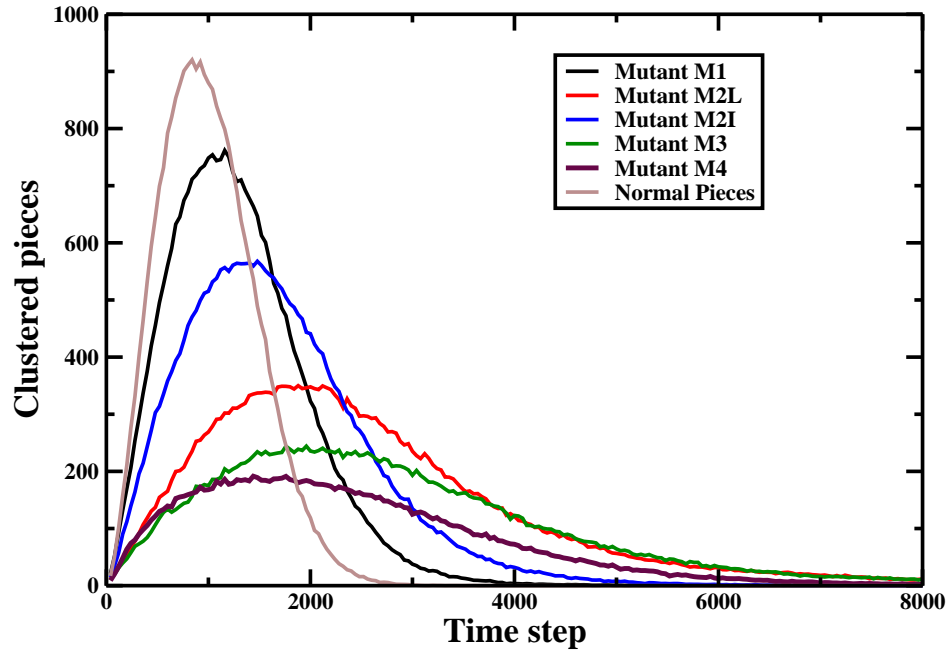


Figure 5.21: Conversion speed for systems with mutant pieces. Initial total density was 0.1 pieces per node in a grid of 400 x 400 nodes. Averages from 20 simulations of each kind of system.

The *perimeter/area* rate is a measure related to the size of compact structures, as the *surface/volume* rate for nanostructures. However, for non compact structures it is rather a measure of structural density at the local level. In our branched structures the *perimeter/area* rate is a way to express how compactly the closest neighbors inside branches are distributed and how much thick such branches are. Branches with the same density but different thickness have different *perimeter/area* rate. It is worthy to remark that how much separated or close the branches are between them does not change *perimeter/area* rate. Thus, for analyzing locally our structures this measure is better than calculating the function  $g(r)$  because our measure isolates the branch structure from global structure.

In figure 5.22 the evolution of *perimeter/area* rate for all the different simu-

lated systems is plotted. There is a valley for all systems on the first 1000 time steps that is related with the initial growth of a denser core when the density of free pieces is still high. After that, the branch structure takes more importance and there is a slight increase with a tendency to go to a stable value. Systems with M2I pieces goes to 1.04, the highest value for all the systems shown, because M2I pieces promote the growth of long and thin branches at the smallest scales. The systems with M2I, M1, M2L and M3 pieces follow a descendant tendency on their *perimeter/area* rates. Such a behavior corresponds to the ability of each kind of mutant piece for inhibiting the growth of branches at the smallest scale. If *perimeter/area* rate is lower then more pieces are inside the main branches and there are lesser “hairs”. This measure provides a way to analyze systems as the one with M4 mutant pieces where it is difficult to evaluate in a visual way the characteristics of branches at different scales. The M4 structure is in some way less branched that all the other systems unless the M3 system, and its branches are thicker. However, it is important to remember that the growth of M4 system is inhibited in two ways: the first is that it has the half of pieces able to attach compared with the other systems, and the second is that M4 pieces act as an environment.

The perimeter of the aggregates are formed by the extremes of the pieces, some of them are able to attach to extremes of free pieces and other are defective extremes of mutant pieces that are not able to establish a connection. If these extremes have different chemical or magnetic properties useful for a next step in an industrial production process it would be interesting to know which is the proportion of these two kinds of extremes. Figure 5.23 shows the proportion between non sticky extremes that are in the perimeter of the aggregate and the total of extremes forming the perimeter. The lowest value is for the system with M4 mutant pieces. It is just zero because M4 pieces can not attach to the cluster and therefore there is not any sticky extreme in the aggregate. For the other mutant pieces it is important to observe that the conditions for adding a new piece to the cluster inhibit the attachment of a piece with a given non sticky extreme, but that does not forbid the existence of a clustered piece aside this non sticky extreme if such piece is aggregated by attaching

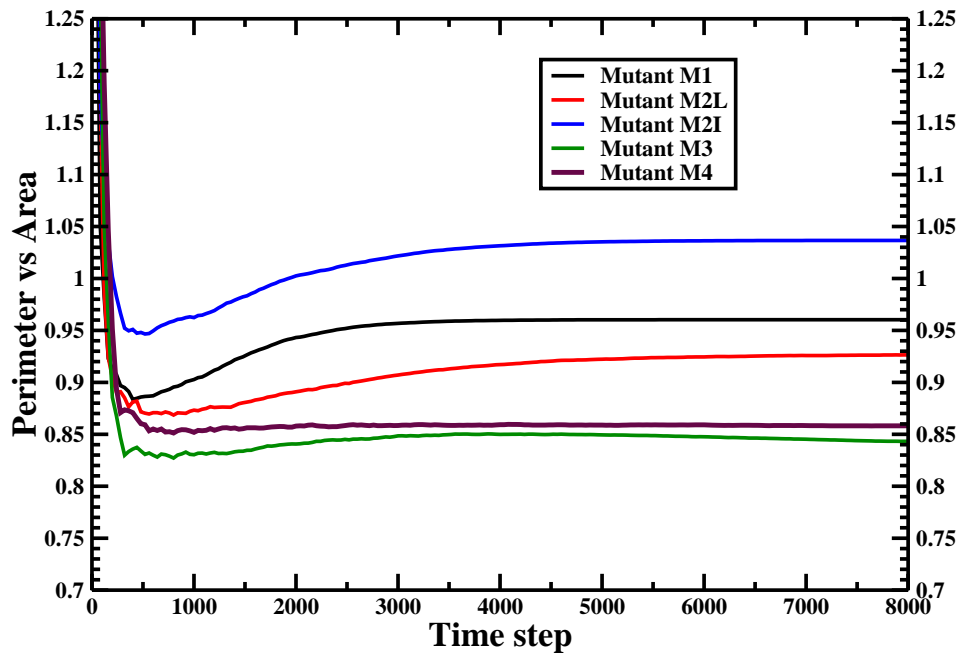


Figure 5.22: Perimeter vs area evolution for systems with mutant pieces. The initial total density is 0.1 pieces per node in a grid of 400 x 400 nodes. Averages from 20 simulations of each kind of system.

to a sticky end of other clustered piece. Non sticky extremes considered here do not have repulsive properties. Therefore, some non sticky extremes can be inside the cluster (not contributing to the perimeter) if the growth of the cluster covers them.

All systems follow an order correspondent with the number of non sticky ends in the mutant pieces but their particular values and dynamics are interesting by themselves. With M1 pieces the value goes to 0.2, that is close to  $\frac{1}{5}$  of the perimeter. The proportion at the beginning of simulation is  $\frac{1}{8}$  but sticky extremes are more prone to get inside the cluster where new pieces are attached to the aggregate. The following value of 0.345 correspond to systems with M2L pieces. This value is higher than that for M1 systems as expected but it is lower than 0.51, the value for M2I system. M2L pieces change the local direction of growth by 90 degrees but, at the same time, it promotes the feature that addition of new pieces to the cluster results in the covering of non sticky extremes, transforming them from perimeter-like to

inner-like. This is not the case for M2I pieces that promotes the growth in a linear fashion and therefore the growth of the perimeter. Finally, M3 pieces make slower the growth of the aggregate, but with enough time these systems reach the highest value.

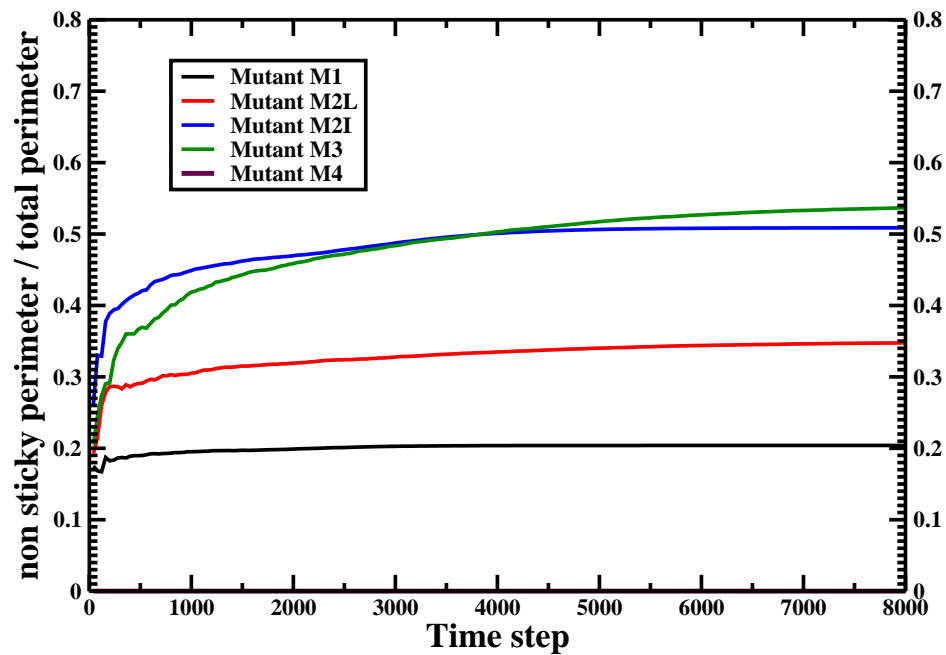


Figure 5.23: The non sticky perimeter vs total perimeter for systems with mutant pieces. The initial total density is 0.1 pieces per node in a grid of 400 x 400 nodes. Averages from 20 simulations of each kind of system

In figure 5.24 it is shown the time evolution of the measure  $F$ . This measure can be considered as a measure of the global density, in an independent way of the local structure or particular characteristics of the branches. The plot shows that the growth of branches at the smallest scale allows to have higher global densities and structures with principal branches more defined reach larger diameters and therefore lower densities. Systems with M2L pieces show a slightly different behavior, although they have branches that are mainly at the medium scale and they have a comparatively low global density.

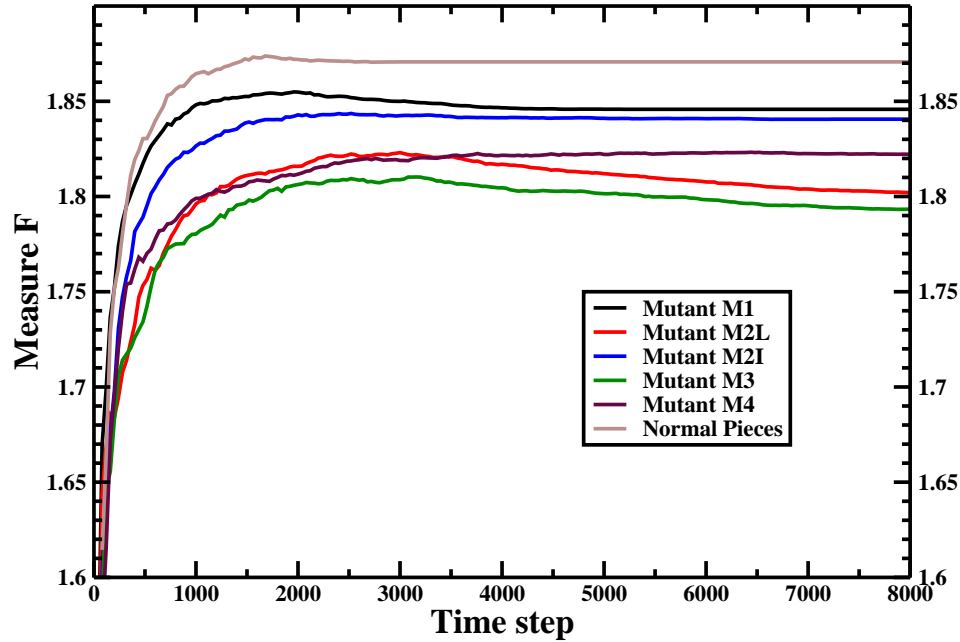


Figure 5.24: Time evolution of the measure  $F$  for systems with mutant pieces. The initial total density was 0.1 pieces per node in a grid of 400 x 400 nodes. Averages from 20 simulations of each kind of system

## 5.4 Conclusions and perspectives

A model for the aggregation of pieces (or molecules), interacting by dynamics rules based on LGCA methods has been described. In addition to traditional models, we have considered that particles are not just point-like, but they have a cross shape. This implies the consideration of rotations and orientation of pieces and gives us the possibility of considering a huge spectra of different pieces by defining different kinds of extremes and interactions between them. This is what makes our model different from previous ones. We have explored only the simplest possibilities as having all extremes of the same kind, complementary extremes in the same piece, two complementary extremes in two different pieces, and combination of pieces that have some extremes that lost their ability to establish a connection.

The conversion rates have been studied as well. All of them showed a main peak

related with the auto-catalytic nature of the growth of the perimeter of the cluster and the posterior scarcity of free pieces. The time step when this peak is located and its height are determined by the initial density of pieces and by the probability of having pieces with complementary sticky extremes in the right orientation and place. Therefore, the definition of interactions between extremes and the kind of pieces are fundamental factors for the conversion rates.

The employed model shows us that the selection of pieces and densities has a major effect on the morphology of the aggregates. For high initial densities, aggregates have a dense core and a less dense outer section. For lower initial densities one can see the effect of pieces with defects on the morphology of aggregates at the smaller and global scale. Different pieces promote different patterns of growth as follows: promotion or inhibition of branches at the smaller scale, changes in the thickness of branches at the medium and global scales, changes in global density, growth on radial or spiral branches. Working with combinations of different densities and pieces would give us an even broader variety of structures.

Three measures have been proposed and involved for the study of the formed structures. The measure  $\mathbf{F}$  gives us an idea of how dense is the structure at the global scale at the same time disregarding local properties. This measure was inspired by the calculation of fractal dimensions through the box counting method. The second measure is the *perimeter/area* rate that is inspired in the *surface/volume* rate for systems at the nanometric scale. This measure gives us an idea about the structure and density of the branches of the aggregates, with the additional property of disregarding global properties of the cluster. The combination of these two measures provides us with a better understanding of the formed structures than would be possible with the well known  $\mathbf{g}(\mathbf{r})$  calculation. The last measure was simply the proportion between the number of non sticky extremes that are part of the perimeter and the total number of extremes forming the perimeter. With this quantity we can have an idea of the size of an “armored against growth” frontier in the aggregates.

All these results suggest that it is possible to create experimental aggregated structures at the micro and nano scales with partial control on their local and global properties. It would be possible to produce aggregates made of alternated sections of different morphologies and densities, going, of course, from higher densities at the core to lower densities at the outsides. The control on local and global densities as well as the kind of branching would allow to produce small structures with enhanced properties for physical absorption of preferred sizes of particles. The control of the proportion of different kind of extremes at the perimeter (and also in the bulk) would do the same from the chemical point of view. It is also possible to consider magnetic and non magnetic extremes for similar purposes. The controlled attachment of several particles over these designed aggregates could be the initial step for industrial production of materials with special surface properties at very low costs due to the easy implementation of the self-assembly process. Some experimental research can be related with the results presented here. We refer to the work presented by Grill *et. al.* [22], where the assembling of crosses has been performed (see figure 5.25).

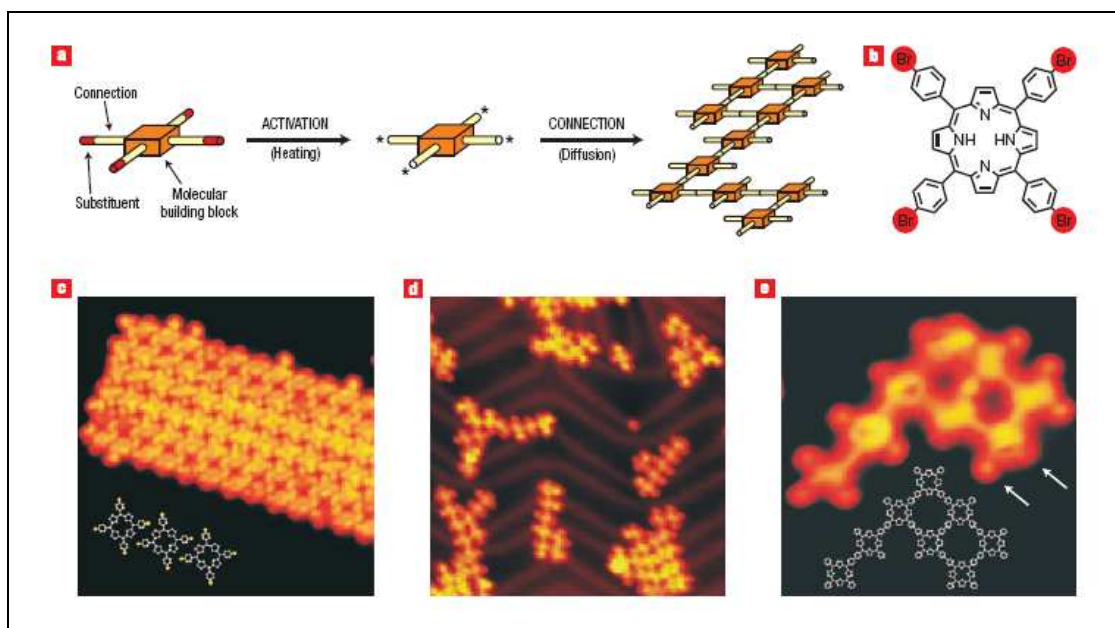


Figure 5.25: Formation of covalently connected networks (CNN). a) Formation of CNN: concept. b) Chemical structure of tetra(4-bromophenyl)porphyrin. c) Structure before activation. d) Formed structures with activation previous to deposition. e) Final formed structures. Figure from [22]

It is noteworthy to observe that the model presented in this chapter is capable of important extensions such as the inclusion of energy considerations for the attachment and detachment of molecules, conformational changes of the pieces, and the implementation of pieces with different geometries (triangles, hexagons). More complex and specifically designed structures can be studied in order to explore how much information is needed for a specific structure and how much information could be structurally carried by pieces under certain restrictions. Hierarchical structures could be also implemented in a far more advanced version of the model presented here.

**REFERENCES**

1. G. M. Whitesides, J. P. Mathias and C. T. Seto, *Science* **254**, 1312 (1991)
2. S. Zhang, *Nature Biotechnology* **21**, 1171 (2003)
3. G. M. Whitesides and B. Grzybowski, *Science* **295**, 2418 (2002)
4. G. M. Whitesides and M. Boncheva, *Proc. Nat. Ac. Sci. U.S.A* **99**, 4769 (2002)
5. J. Oullete, *The Industrial Physicist* (26-29) Dec 2000
6. N. Bowden, A. Tetfort, J. Carbeck and G. M. Whitesides, *Science* **276**, 233 (1997)
7. T. L. Breen, J. Tien, S. R. J. Oliver, T. Hadzic and G. M. Whitesides, *Science* **284**, 948 (1999)
8. J. E. Padilla, C. Colovos and T. O. Yeates, *Proc. Nat. Ac. Sci. U.S.A* **98**, 2217 (2001)
9. P. W. K. Rothmund, *Nature* **440**, 297 (2006)
10. P. W. Rothmund, N. Papadakis and E. Winfree, *PLoS Biol.* **2**, 2041 (2004)
11. D. C. Rapaport, J. E. Thompson and J. Skolnick, *Computer Physics Communications* **121**, 231 (1999)
12. A. Troisi, V. Wong and M. A. Ratner, *Proc. Nat. Ac. Sci. U.S.A* **102**, 255 (2005)
13. M. Nilsson and S. Rasmussen, *Discrete Mathematics and Theoretical Computer Science AB(DMCS)*, **31** (2003)
14. R. Schulman and E. Winfree, in *DNA Computing*, *Lect. Notes in Comp. Sci.* 3384, 319-328 (2005), arXiv: cond-mat/0607317
15. R. L. Thompson and N. S. Goel, *J. Theor. Biol.* **131**, 351 (1988)

16. U. Frisch, B. Hasslacher and Y. Pomeau, *Phys. Rev. Lett.* **56**, 1505 (1986)
17. B. Chopard and M. Droz, *Cellular Automata Modeling of Physical Systems*, Cambridge University Press, Cambridge (1998)
18. L.-S. Luo, “The Lattice-Gas and Lattice Boltzmann Methods: Past, Present and Future”, in *Proceedings of the International Conference on Applied Computational Fluid Dynamics*, Beijing, 2000, edited by J.-H. Wu and Z.-J. Zhu (Beijing, China, 2000), p. 52. Available at <http://www.lions.odu.edu/~lluo/>
19. A. Deutsch and S. Dormann, *Cellular Automata Modeling of Biological Pattern Formation*, Birkhäuser (2005)
20. B. Chopard and M. Droz, *Cellular Automata Modeling of Physical Systems*, Cambridge University Press, New York (1998)
21. S. T. Griffith, *Growing Machines*, PhD Thesis, Media Art and Sciences at the Massachusetts Institute of Technology (2004)
22. L. Grill, M. Dyer, L. Lafferentz, M. Persson, M. V. Peters and S. Hecht, *Nature Nanotechnology* **2**, 687 (2007)

# Chapter 6

## Wavelet Analysis of Elementary Cellular Automata Signals

### 6.1 Overview

#### 6.1.1 Elementary Cellular Automata

General cellular automata have been defined in chapter two, they can be  $n$ -dimensional and have a set of  $q$  states for cell states ( $n$  and  $q \in \mathbb{N}$ ). There are multiple neighborhood options and the rules can be defined in several ways. However, the simplest cellular automata are defined in an infinite 1-D arrangement of cells, each of them being in one of only two states (black or white, 0 or 1) and the rules are explicitly defined using a neighborhood composed by the central cell and its closest two neighboring cells. These class of cellular automata are called *Elementary Cellular Automata* (ECA) [1].

ECA's can be formally defined as follows: Each cell (labeled  $i$ ) has, at a given time, two possible states  $s_i = \mathbf{0}$  or  $\mathbf{1}$ . The state  $s_i$  at time  $t + 1$  depends only on the triplet  $(s_{i-1}, s_i, s_{i+1})$  at time  $t$ :

$$s_i(t + 1) = \Phi(s_{i-1}(t), s_i(t), s_{i+1}(t)) . \quad (6.1)$$

To each of the eight possible configurations of a triplet of sites it is associated a

value  $\alpha_k = 0$  or  $1$  according to the following list:

$$\underbrace{111}_{\alpha_7} \quad \underbrace{110}_{\alpha_6} \quad \underbrace{101}_{\alpha_5} \quad \underbrace{100}_{\alpha_4} \quad \underbrace{011}_{\alpha_3} \quad \underbrace{010}_{\alpha_2} \quad \underbrace{001}_{\alpha_1} \quad \underbrace{000}_{\alpha_0} . \quad (6.2)$$

Each possible cellular automata rule  $R$  is characterized by the values  $\alpha_0, \alpha_1, \alpha_2, \alpha_3, \alpha_4, \alpha_5, \alpha_6, \alpha_7$ . There are clearly 256 possible choices. Each rule can be identified by an index  $\mathcal{N}_R$  computed as follows

$$\mathcal{N}_R = \sum_{i=0}^7 2^i \alpha_i , \quad (6.3)$$

which corresponds to the binary representation  $\alpha_7, \alpha_6, \alpha_5, \alpha_4, \alpha_3, \alpha_2, \alpha_1, \alpha_0$ .

An example is presented in Fig. 6.2 for rule 90 for a initial condition where only one cell is in the state “1” and all others are in the “0” state. In the top it is shown the neighborhood, made up by the central cell and its two closest neighboring cells. Then, the eight possibilities for the triplet configuration are presented in binary order, with the future state for the central cell correspondent to rule number 90 (01011010 in binary). Finally, it is shown the evolution of the system by the successive application of the rule.

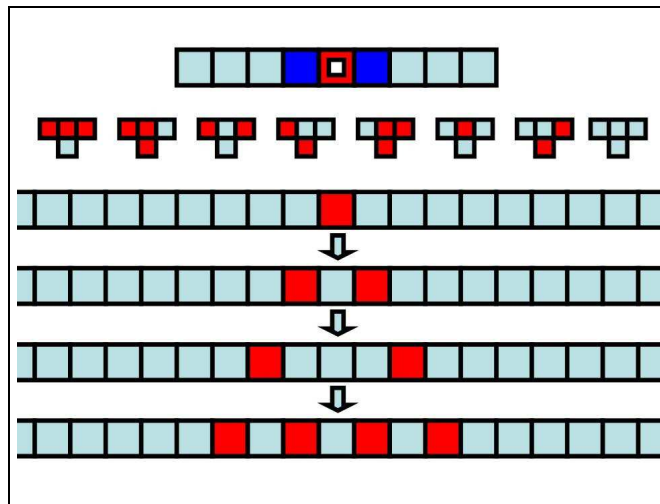


Figure 6.1: ECA number 90 evolution. It is depicted the neighborhood, the schematic representation of rule number 90, and the evolution of the system by applying three times the rule.

Despite its simplicity, these systems have presented interesting properties; for instance, rule 30 can be used as a random number generator, rule 90 is able to generate a Sierpinski triangle and rule 110 is capable of universal computation [2].

Given a rule and an initial state (random or not), one can study the time evolution of ECA's. Some results can be deduced analytically using algebraic techniques, but most of the conclusions follow from numerical iterations of the rules. A systematic study of these rules was undertaken by S. Wolfram in 1983 [1]. According to their behavior, he grouped the different rules in four different classes [2,3]:

Class 1 Evolve after a finite number of time steps from almost all initial states of the system to a unique homogeneous state (simple limit point).

Class 2 A pattern consisting of separated periodic regions (limit cycles) is produced from almost all initial states.

Class 3 These cellular automata evolve from almost all initial states to chaotic, aperiodic patterns (strange attractors).

Class 4 Persistent complex structures are formed for a large class of initial states (determined only by explicit simulation of their time evolution).

Although this classifications suffers of some drawbacks it shows that these simple systems are capable of generating quite complex behaviors and are worth of research.

### 6.1.2 Wavelet Method

The Fourier transform is the most popular method for signal analysis. It is a suitable technique for stationary signals because it is based on sinusoidal-like waves for decomposing signals. However, it has problems with providing the proper information

where non-stationary signals are studied. Therefore other methods of analysis, such as the Wavelet transform, have been developed in order to deal with non-stationary signals.

A wavelet is defined as a function  $\Psi(t)$  with finite energy that oscillates in a small time interval. This function satisfy that

$$\int_{-\infty}^{\infty} \Psi(t) dt = 0, \quad (6.4)$$

*i.e.* the mean value is zero.

From this wavelet (called *mother wavelet*), it is built an entire family of “daughter wavelets”, defined as:

$$\Psi_{a,b}(t) = \frac{1}{\sqrt{a}} \Psi\left(\frac{t-b}{a}\right), \quad (6.5)$$

where  $a > 0$  is the *scale parameter*, and  $b \in \mathbf{R}$  is the *translation parameter*.

If the parameters  $a$  and  $b$  are varied in a continuous way it is possible to analyze a signal by calculating the convolutions between the signal and the daughter wavelets. As occurs in the Continuous Fourier Transform, the original signal can be reconstructed from these convolution values although there is a great amount of redundant information.

Besides the Continuous Wavelet Transform (CWT) presented in more detail in Appendix B, there is also a discrete version, called Discrete Wavelet Transform (DWT), that decomposes a signal in an orthonormal basis without redundant information. This approach is specially appropriate for our work given that elementary cellular automata are discrete by definition.

If the scale and translation parameters are defined as:

$$a = 2^{-j} \quad \text{and} \quad b = k2^{-j}, \quad (6.6)$$

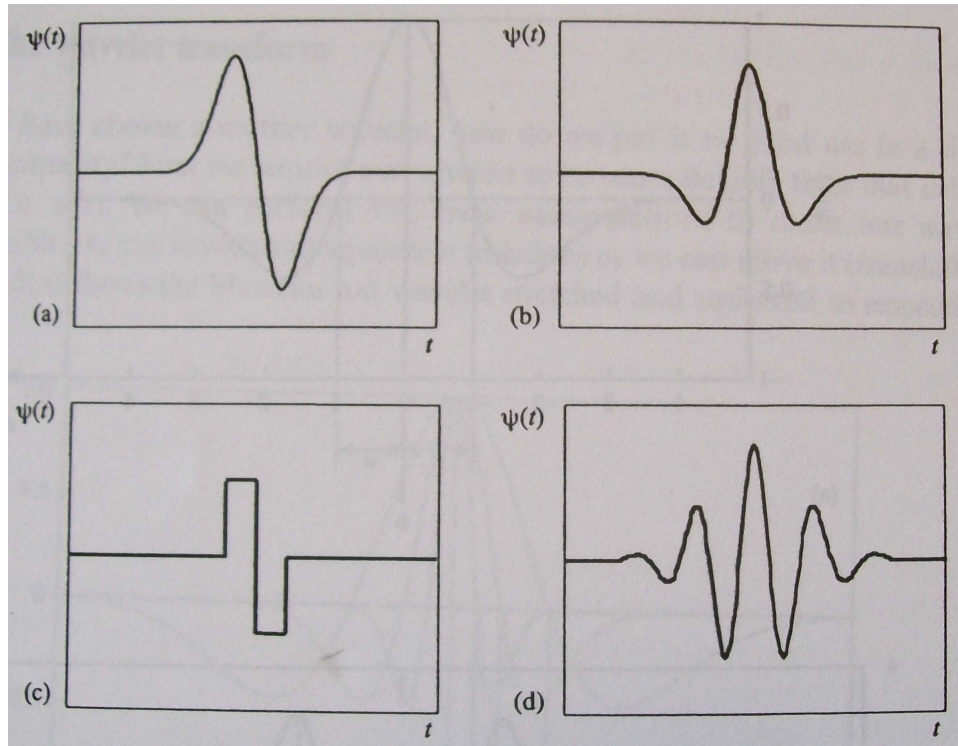


Figure 6.2: Four wavelets. a) Gaussian wave (first derivative of a Gaussian). b) Mexican hat (second derivative of a Gaussian). c) Haar. d) Morlet (real part). Figure from [4]

where  $j, k \in \mathbf{Z}$ , a Fast Wavelet Transform algorithm can be applied. Therefore, the family of wavelets can be represented by:

$$\Psi_{j,k}(t) = 2^{j/2} \Psi(2^j t - k). \quad (6.7)$$

Then,  $d_{j,k}$  coefficients are defined in the following way:

$$d_{j,k} = W_{\Psi} f(2^{-k}, k2^{-j}) = \int_{-\infty}^{\infty} f(t) \Psi_{j,k}(t) dt, \quad (6.8)$$

where  $f(t)$  is the signal to analyze. Therefore, the signal reconstruction corresponds to:

$$f(t) = \sum_{j=-\infty}^{\infty} \sum_{k=-\infty}^{\infty} d_{j,k} \Psi_{j,k}(t), \quad (6.9)$$

However, decomposition of the signal requires the use of Multi-Resolution Analysis (MRA) method; that consists in decomposing the signal level by level, performing convolution from the more localized wavelets to the less localized. The information

that can be represented by the wavelets at a given level is understood as “details” information, In each level, the MRA procedure works on the information that remains after subtracting the “details” information that can be represented by the previous level. So the information is separated at each level in “details” information and an “average” information that is passed to be decomposed in the next level. Reconstruction can be achieved by following this process in reversed order. In Appendix B the Wavelet formalism is presented in further detail.

## **6.2 Multifractal properties of elementary cellular automata in a discrete wavelet approach of MF-DFA**

In this section we analyze the behavior of the time signals produced by ECAs. As a main objective we are interested in detecting monofractal, multifractal and  $1/f^\alpha$ -like behavior. The work described here resulted from the collaboration between Ph. D. José Salomé Murguía, M. Sc. Jaime E. Pérez Terrazas and Ph. D. Haret Codratian Rosu; the results have been published in Europhysics Letters 87, 28003 (2009).

### **6.2.1 Introduction**

In 2005 Nagler and Claussen [16] investigated the time series of the elementary cellular automata (ECA) for possible (multi)fractal behavior. They eliminated the polynomial background  $at^b$  through the direct fitting of the polynomial coefficients  $a$  and  $b$ . We here reconsider their work eliminating the polynomial trend by means of the multifractal-based detrended fluctuation analysis (MF-DFA) in which the wavelet multiresolution property is employed to filter out the trend in a more speedy way than the direct polynomial fitting and also with respect to the wavelet transform modulus maxima (WTMM) procedure. In the algorithm, the discrete fast wavelet transform is used to calculate the trend as a local feature that enters the so-called

details signal. We illustrate our result for three representative cellular automata rules: 90, 105, and 150. We confirm their multifractal behavior and provide our results for the scaling parameters.

At the present time, a number of different algorithms are well established to analyze the singular behavior that may be hidden in time series data, such as the structure function method [5], the wavelet transform modulus maxima (WTMM) method [1, 5, 7, 8], the detrended fluctuation analysis (DFA) [9] and its variants [10–12]. DFA is a method used to analyze the behavior of the average fluctuations of the data at different scales after removing the local trends. In 2002, Kantelhardt *et. al.* [10] provided a generalization of DFA to the case of multifractal time series. Subsequently, the latter method started to be widely employed in the literature under the name of MF-DFA. Kantelhardt wrote a recent review of the techniques used in processing the fractal and multifractal time series [11]. On the other hand, a lot of research has been done on fractal signals and objects with wavelet transforms (WTs) because the multiscale decompositions implied by the WTs are well adapted to evaluate typical self-similarity properties. The efficiency of WTs as “mathematical microscopes” for capturing the local scaling properties of fractals have been noticed since more than two decades [13].

It is thus no wonder that there are current efforts towards merging the WTs with DFA procedures [14] as a natural union of powerful methods for quantifying the scaling properties of the fluctuations. In this short note, based on this unifying standpoint, which we call WMF-DFA, we focus on the MF properties of elementary CA with periodic boundary conditions. At the best of our knowledge, there is only one previous work dedicated to the MF features of CA [15] but there the analysis is performed on the time series of random walk processes generated by some of the evolution rules of cellular automata and not directly as we do here. In addition, Nagler and Clausen [16] mention in the final part of their work the possibility of considering their spectral analysis for multifractal signals instead of monofractal ones. We recall that many important applications of CA are in biology, chemistry,

and soft materials, where multifractal properties are to be expected. For example, an interpretation of CA rules 90 and 150 can be made in the context of catalytic processes [16], also rule 126 can be used as a conceptual model of biological cell growth [17]. On the other hand, rule 110 is interesting because it has been proven that any mathematical algorithm can be mapped to a CA having this rule and rule 30 can be considered as an intrinsic generator of randomness [2].

### 6.2.2 DFA with wavelets

An important advantage of the vanishing moment property of wavelets (see the Appendix) is that it helps detrending the data. We are interested in revealing the (multi)fractal properties [18] of elementary cellular automata. To separate the trend from fluctuations in the CA time series, we follow the discrete wavelet method proposed by Manimaran et al [14]. This method exploits the fact that the low-pass version resembles the original data in an “averaged” manner in different resolutions. Instead of a polynomial fit, we consider the different versions of the low-pass coefficients to calculate the “local” trend. Let  $\mathbf{x}(t_k)$  be a time series type of data, where  $t_k = k\Delta t$  and  $k = 1, 2, \dots, N$ . Then the algorithm that we employ contains the following steps:

1. Determine the profile  $\mathbf{Y}(\mathbf{k})$  of the time series, which is the cumulative sum of the series from which the series mean value is subtracted:

$$\mathbf{Y}(\mathbf{k}) = \sum_{i=1}^k (\mathbf{x}(t_i) - \langle \mathbf{x} \rangle) \quad (6.10)$$

2. Compute the FWT, i.e., the multilevel wavelet decomposition of the profile. For each level  $\mathbf{m}$ , we get the fluctuations of the  $\mathbf{Y}(\mathbf{k})$  by subtracting the “local” trend of the  $\mathbf{Y}$  data, i.e.,

$$\Delta \mathbf{Y}(\mathbf{k}; \mathbf{m}) = \mathbf{Y}(\mathbf{k}) - \tilde{\mathbf{Y}}(\mathbf{k}; \mathbf{m}), \quad (6.11)$$

where  $\tilde{\mathbf{Y}}(\mathbf{k}; \mathbf{m})$  is the reconstructed profile after removal of successive details

coefficients at each level  $m$ . These fluctuations at level  $m$  are subdivided into windows, i.e., into  $M_s = \text{int}(N/s)$  non-overlapping segments of length  $s$ . This division is performed starting from both the beginning and the end of the fluctuations series (i.e., one has  $2M_s$  segments). Next, one calculates the local variances associated to each window  $\nu$

$$F^2(\nu, s; m) = \text{var}\Delta Y((\nu - 1)s + j; m) , \quad (6.12)$$

where  $j = 1, \dots, s$  ,  $\nu = 1, \dots, 2M_s$  ,  $M_s = \text{int}(N/s)$  .

3. Calculate a  $q$ th order fluctuation function defined as

$$F_q(s; m) = \left\{ \frac{1}{2M_s} \sum_{\nu=1}^{2M_s} |F^2(\nu, s; m)|^{q/2} \right\}^{1/q} \quad (6.13)$$

where  $q \in \mathbb{Z}$  with  $q \neq 0$ . Because of the diverging exponent when  $q \rightarrow 0$  we employed in this limit a logarithmic averaging

$$F_0(s; m) = \exp \left\{ \frac{1}{2M_s} \sum_{\nu=1}^{2M_s} \ln |F^2(\nu, s; m)| \right\} , \quad (6.14)$$

as in [10, 19].

In order to determine if time series, under analysis, have a fractal scaling behavior, the fluctuation function  $F_q(s; m)$  should reveal a power law scaling

$$F_q(s; m) \sim s^{h(q)} , \quad (6.15)$$

where  $h(q)$  is called the generalized Hurst exponent [19] since it can depend on  $q$ , while the original Hurst exponent is  $h(2)$ . If  $h$  is constant for all  $q$  then the time series is monofractal, otherwise it has a multifractal behavior. In the latter case, one can calculate various other multifractal scaling exponents, such as  $\tau(q)$  and  $f(\alpha)$  [18].

### 6.2.3 Application to one-dimensional CAs

We apply the previous algorithm to the time series of three illustrative one-dimensional elementary cellular automata (ECA) as classified by Wolfram in 1984 [20]. The chosen rules are the following: 90, 105, and 150. For the first and the last rules the updates are given by

$$\mathbf{x}_n^{t+1} = [\mathbf{x}_{n-1}^t + r\mathbf{x}_n^t + \mathbf{x}_{n+1}^t] \bmod 2, \quad (6.16)$$

where  $r = 0$  and  $r = 1$ , respectively. It is well known that rule 90 has the appearance of a Sierpinski triangle when responding to an impulse (first row is all 0s with a 1 in the center). Nagler and Claussen [16] found that the ECA with rule 150 displays a Sierpinski-like self-similar structure of fractal dimension  $\mathbf{d}_F = 1.69$  (golden mean) instead of the standard one of 1.58. In a subsequent paper [21], Claussen showed that its time behavior can be solved as a two-step vectorial, or string, iteration, which can be viewed as a generalization of Fibonacci iteration generating the time series from a sequence of vectors of increasing length. This could explain the difference in the fractal dimension. Finally, it is known that rule 105 is complementary to the rule 150, i.e.  $\mathbf{f}_{105} = \mathbf{1} - \mathbf{f}_{150}$ , where  $\mathbf{f}$  is the neighborhood-dependent updating rule.

Data for rules 90 and 150 are valid for periodic conditions as well as for infinite CA because CA size has been chosen large enough (cells in CA are more than twice the number of time steps) and the few cells with a “1” in the initial setup (three or less) were put at the center so data generated is the same for both cases. It is possible due to these rules are pair and a strip of zeros produces a strip of zeros in the next iteration. Then, it can be considered that “information” or “effect” due to initial conditions does not cross the boundaries. It is not the case for rule 105, where a strip of zeros produces a strip of ones in the next iteration; and a strip of ones produces a strip of zeroes. For rule 105 we isolated the effect of the initial conditions (ones in the setup) by substrating the data from the total number of cells when the data is generated after a number odd of iterations. It is at least as significant as the detrending made by Nagler and Claussen [16] but with the advantage that the data

used for analysis is independent of the number of cells selected for the CA simulation.

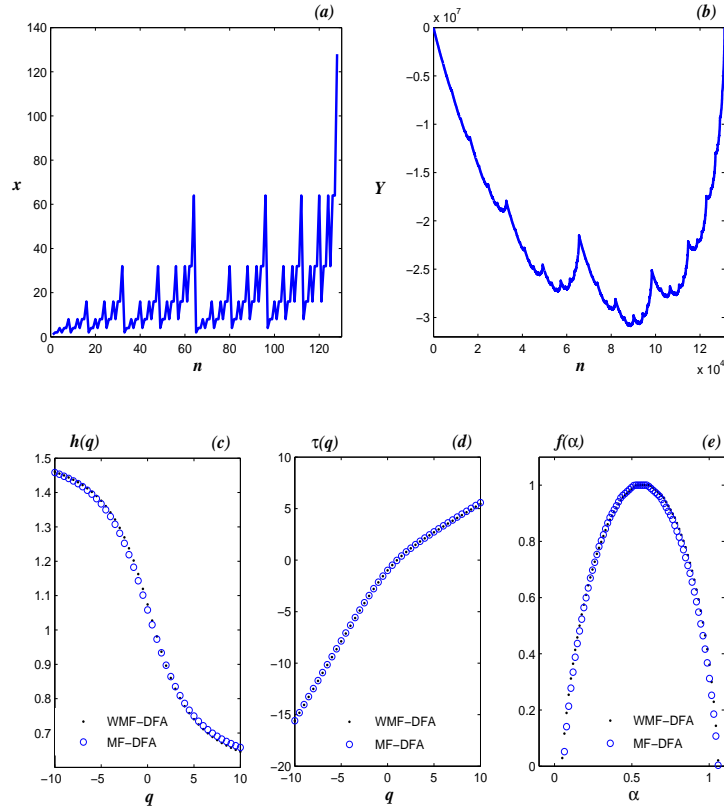


Figure 6.3: Rule 90: (a) Time series of the CA row signal. Only the first  $2^7$  points are shown of the whole set of  $2^{17}$  data points. (b) Profile  $Y$  of the row signal. (c) Generalized Hurst exponent  $h(q)$ . (d) The  $\tau$  exponent,  $\tau(q) = qh(q) - 1$ . (e) The singularity spectrum  $f(\alpha) = q \frac{d\tau(q)}{dq} - \tau(q)$ . The calculations of the multifractal quantities  $h$ ,  $\tau$ , and  $f(\alpha)$  are performed both with MF-DFA and the wavelet-based MF-DFA.

### 6.2.4 Conclusions

We have analyzed the time series of the so-called row sum (or total activity) of the ECA signals, i.e., the sum of ones in sequences of rows, employing Daubechies (Db) wavelets. Various types of Db wavelets have been used but we have found that a better matching of the results given by the wavelet-based MF-DFA method with those of other methods is provided by the Db-4 wavelets with four filter coefficients. Our results are illustrated in Figs. (6.3)-(6.5). The fact that the generalized Hurst

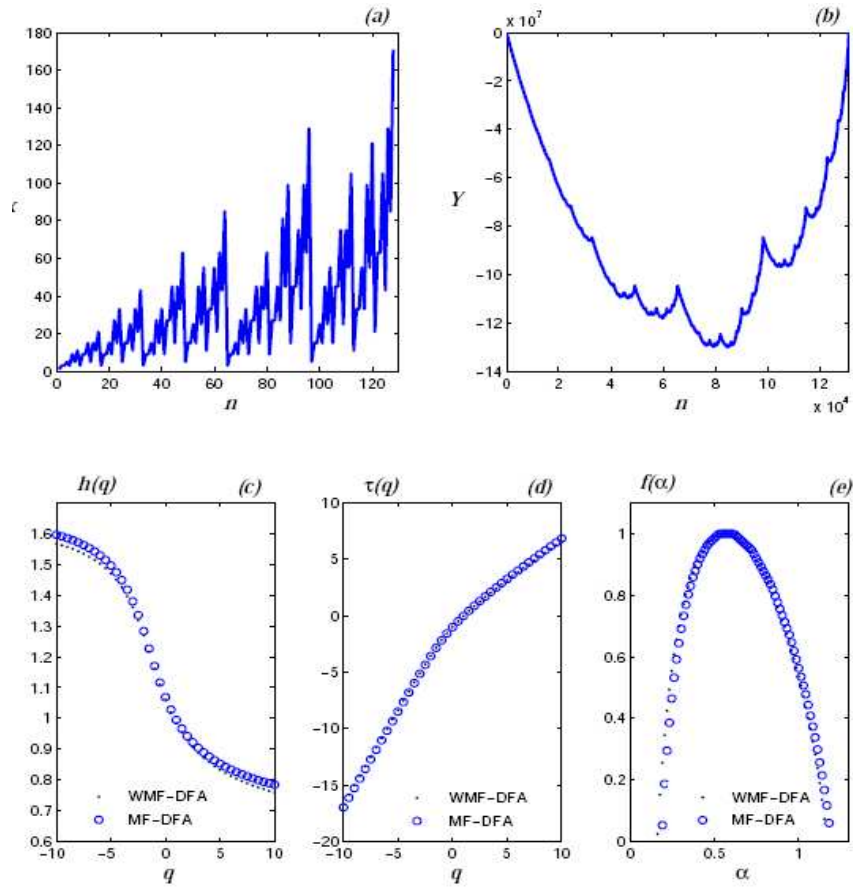


Figure 6.4: Rule 150: (a) Time series of the CA row signal. Only the first  $2^7$  points are shown of the whole set of  $2^{17}$  data points. (b) Profile  $Y$  of the row signal. (c) Generalized Hurst exponent  $h(q)$ . (d) The  $\tau$  exponent,  $\tau(q) = qh(q) - 1$ . (e) The singularity spectrum  $f(\alpha) = q \frac{d\tau(q)}{dq} - \tau(q)$ . The calculations of the multifractal quantities  $h$ ,  $\tau$ , and  $f(\alpha)$  are performed both with MF-DFA and the wavelet-based MF-DFA.

Table 6.1: The Hurst exponent  $h(2)$  for the three CA rules examined in this paper as obtained by means of the MF-DFA method and in each of the cases for four different initial setup (first row) as indicated.

	MF-DFA			
	I (...010...)	II (...0110...)	III (...01010...)	IV (...01110...)
R90	0.8972	0.8972	0.8898	0.9451
R150	0.9427	0.9413	0.9541	0.9296
R105	0.9427	0.9413	0.9542	0.9296

exponent is not a constant horizontal line is indicative of a multifractal behavior in all three cases. In addition, the fact that the  $\tau$  index is not of a single slope is an-

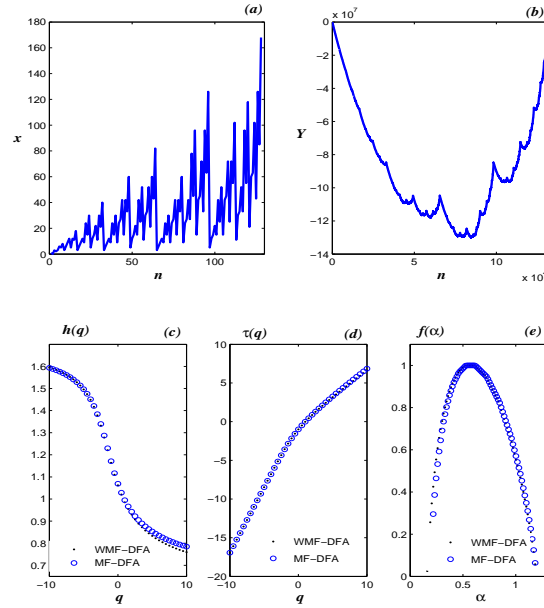


Figure 6.5: Rule 105: (a) Time series of the CA row signal. Only the first  $2^7$  points are shown of the whole set of  $2^{17}$  data points. (b) Profile  $Y$  of the row signal. (c) Generalized Hurst exponent  $h(q)$ . (d) The  $\tau$  exponent,  $\tau(q) = qh(q) - 1$ . (e) The singularity spectrum  $f(\alpha) = q \frac{d\tau(q)}{dq} - \tau(q)$ . The calculations of the multifractal quantities  $h$ ,  $\tau$ , and  $f(\alpha)$  are performed both with MF-DFA and the wavelet-based MF-DFA.

Table 6.2: The Hurst exponent  $h(2)$  for the three CA rules examined in this paper as obtained by means of the WMF-DFA method and in each of the cases for four different initial setup (first row) as indicated.

	WMF-DFA			
	I (...010...)	II (...0110...)	III (...01010...)	IV (...01110...)
R90	0.8961	0.8961	0.9229	0.9787
R150	0.9293	0.9529	0.9513	0.9407
R105	0.9294	0.9529	0.9514	0.9407

other clear feature of multifractality. The values of the Hurst exponent  $h(2)$  for four types of initial conditions are given in Table 1. We also present the corresponding fluctuation function  $F_2$  in Fig. (6.6) for the impulsive initial condition. The strength of the multifractality is roughly measured with the width  $\Delta\alpha = \alpha_{\max} - \alpha_{\min}$  of the parabolic singularity spectrum  $f(\alpha)$  on the  $\alpha$  axis. For example, for the impulsive initial condition,  $\Delta\alpha_{90} = 0.9998(1.0132)$ ,  $\Delta\alpha_{150} = 1.011(1.0075)$ , and

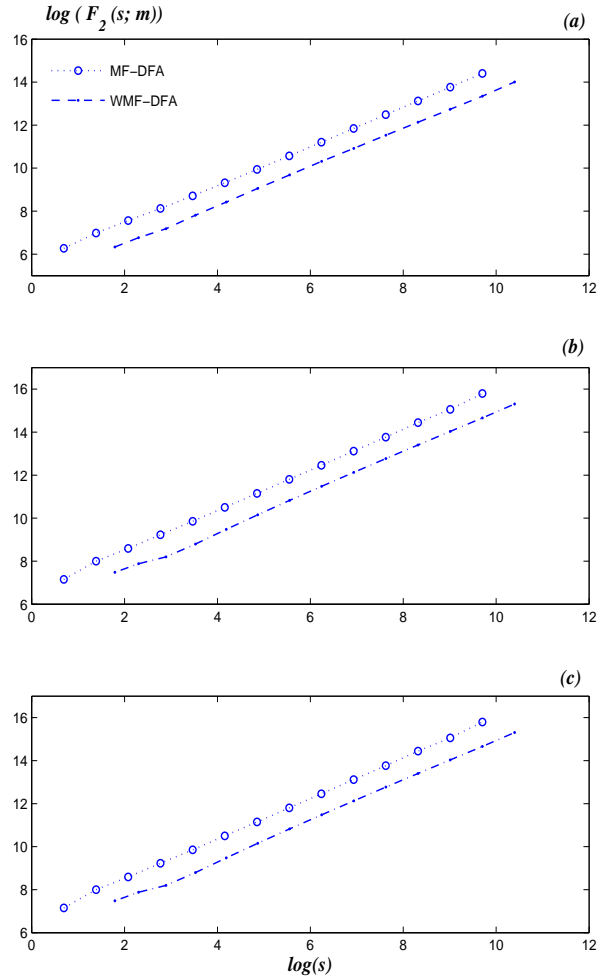


Figure 6.6: Log-log plot of the fluctuation function  $F_2$  versus scale for: (a) rule 90, (b) rule 150, and (c) rule 105.

$\Delta\alpha_{105} = 1.0083(1.0325)$  when the MF-DFA (WMF-DFA) are employed. We notice that the most “frequent” singularity for all the analyzed time series occurs at  $\alpha = 0.568$ , where the width  $\Delta\alpha$  of rule 90 is shifted to the right with respect to those of 105 and 150. According to our results, the strongest singularity  $\alpha_{min}$ , of all time series corresponds to the rule 90 and the weakest singularity,  $\alpha_{max}$ , to the rule 150.

In conclusion, in general terms, our algorithm implementation shows that embedding the discrete wavelet transform in the MF-DFA technique is a well-suited

procedure to analyze the multifractal properties of the ECA. Indeed, we get similar results to the other methods but computationally faster because we employ a lesser number of windows. Our results represent a confirmation of the fact that ECA patterns of different magnitudes follow different scaling laws, *i.e.*, the ECA have intrinsic multifractality that does not depend on the set of initial data that we used. Therefore, when processes thought to be multifractal are simulated with (E)CA, their intrinsic multifractal behavior should be taken into account as a feature of the simulation procedure rather than of the multifractal behavior of the simulated processes.

***REFERENCES***

1. S. Wolfram, Rev. Mod. Phys. **55**, 601 (1983)
2. S. Wolfram, A New Kind of Science, Wolfram Media, Inc. (2002)
3. S. Wolfram, Nature **311**, 419 (1984)
4. P. S. Addison, *The Illustrated Wavelet Transform Handbook, Introductory Theory and Applications in Science, Engineering, Medicine and Finance*, published by Taylor & Francis Group, New York (2002)
5. J. F. Muzy, E. Bacry and A. Arneodo, Phys. Rev. E **47**, 875 (1983)
6. E. Bacry, J. F. Muzy and A. Arneodo, J. Stat. Phys. **70**, 635 (1993)
7. J. F. Muzy, E. Bacry and A. Arneodo, Int. J. of Bifurcation and Chaos **4**, 245 (1994)
8. A. Arneodo, E. Bacry and J. F. Muzy, Physica A **213**, 232 (1995)
9. C. K. Peng, S. V. Buldyrev, S. Havlin, M. Simons, H. E. Stanley and A. L. Goldberger, Phys. Rev. E **49**, 1685 (1994).
10. J. W. Kantelhardt, S. A. Zschiegner, E. Koscielny-Bunde, S. Havlin, A. Bunde, H. E. Stanley, Physica A **316**, 87, (2002)
11. J. W. Kantelhardt, *Fractal and multifractal time series*, in Springer Encyclopedia of Complexity and System Science, to appear.
12. P. Oswiecimka, J. Kwapien and S. Drozd, Phys. Rev. E **74**, 016103 (2006)
13. F. Argoul, A. Arneodo, J. Elezgaray, G. Grasseau and R. Murenzi, Phys. Lett. A **135**, 327 (1989).
14. P. Manimaran, P. K. Panigrahi and J. C. Parikh, Phys. Rev. E **72**, 046120 (2005)
15. J. R. Sanchez, Int. J. Mod. Phys. C **14**, 491 (2003).

16. J. Nagler and C. Claussen, Phys. Rev. E **71**,067103 (2005)
17. M. T. Matache and J. Heidel, Phys. Rev. E **71**, 026232 (2005)
18. T. C. Halsey, M. H. Jensen, L. P. Kadanoff, I. Procaccia and B. I. Shraiman, Phys. Rev. A **33**, 1141 (1986)
19. L. Telesca, G. Colangelo, V. Lapenna and M. Macchiato, Phys. Lett. A **332**, 398 (2004)
20. S. Wolfram, Physica D **10**, 1 (1984).
21. J.C. Claussen, J. Math. Phys. **49**, 062701 (2008).

# Chapter 7

## Concluding remarks and future work

### 7.1 Contributions

In this work we have presented results from simulations according to two computational models. The first one referred to a chemical system within a Continuously Stirred Tank Reactor (CSTR) while the second dealt with a physical system of self-assembling pieces under different conditions. In addition, were presented mathematical analysis, for waves along microtubules at the brain scale, and of wavelet processing of data from time series of Elementary Cellular Automata (ECA). The main results of this thesis work are briefly recalled in the following.

A cellular automata approach for the CSTR with a cooling jacket has been presented in Chapter 3. It could reproduce the CSTR dynamical behavior calculated by ODE's with a good approximation and in an easy way. The presented stochastic model allow us to study what could be the behavior of the variables of the tank when the reaction probability depends on the local temperature. It also gives us an approach to study systems of reduced content, such as micro and nanoreactors, or catalytic membranes separating two phases. The main advantages of the employed CA approach are its stochastic nature and the direct involvement of a spatial structure. This also represents a tool for studying the role of initial configuration

and stochastic fluctuations in systems of reduced content. Additionally, the CA approach is a clear improvement of the CSTR modeling and moreover can be applied to different reactor and jacket geometries, as well as for considering in greater detail the real mass flow for different geometries of the tank reactors.

We have found that in our CA-CSTR implementation at lattice dimensions beyond 400x400 and below time steps of 0.001 the ODE-based solutions (curves) are very well reproduced thus indicating that for those values the stochastic noise is very small. On the other hand, at small lattice dimensions the CA procedure gives strong fluctuations which are due to the CA discretization that sometimes could match the discretization of Nature at those scales. Besides, CA-type models can be used to analyze local microorganism densities which are directly related to the production yields of important fermentation products, such as bacterial cellulose obtained in generalized stirring reactors.

In Chapter 4 the mathematical technique of factorization of differential operators has been applied to two different problems. After a brief overview on microtubules, there were reviewed previous results related to the supersymmetry of the Montroll kinks moving onto the microtubule walls as well as mentioning the sine-Gordon model for the microtubule nonlinear excitations. Next, analytic formulas have been found for a class of one-parameter solutions of a sort of diffusion equation of Bessel type that is obtained by supersymmetry from the homogeneous form of a simple damped wave equations derived from previous work in the literature for the corticothalamic system. A possible interpretation of the diffusion equation in the brain context was presented.

In Chapter 5 the discussion focused on a model for the aggregation of pieces (or molecules), dynamically interacting according to LGCA methods. In addition to traditional models we considered that particles are not just point-like, but they have a cross shape. This implies the consideration of rotations and orientation of pieces and gives us the possibility of considering a huge spectra of different pieces

by defining different kinds of extremes and interactions between them. This is what makes our model different. We explored only the simplest possibilities of having all extremes of the same kind, complementary extremes in the same piece, two complementary extremes in two different pieces, and combination of pieces that have some extremes that lost their ability to establish a connection.

It was noticed that selection of pieces and densities have a major effect on the morphology of the aggregates at different scales. Different pieces promote different patterns of growth: promotion or inhibition of branches at the smaller scale, changes in the thickness of branches at the medium and global scales, changes in global density, growth on radial or spiral branches. Working with combinations of different densities and pieces certainly will provide a broader variety of structures.

Three measures were proposed for the study of the formed structures. The measure  $F$  gives us an idea of how dense is the structure at the global scale at the same time that neglect local properties. The second measure is the *perimeter/area* rate that gives us an idea about the structure and density of the branches of the aggregates, with the additional property of discarding global properties of the cluster. The combination of these two measures provides us with a better understanding of the formed structures than would be possible with the well known  $g(r)$  calculation. The last measure was simply the proportion between the number of non sticky extremes that are part of the perimeter and the total number of extremes forming the perimeter.

The results suggest that it is possible to create experimental aggregated structures at the micro- and nano-scales with partial control on their local and global structural properties. This would allow to produce small structures with enhanced properties for physical or chemical absorption of preferred sizes of particles. The controlled attachment of several particles over these designed aggregates could be the initial step for industrial production of materials with special microlocal surface properties at very low costs due to the easy implementation of the self-assembly

process.

Chapter 6 focuses on the analysis of the time series of the so-called row sum (or total activity) ECA signals, i.e., the sum of ones in sequences of rows, employing Daubechies (Db) wavelets. Various types of Db wavelets were used but the better matching of the results given by the wavelet-based MF-DFA method with those of other methods were provided by the Db-4 wavelets with four filter coefficients. The fact that the generalized Hurst exponent is not a constant horizontal line is indicative of a multifractal behavior in all analyzed cases. In addition, the fact that the  $\tau$  index is not of a single slope is another clear feature of multifractality. The strength of the multifractality is roughly measured with the width  $\Delta\alpha = \alpha_{\max} - \alpha_{\min}$  of the parabolic singularity spectrum  $f(\alpha)$  on the  $\alpha$  axis. We noticed that the most “frequent” singularity for all the analyzed time series occurs at  $\alpha = 0.568$ , where the width  $\Delta\alpha$  of rule 90 is shifted to the right with respect to those of rules 105 and 150. According to our results, the strongest singularity  $\alpha_{\min}$ , of all time series corresponds to the rule 90 and the weakest singularity,  $\alpha_{\max}$ , to the rule 150.

In conclusion, in general terms, the algorithmic implementation shows that embedding the discrete wavelet transform in the MF-DFA technique is a well-suited procedure to analyze the multifractal properties of the ECA. Indeed, we get similar results to the other methods but computationally faster because we employ a lesser number of windows. Our results represent a confirmation of the fact that ECA patterns of different magnitudes follow different scaling laws, *i.e.*, the ECA have intrinsic multifractality that does not depend on the set of initial data that we used. Therefore, when processes thought to be multifractal are simulated with (E)CA, their intrinsic multifractal behavior should be taken into account as a feature of the simulation procedure rather than of the multifractal behavior of the simulated processes.

Therefore, it is possible to say that the aims of this work have been accomplished at a great extent. They were

- To study, model, and simulate chemical and biological systems where spatio-temporal structures, probabilistic fluctuations and/or spatial inhomogeneities can be important for their behavior.
- To study, model, and simulate self-assembly systems, trying to find archetyp-ical self-assembly systems, by means of the abstract representation of compo-nents and their internal states and interactions.
- To reinforce the use of cellular automata by performing multidisciplinary stud-ies and modeling of the systems presented above, with cross-over of Biology, Physics, Chemistry and Mathematics.

## 7.2 Future research

Each of the studies presented here can be expanded and enhanced with further work. And I hope to be so, because am decided to continue my investigations along these research lines.

Some of the main points that I have in mind are:

- To implement different tank geometries to CA-CSRT model
- To analyze, under more specific conditions, the dynamic activity of nanoreac-tors
- To study wave propagation on computational models of microtubules
- To include energy considerations for the attachment and detachment of molecules in self-assembled systems
- To include conformational changes of the pieces as well as different piece ge-ometries
- To study more complex and specifically designed structures in order to explore how much information is needed for a specific structure and how much infor-mation could be structurally carried by the pieces under certain restrictions.

It is also desired to implement self-assembled systems with a molecular dynamics approach, in order to overcome geometrical restrictions inherent to lattice methods.

# Appendix A

## Cellular Automata Model for Reaction-Diffusion Systems

In this appendix it is presented in a brief way the Moving Average Cellular Automata that was developed by Weimar [1], [2]. This model was reproduced by us (a working code written in Fortran for 2D) and several key ideas were implemented as part of the Cellular Automata Model for Continuous Stirred Tank Reactor [3] presented in chapter 3. We also improved our code in order to manage systems with any number of chemical species (under computational restrictions), that can be used in future work on pattern generation on reaction-diffusion systems as those proposed by Turing in his seminal paper [4].

The summary of the method is depicted in Fig. A.1 for a 2-dimensional squared array and two reactants. Each cell has two values, one representing the concentration of chemical A in that point and the other for the concentration of reactant B at the same point. The concentration is represented by an integer that is inside a range from zero to  $\mathbf{N}$ . The greater the  $\mathbf{N}$ , the smoother the evolution of the system.

The first step in the iterations is the simulation of diffusion. It is made by performing the sum of concentrations of reactant A (B) from the neighboring cells in the vertical way that are closer than a distance  $\mathbf{R}$  from a given cell. This is made for all cells in the grid. This procedure allows to calculate the value for a cell  $\mathbf{i}$  from

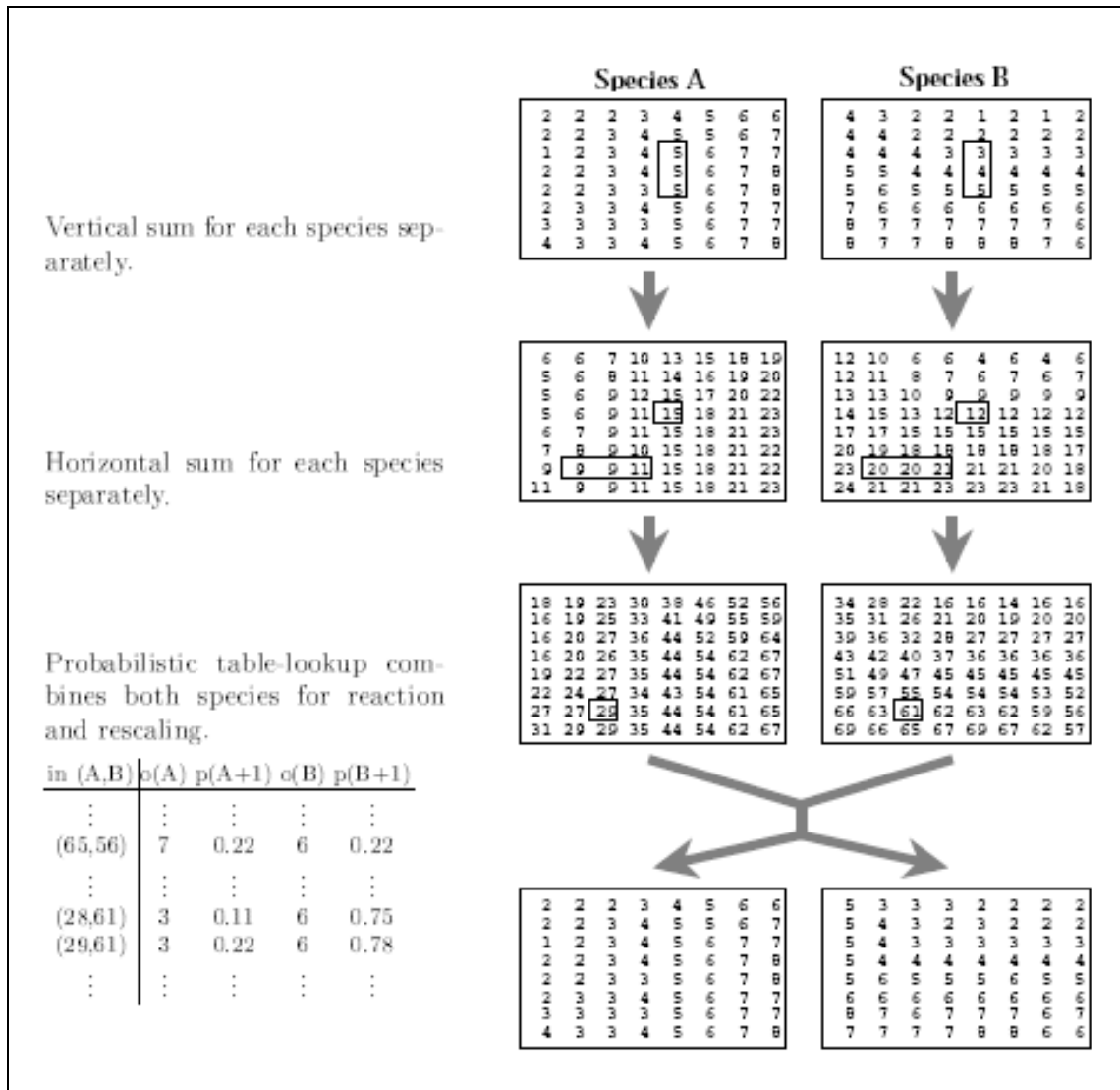


Figure A.1: Summary of moving average cellular automaton. Figure from [1].

the previously calculated value for the cell  $j$  above this one by subtracting the value of one cell (that one neighbor of  $j$  but not of  $i$ ) and adding the value of another cell (that one neighbor of  $i$  but not of  $j$ ). The process is repeated in the horizontal way with the values obtained in the vertical way. This process is equivalent to the diffusion of chemical A (B), as shown by Weimar (second order approximation) [2], with a magnitude that is related with the value  $R$ . The relation between diffusion of species A and species B can be controlled by giving them different  $R$  values. The calculation is made for all chemical species.

Instead of dividing the obtained value between the number of neighbors ( $(2R +$

1)<sup>2</sup>) in order to assure matter conservation, it is used a look-up table. This table is made before the iterations are performed, and represents the results from the chemical reaction between reactants A and B on all possible concentration combinations. The table can be seen as having five columns, and the first of them is composed by all possible results for the calculation explained above. The explanation for the other four columns will be done using the look-up table in Fig. A.1. The line where is written (65,56) represents a cell where the concentration of reactant A corresponds to  $65/9 = 7.222$  and  $56/9 = 6.222$ . The factor 9 comes from the fact that neighborhoods for diffusion in both cases was a square with 9 cells in the example of Fig. A.1 example. As can be seen in the table this values has been decomposed in four values: 7 and 0.222 from 7.222 and 6 and 0.222 from 6.222. These numbers are for a system where there is only diffusion and chemical species A and B do not react. If reaction were considered the values resulting after the reaction would have been calculated using the equations describing the reaction. The results from reaction would have been decomposed in integers and decimal parts in the same way.

The look-up table was calculated for all options according with the mathematical description of the system. Therefore, when the evolution of the system is calculated, the values are taken directly from the table and almost all calculations are made with integers, yielding a higher calculation speed of the system.

The last part of the method is related with how to use the numbers obtained from the look-up table. The integer  $\alpha$  from the table is the possible result for concentration of species A (B) in the cell in the beginning of the next iteration. The fractional part  $p$  is the probability of using  $\alpha + 1$  as the value in the next iteration and comes from the fact that  $\alpha + p$  is the value expected. The selection is done by comparison with a randomly generated number. This technique allows to maintain, in a statistical way, the real value that should be obtained from reaction, i.e., the average between values used ( $x$  times  $\alpha$  and  $y$  times  $\alpha + 1$ ) goes to the expected value  $\alpha + p$ .

Therefore, as a whole, this method is a flexible algorithm for simulating chemical systems with reduced noise, discrete nature and for fast computation.

### *REFERENCES*

1. J. R. Weimar, Cellular Automata for Reactive Systems, PhD Thesis, Université Libre de Bruxelles, Faculté des Sciences Service de Chimie Physique (1995)
2. J. R. Weimar and J. P. Boon, Phys. Rev. E **49**, 1749 (1994)
3. J.E. Pérez-Terrazas, V. Ibarra-Junquera and H.C. Rosu, Korean J. Chem. Eng. **25**(3), 461 (2008)
4. A. M. Turing, Phil. Trans. R. Soc. Lond. B **237**, 37 (1952)

# Appendix B

## Multi-Resolution Analysis

This appendix gives the basic concepts about the wavelet formalism used in order to produce the results presented in Chapter 6.

*WT: continuous and discrete.* - The WT of a function or distribution function  $\mathbf{x}(t)$  is given by

$$\mathbf{W}_x(\mathbf{a}, \mathbf{b}) = \frac{1}{\mathbf{a}} \int_{-\infty}^{\infty} \mathbf{x}(t) \bar{\psi} \left( \frac{t - \mathbf{b}}{\mathbf{a}} \right) dt, \quad (\text{B.1})$$

where  $\psi$  is the analyzing wavelet,  $\mathbf{b} \in \mathbb{R}$  is a translation parameter, whereas  $\mathbf{a} \in \mathbb{R}^+$  ( $\mathbf{a} \neq \mathbf{0}$ ) is a dilation or scale parameter, and the bar symbol denotes complex conjugation. One fundamental property that we require in order to analyze the singular behavior of a signal is that  $\psi(t)$  has enough vanishing moments [1, 2]. A wavelet has  $\mathbf{n}$  vanishing moments if and only if it satisfies

$$\int_{-\infty}^{\infty} t^k \psi(t) dt = 0, \quad \text{for } k = 0, 1, \dots, \mathbf{n} - 1, \quad \int_{-\infty}^{\infty} t^k \psi(t) dt \neq 0, \quad \text{for } k = \mathbf{n}. \quad (\text{B.2})$$

This means that a wavelet with  $\mathbf{n}$  vanishing moments is orthogonal to all polynomials up to order  $\mathbf{n} - 1$ . Thus, the WT of  $\mathbf{x}(t)$  performed with a wavelet  $\psi(t)$  with  $\mathbf{n}$  vanishing moments is nothing else but a “smoothed version” of the  $\mathbf{n}$ -th derivative of  $\mathbf{x}(t)$  on various scales.

However, the cellular automata data are notoriously discrete, so it is important to consider a discrete version of the CWT (B.1). Generally, the orthogonal (dis-

crete) wavelet transform (DWT) is employed. This is one of the different forms of the wavelet transform [3], and this method associates the wavelets to orthonormal bases of  $L^2(\mathbb{R})$ . In this case, the wavelet transform is performed only on a discrete grid of the parameters of dilation and translation, i.e.,  $\mathbf{a}$  and  $\mathbf{b}$  take on only integral values, as will be seen. In fact, for the numerical implementation of the DWT the multiresolution analysis (MRA) have been introduced.

The representation of a function or process  $\mathbf{x}(t)$  with the DWT is given in terms of shifted and dilated versions of the wavelet function  $\psi(t)$ , and its associated scaling function  $\varphi(t)$  [3, 4]. Within this framework and considering that the scaling and wavelet functions

$$\varphi_{m,n}(t) = 2^{m/2}\varphi(2^m t - n), \quad \psi_{m,n}(t) = 2^{m/2}\psi(2^m t - n), \quad m, n \in \mathbb{Z} \quad (\text{B.3})$$

form an orthonormal basis, then one can write the expansion of  $\mathbf{x}(t)$  as follows

$$\mathbf{x}(t) = \sum_n \left( c_{m_0,n} \varphi_{m_0,n}(t) + \sum_{m=m_0}^{M-1} d_{m,n} \psi_{m,n}(t) \right), \quad (\text{B.4})$$

where the scaling or approximation coefficients  $c_{m,n}$ , and the wavelet coefficients  $d_{m,n}$  are defined as

$$c_{m,n} = \int \mathbf{x}(t) \varphi_{m,n}(t) dt, \quad d_{m,n} = \int \mathbf{x}(t) \psi_{m,n}(t) dt, \quad (\text{B.5})$$

with  $m$  and  $n$  denoting the dilation and translation indices, respectively.

*Fast wavelet transform.* - To calculate  $c_{m,n}$  and  $d_{m,n}$ , Mallat [3] developed the fast wavelet transform (FWT) in which the MRA approach is involved. The FWT algorithm connects, in an elegant way, wavelets and filter banks, where the multiresolution signal decomposition of a signal  $\mathbf{X}$ , based on successive decomposition, is composed by a series of approximations and details which become increasingly coarse. At the beginning, the signal is split into an approximation and a detail part

that together yield the original one. The subdivision is such that the approximation signal contains the low frequencies, while the detail signal collects the remaining high frequencies. By repeated application of this subdivision rule on the approximation, details of increasingly coarse resolution are separated out, while the approximation itself grows coarser and coarser.

The FWT calculates the scaling and wavelet coefficients at scale  $m$  from the scaling coefficients at the next finer scale  $m + 1$  using the following formulas

$$c_{m,n} = \sum_k h[k - 2n]c_{m+1,k}, \quad (\text{B.6})$$

$$d_{m,n} = \sum_k g[k - 2n]c_{m+1,k}, \quad (\text{B.7})$$

where  $h[n]$  and  $g[n]$  are typically called low pass and high pass filters in the associated analysis filter bank. In fact, the signals  $c_{m,n}$  and  $d_{m,n}$  are the convolutions of  $c_{m+1,n}$  with the filters  $h[n]$  and  $g[n]$  followed by a downsampling of factor 2, respectively [3].

Conversely, a reconstruction of the original scaling coefficients  $c_{m+1,n}$  can be made from the following combination of the scaling and wavelet coefficients at a coarse scale

$$c_{m+1,n} = \sum_k (h[2k - n]c_{m,k} + g[2k - n]d_{m,k}) . \quad (\text{B.8})$$

It corresponds to the synthesis filter bank, and this part can be viewed as the discrete convolutions between the upsampled signal  $a_i^m$  and the filters  $h[n]$  and  $g[n]$ , that is, following an “upsampling” of factor 2 calculate the convolutions between the upsampled signal and the filters  $h[n]$  and  $g[n]$ . The number of levels depends on the length of the signal, i.e., a signal with  $2^L$  values can be decomposed into  $(L + 1)$  levels. To initialize the FWT, we consider a discrete time signal  $\mathbf{X} = \{x[1], x[2], \dots, x[N]\}$  of length  $N = 2^L$ . The first application of (B.6) and (B.7),

beginning with  $\mathbf{a}_n^{m+1} = \mathbf{x}[n]$ , define the first level of the FWT of  $\mathbf{X}$ . The process goes on, always adopting the “ $m+1$ ” scaling coefficients to calculate the “ $m$ ” scaling and wavelet coefficients. Iterating (B.6) and (B.7)  $M$  times, the transformed signal consists of  $M$  sets of wavelet coefficients at scales  $m = 1, \dots, M$ , and a signal set of scaling coefficients at scale  $M$ . There are exactly  $2^{(L-m)}$  wavelet coefficients  $\mathbf{d}_n^m$  at each scale  $m$ , and  $2^{(L-M)}$  scaling coefficients  $\mathbf{a}_n^M$ . The maximum number of iterations  $M_{\max} = L$ . A three-level decomposition process of the FWT is shown in Figure B.1.

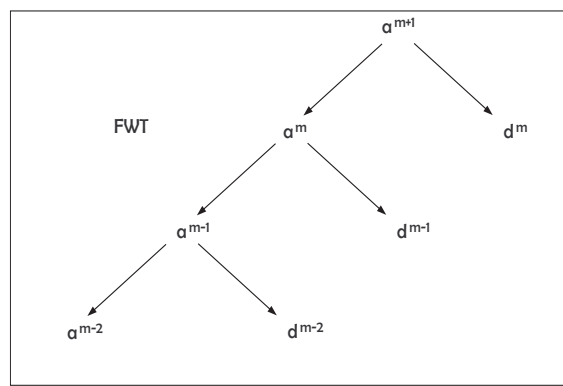


Figure B.1: The structure of a three-level FWT.

## REFERENCES

1. E. Bacry, J. F. Muzy and A. Arneodo, *J. Stat. Phys.* **70**, 635 (1993)
2. S. Mallat, W. L. Hwang, *IEEE Trans. Inform. Theory* **38**(2), 617 (1992)
3. S. Mallat, *A Wavelet Tour of Signal Processing*, 2nd. Edition, Academic Press (1999).
4. Ingrid Daubechies, *Ten lectures on Wavelets*, SIAM, Philadelphia, PA (1992).